INVESTIGATION OF TOLL-LIKE RECEPTOR 9 LIGAND RECOGNITION AND FUNCTION VIA MULTIVALENT OLIGODEOXYNUCLEOTIDE-POLYMER CONJUGATES

by

Eric Andrew Levenson

A dissertation submitted to the Faculty of the University of Delaware in partial fulfillment of the requirements for the degree of Doctor of Philosophy in Chemistry and Biochemistry

Spring 2014

ProQuest LLC.
789 East Eisenhower Parkway
P.O. Box 1346
Ann Arbor, MI 48106 - 1346

INVESTIGATION OF TOLL-LIKE RECEPTOR 9 LIGAND RECOGNITION AND FUNCTION VIA MULTIVALENT OLIGODEOXYNUCLEOTIDE-POLYMER CONJUGATES

by

Eric Andrew Levenson

Approved: _____
Murray Johnston, Ph.D.
Chair of the Department of Chemistry and Biochemistry

Approved: _____
George H. Watson, Ph.D.
Dean of the College of Arts and Sciences

Approved: _____
James G. Richards, Ph.D.
Vice Provost for Graduate and Professional Education

I certify that I have read this dissertation and that in my opinion it meets the academic and professional standard required by the University as a dissertation for the degree of Doctor of Philosophy.

Signed: _____

Zhihao Zhuang, Ph.D.
Professor in charge of dissertation

I certify that I have read this dissertation and that in my opinion it meets the academic and professional standard required by the University as a dissertation for the degree of Doctor of Philosophy.

Signed: _____

Kristi L. Kiick, Ph.D.
Professor in charge of dissertation

I certify that I have read this dissertation and that in my opinion it meets the academic and professional standard required by the University as a dissertation for the degree of Doctor of Philosophy.

Signed: _____

Roberta Colman, Ph.D.
Member of dissertation committee

I certify that I have read this dissertation and that in my opinion it meets the academic and professional standard required by the University as a dissertation for the degree of Doctor of Philosophy.

Signed: _____

Kishore Alugupalli, Ph.D.
Member of dissertation committee

ACKNOWLEDGMENTS

The PhD is a degree of independence, but there are some whom I wish to acknowledge for their support over the course of my degree.

My wife Courtney, and now my son, Troy, are part of what make achievements, like the completion of this degree, worth it. My family and extended family have also lent significant moral support over the years (and time!) and I thank them for it.

I would like to wholeheartedly thank my advisor, Kristi Kiick, for providing an environment, which allowed me to grow as a scientist within my capabilities and needs. The true interdisciplinary nature of the work presented in this thesis would not be possible without her scientific curiosity and willingness to take a chance. The Kiick group was always known as friendliest and most welcoming group in the department. I would also like to thank the counsel of Roberta Colman, who recruited me to Delaware and the CBI program. Also Zhihao Zhuang, Colin Thorpe, Sharon Rozovsky, and John Koh for their helpful advice over the years. I would also like to acknowledge colleagues and friends Jeffery Caplan and Michael Moore for all their help at the Delaware Biotechnology Institute Bio Imaging Center.

I also had an opportunity to interact with many of the Faculty members at Thomas Jefferson University. I owe special thanks to Lawrence Eisenlohr for allowing me to join in his group meetings for two years, mentoring and introducing me to the microbiology and immunology department. I would also like to

acknowledge the mentoring of Tim Manser and Kishore Alugupalli, and the friendship and contributions of Raja Vuyyuru and Gregory Dickinson to this work.

I would like to acknowledge the financial support of this work, provided by the National Institutes of Health for the Chemistry Biology Interface Program at the University of Delaware (NIH/NIGMS CBI Training Grant 5T32 GM 08550-15). This work was also supported in part by the Center for Neutron Science at UD under award (U.S. Department of Commerce) #70NANB7H6178, as well as by the National Institutes of Health (1-RO1-EB006006).

I would like to acknowledge C. Gürtler and A. G. Bowie for the use of Fig. 1.1 as well as Hiromi Tanji and colleagues for Figure 1.2.

TABLE OF CONTENTS

LIST OF TABLES

LIST OF FIGURES

LIST OF ABREVIATIONS

AIM2	**absent in melanoma 2**
BCR	**B cell receptor**
BTK	**Bruton's tyrosine kinase**
CD14	**cluster of differentiation 14**
CD40	**cluster of differentiation 40**
CD80	**cluster of differentiation 80**
CD86	**cluster of differentiation 86**
CNPY3	**canopy FGF signaling regulator 3**
CXCL10	**C-X-C motif chemokine 10**
DLS	**dynamic light scattering**
DMSO	**dimethylsulfoxide**
DNA	**deoxyribonucleic acid**
EDC	**N-(3-dimethylaminopropyl)-N'-ethylcarbodiimide hydrochloride**
EEA-1	**early endosomal antigen 1**
ELISA	**enzyme linked immunosorbant assay**
GPC	**gel permeation chromatography**
HABA	**4'-hydroxyazobenzene-2-carboxylic acid)**
HBTU	**O-(Benzotriazol-1-yl)-N,N,N',N'-tetramethyluronium hexafluoro phosphate**
HEPES	**2-[4-(2-hydroxyethyl)piperazin-1-yl]ethanesulfonic acid**
HMGB1	**high mobility box group 1**
hSAP	**human serum amyloid P**
HSP	**heat shock protein**

IFN	**Interferon**
IL-10	**Interleukin 10**
IL-6	**Interleukin 6**
IRAK	**Interleukin 1 receptor associated kinase 1**
IRF	**Interferon regulatory factor**
LAL	**limulus amoebocyte assay**
LAMP-1	**lysosomal associated membrane protein 1**
LGP2	**laboratory of physiology and genetics 2**
LRR	**leucine-rich repeat**
M.W.	**molecular weight**
MAC-1	**Macrophage-1 antigen**
MBP	**Mannose binding protein**
MDA5	**Melanoma differentiation-associated protein 5**
MES	**2-(N-morpholino)ethanesulfonic acid sodium salt**
MHC	**major histocompatibility complex**
MWCO	**molecular weight cutoff**
NEAM	**N-(2-aminoethyl)maleimide trifluoroacetate salt**
NF-κB	**nuclear factor kappa-light-chain-enhancer of activated B cells**
NMR	**nuclear magnetic resonance**
ODN	**Oligodeoxynucleotide**
PAA	**poly(acrylic acid)**
pDC	**plasmacytoid dendritic cells**
PDI	**poly dispersity index**
PES	**polyethersulfone**
PRR	**pattern recognition receptor**
RA	**rheumatoid arthitis**
RAGE	**receptor for advanced glycation end-products**
RIG-I	**retinoic acid induced gene I**
RNA	**ribonucleic acid**

SLE	**systemic lupus erythematosus**
STING	**stimulator of interferon genes**
TAK1	**TGFβ-activated kinase**
TCR	**T cell receptor**
TEA	**triethylamine**
TIR	**Toll interleukin 1 receptor**
TLR9	**Toll-like Receptor 9**
TNF-α	**tumor necrosis factor alpha**
TRAF6	**TNF receptor associated factor 6**
TRIF	**TIR-domain-containing adapter-inducing interferon-β**
UNC93B1	**unc93 homolog B1**
UV-Vis	**ultraviolet visible**

ABSTRACT

DNA is used as the template for genetic information in all pathogen types sensed by the innate immune system– viruses, bacteria, fungi, and parasites – making it a critical signal of infection. Toll-like receptor 9 (TLR9) recognizes DNA encoding unmethylated CpG motifs and upon activation, promotes signaling through NF-κB in B-cells or plasmacytoid dendritic cells (pDC) for the generation of adaptive immunity or IRF3/7 in pDC for antiviral responses. TLR9 is an integral part of innate response for many major pathogens including *M. tuberculosis, T. cruzi*, *P. falciparum, and Herpes simplex,* underscoring the importance of discerning the biological function of this receptor. Oligodeoxynucleotides (ODN) containing unmethylated CpG dinucleotide motifs are currently being investigated for use as vaccine adjuvants through promotion of type I immunity. Several classes of ODN have been developed which differ in their propensity to aggregate, which in turn, alter cytokine profiles and immune cell subsets activated. Although aggregation state is correlated with the change in cytokine response, subcellular location and other factors, it is not clear how differences in spatial presentation lead to this divergent immune response.

Here, we examined the role of ligand valency on the activation of TLR9 through the synthesis of ODN-poly(acrylic acid) (PAA) conjugates. The composition and size of the conjugates were characterized by UV-Vis spectroscopy, ^{1}H NMR, gel permeation chromatography, and dynamic light scattering. ELISA-based assays of cytokine secretion by murine-like macrophages indicate that these ODN-PAA polymer conjugates show enhanced immunostimulation at 100-fold lower concentrations than

those required for ODN alone, for both TNF-α and IL-6 release, and are more potent than any other previously reported multivalent ODN constructs. Increasing valency was shown to significantly enhance cytokine expression, particularly for IL-6. Knockdown by siRNA demonstrates that these polymer conjugates are specific to TLR9.

To further define the role of ligand number and density, we directly labeled ODN-PAA conjugates with the fluorophore Alexa 647. The compositions of the labeled ODN-PAA conjugates were characterized by UV-Vis spectroscopy using this internal Alexa 647 standard. ELISA-based assays for TNF-α, IL-6 and IL-10 demonstrate an ODN valency dependent increase in cytokine output. IL-6 expression is shown to require a critical valency, suggesting localized engagement of multiple TLR9 dimers results in a functionally higher inflammatory response. The observed increase in IL-10 with increasing ODN functionality was shown to correlate with intracellular ODN concentration (flow cytometry) indicating high valency conjugates were more efficient delivery vehicles. However, ODN spatial density was found to be directly proportional to observed IL-10 expression across all conjugates assayed regardless of scaffold. TNF-α expression is influenced by scaffold molecular weight and ODN presentation density. Low molecular weight scaffolds demonstrate increasing expression with increasing valency while higher molecular weight scaffolds show highest expression at low density and valency. This divergent cytokine response was examined with respect to endocytosis (time dependence and inhibition) and

subcellular localization. Cellular internalization is shown to be a clathrin-mediated process blocked by monodansylcadaverine. Subcellular localization indicated rapid conjugate endocytosis with enhanced accumulation in LAMP-1 staining compartments compared to labeled ODN or scaffold. Our results define valency and density as critical design parameters and polymer conjugation as a potentially advantageous strategy for ODN immunomodulatory agents.

Under pathological conditions, activation of the innate immune system by 'self'-DNA has been definitively linked to autoimmune diseases including systemic lupus erythematosus (SLE), rheumatoid arthritis (RA), psoriasis, and heart disease. Innate antagonists are thus currently in development for these diseases in addition to sepsis and pathological inflammation. Many autoimmune disorders, such as Systemic Lupus Erythematosus (SLE) and psoriasis, are now correlated with improper nucleic acid recognition by TLR9. Current TLR9 ODN therapies in development rely upon phosphorothioate-based derivatives to increase serum half-life and enhance intracellular delivery; however, safety concerns warrant the development of alternatives. Oligodeoxynucleotide (ODN)-Poly(acrylic acid)(PAA) conjugates were synthesized via Michael-type addition and characterized by ^{1}H nuclear magnetic resonance and UV-Vis spectroscopy. Conjugate alteration of ODN antagonism was characterized by *in vitro* dose response curves in RAW264.7 cells. Here, our results demonstrate polymer conjugation of an antagonistic phosphodiester-based oligodeoxyribonucleic (ODN) sequence (4380) enhances exo- and endonuclease resistance in addition to intracellular delivery with a ~15X reduction in IC_{50} values, similar to the phosphorothioate-based derivative. Additionally, intracellular delivery and activity are influenced by valency with the most efficient conjugate showing IC_{50}

values roughly 2-fold lower than the corresponding phosphorothioate sequence. These results suggest antagonistic ODN-polymer conjugates as a potential strategy for autoimmune disease therapy.

Chapter 1

INTRODUCTION

1.1 Innate Recognition of Nucleic Acids

The innate immune system is critical in early response to pathogens as well as the progression to effective adaptive immune response(1), and approaches to control innate responses thus have significance in the development of vaccines and in the treatment of autoimmune diseases. Pathogens such as viruses, bacteria, fungi, and parasites all have non-endogenous chemical structures called pathogen associated molecular patterns (PAMPs) that are recognized by pattern recognition receptors (PRR).(2) Sensing of pathogens by PRRs allows accurate identification and also promotes proper processing and presentation of antigen;(3) for these reasons, PRR ligands are currently in phase I, II and II clinical trials for numerous vaccines including influenza, hepatitis B/C, and cancer.(4) Nucleic acid sensing PRRs are a special group that plays an important role in pathogen recognition but under stringent regulation to not respond to endogenous DNA and RNA.(5, 6) The breakdown of PRR regulation has been correlated with many autoimmune diseases.(7) This introduction highlights the nucleic acid sensing receptor Toll-like receptor 9 (TLR9) and the birfurcated response observed with the alteration of aggregation state in

unmethylated CpG dinucleotide containing DNA. Additionally, methods and examples of receptor clustering and signaling are briefly reviewed.

1.1.1 Nucleic Acid Receptors

Nucleic acid recognition is central to innate immune response as all pathogens use nucleic acids to encode or transcribe their genes. Fungal pathogens, bacteria and DNA-based viruses are recognized through TLR9 and other putative or unidentified cytosolic receptors.(8-10) Nucleic acid recognition is tightly controlled to limit identification of endogenous sources. There are an increasing number of intracellular receptors capable of sensing DNA, RNA, or cyclic dinucleotides with specific signatures characteristic of bacterial or viral infection. These include RIG-I, MDA5, AIM2, RNA Polymerase III, STING, and a host of other putative receptors.(10) The nucleic acid sensing Toll-like receptors (TLRs), TLR3, 7, 8, 9, and 13 (mice) are all endosomally localized to only recognize endocytosed material.(10) They also recognize unique motifs that help to restrict recognition of self-nucleic acids(7), which will be described below. Figure 1.1 schematically depicts the location, ligand, signaling pathways, and downstream transcriptionally-activated gene products for all of the known nucleic acid receptors.(5)

1.1.1.1 Intracellular Receptors

Replicating pathogens that gain entrance to the cytoplasm, and are subsequently detected, synthesize nucleic acids with unique molecular characteristics. A growing number of characterized intracellular receptors have been identified that function as PRRs against these intracellular pathogens. The first receptors characterized are the DExD/H box (RNA binding motif) helicase family containing RIG-I, MDA5, and LGP2, recognizing single-stranded and double-stranded RNA respectively, and leading to the production of both type I interferons (IFN) and proinflammatory cytokines.(10) Cytosolic DNA recognition receptors or mediators also exist. RNA polymerase III converts dsDNA to dsRNA, which is then recognized by RIG-I.(10) The DExD/H box helicase DDX41 binds DNA and knockdown shows a role in IFN production to cytoplasmic DNA.(10) There are also secondary messengers, cyclic dinucleotides (CDNs), which are produced in response to DNA binding by proteins including cGAMP synthase.(11, 12) CDNs are recognized by both the stimulator of interferon genes (STING) and DDX41, with both leading to IFN production.(10) Additional uncharacterized receptors are still thought to exist, and the interplay between these described receptors, and others, must still be determined.

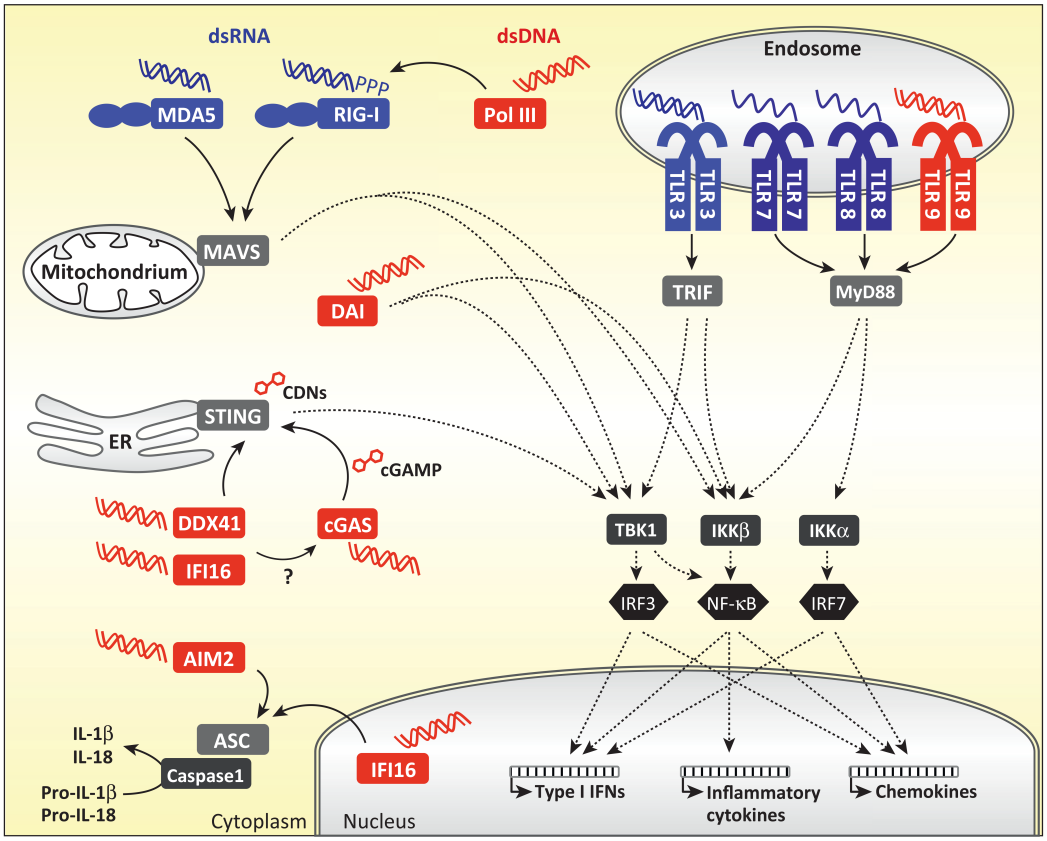

Figure 1.1 Nucleic acid sensing by pattern recognition receptors (PRRs) in distinct cellular compartments.The four Toll-like receptor (TLR) family members TLR3, TLR7/8, and TLR9 are located in the endosome leading to activation of TIR domain-containing adaptor inducing IFN-b (TRIF)- or myeloid differentiation factor-88 (MyD88)-dependent pathways and the upregulation of type I IFNs, inflammatory cytokines, and chemokines via IFN regulatory factor (IRF) and nuclear factor κB (NF-κB) transcription factors. Cytosolic RNA detection is mediated by retinoic acid-inducible gene I (RIG-I)- like receptors (RLRs), i.e., RIG-I and melanoma differentiation-associated gene 5 (MDA5), that subsequently signal via mitochondrial antiviral signaling (MAVS) adaptor. Upstream candidate DNA receptors include DEAD box protein 41 (DDX41) and the absent in melanoma 2 (AIM2)-like receptor (ALR) family member IFI16. Furthermore, the ALRs AIM2 and IFI16 trigger the formation of an inflammasome following detection of cytosolic DNA, respectively to induce processing of the inflammatory cytokines IL-1b and IL-18.(5)

1.1.1.2 Endosomal Partitioned Receptors

The endosomal nucleic acid receptors all belong to the TLR family of PRRs. TLR receptors belong to the solenoid-shaped leucine-rich repeat (LRR) group of receptors; they are type-I integral membrane proteins that exist as preformed dimers, which when bound to their respective ligands, undergo allosteric conformational changes.(13, 14) TLR3, 7, 8, and 9's endosomal location requires all ligands to be endocytosed from the extracellular space (Figure 1.1).(15) TLR3 binds double stranded RNA, a replication intermediate for RNA viruses, and is commonly activated in vitro by poly(I:C).(5) TLR7 and 8 recognize virus-derived single stranded RNA and are pharmacologically activated by small molecule nucleoside derivative agonists.(5) The final human TLR, TLR9, recognizes unmethylated cytosine-guanine motifs in DNA or synthetic oligodeoxyribonucleic acids (ODN).(16, 17) This motif is more common in bacterial or viral-derived DNA where epigenetic methylation of cytosine does not occur, and is one of the layers of TLR9 regulation.(7) TLR recognition of nucleic acids is most effective for specific molecular signatures; there are instances where this specificity breaks down.

Nucleic acid sensing TLR, have layers of regulation to limit inappropriate recognition, in addition to molecular specificity, which include the requirement for endocytosis of extracellular material and proteolytic processing events.(7) All TLRs have similar sequence and structure, belonging to the leucine-rich repeat (LRR) family of solenoid shaped receptors.(9, 13) The proteolytic processing of nucleic acid sensing TLRs by cathepsins(18, 19), was first identified in TLR9. Receptor processing was

then extended to TLR3, 7, and 8 with the hypothesis that proteolytic processing is another control step to limit improper recognition of endogenous nucleic acids.(20-22) TLR3 and 8 have both had crystal structures determined(22-24) , however, earlier interpretations of the TLR3 structure, including the uncleaved receptor, bound to dsRNA, are now in doubt. The TLR8 structure is cleaved, but shows the membrane bound C-terminal segment still in association with the cleaved portion of the receptor.(22) Recently, the N-terminal cleavage product of TLR9 was shown to be critical for TLR-dependent cytokine expression(25), further supporting the necessity of cleavage and association of this cleavage product for nucleic acid sensing.

1.1.2 Role of DNA Sensing in Adaptive Immunity

The enhancement in presentation of antigen and the adaptive generation of specific clonal populations of B and T cells is one of the main functions of the innate immune system. All PRR ligands serve as early markers of infection and have potential use as adjuvants to promote potent and lasting immunological response and memory.(4) Nucleic acids are not the most potent PRR ligands(26), but the relative ease of synthesis and low cost make them ideal candidates as adjuvants.(6) Maurer et al first showed CpG antigen conjugates are efficiently endocytosed and promote cellular stimulation.(27) Exposure of immune cells to DNA with CpG motifs stimulates a potent T helper 1 (T_H1) inflammatory response(16), which is beneficial for activation of CD4+ T cells(28) and allergic immunotherapy.(29) CpG ODN have been covalently attached to antigens as diverse as major short ragweed allergen Amb a

1(29), *E. coli* ß-galactosidase(29), HIV envelope glycoprotein gp120(30), and ovalbulmin (OVA).(27, 31-33) The physical conjugation of antigen to CpG-containing DNA enhances uptake, elicits potent cytokine release, and promotes antibody production.(34) The enhanced endocytosis of these antigen-CpG-DNA conjugates is independent of TLR9. However, TLR9 is responsible for the maturation of the antigen presenting cell and productive T cell activation.(35) Current efforts to improve vaccine response also include the activation of plasmacytoid dendritic cells (pDC) by nucleic acid adjuvants for potent type I interferon production.(34) More selective and efficient stimulation of the T_H1 response yields better immunological activation and memory, and therefore, appropriate response and protection.

1.1.3 Accessory Molecules of Toll-like Receptor 9

An ever increasing number of proteins have been identified as possible accessory proteins or receptors involved in TLR9 DNA recognition and activation.(36-38) A general theme of all the currently identified proteins and receptors are their already identified role in immunological function. Further efforts to characterize the structure, ligand binding, and role of accessory molecules in ligand recognition for all nucleic acid sensing TLRs has been complicated by the dynamic cellular transport of both TLR and ligand, as well the multiple roles and activities already identified for most of these proteins.(39) These efforts, however, will be critical to clarify the complexities of innate nucleic acid signaling.

Proteins involved in the regulation of TLR9 trafficking and processing include the heat shock proteins (Hsp) GP96 and Hsp90, and Unc93b1. Heat shock protein gp96, a paralogue of Hsp90, provides conformational stability and protection from degradation in endosomes.(40) The association of gp96 was further shown to rely upon another accessory molecule, CNPY3, and the ternary complex formation was sensitive to ATP.(41) Hsp90 binds both CpG A-type ODN and endogenous DNA, promoting endocytosis and localization with static early endosomes. This localization promotes IFN-α release by plasmacytoid dendritic cells.(42) Unc93b1 is an endoplasmic reticulum (ER)-associated transmembrane protein, which regulates the intracellular trafficking of nucleic acid sensing TLRs from the ER to endolysosomes. It not only biases dendritic cells (DC) from RNA to DNA(43), but also associates with the protein AP3 to regulate trafficking to lysosome-related organelles required for the DC production of type I interferons (IFN).(44)

Several proteins have been implicated in the binding, endocytosis, and recognition of CpG DNA or ODNs, including CXCL10, Complement C3A, Granulin, CD14, Raftlin and the mannose receptor. The scavenger receptor CXCL10 aids in the endocytosis of CpG A type ODN and is hypothesized to be partly responsible for the selective recognition of this ODN type by pDC.(45) Complement C3a has also been shown to promote IFN production by pDC through a ternary complex with the receptor for advanced glycation end products (RAGE), and CpG A ODN.(46) Granulin, a secreted and soluble cysteine-rich protein directly binds to all ODN types and promotes their delivery to endolysosomal compartments(47), hypothesized to be the site of TLR9-mediated production of proinflammatory cytokines.(48)The last of

this group, CD14, was already identified as a co-receptor for TLR4.(49) CD14 was first identified as a co-receptor for TLR3 by binding double stranded RNA (dsRNA).(50) This finding was then extended to TLR9 showing that CD14 aids in the endocytosis of nucleic acids and aids in the production of proinflammatory cytokines.(51) Through CD14, the cytoplasmic lipid raft protein Raftlin functions as a required protein for endocytosis of both dsRNA and ssDNA.(52, 53) Finally, the mannose receptor was recently identified and as being responsible for the hyper responsiveness of common laboratory strains of mice to ODN and further investigation will be required to demonstrate this receptors importance in humans.(54)

TLR9 intracellular signaling is promoted by Viperin, major histocompatibility complex (MHC) class II, and the Bruton's Tyrosine Kinase (BTK); the core signaling proteins and adapters of TLR9 will be covered in section 1.1.4. Viperin is a cytoplasmic protein with induced expression after pDC activation by TLR7 or TLR9.(55) Viperin interacts with both the Interleukin-1 receptor-associated kinase 1 (IRAK1) and the TNF receptor-associated factor-6 (TRAF6) to promote the K63-linked ubiquitination of IRAK1, promoting the transcription factor IRF7 for IFN production. BTK has recently shown two important activities to promote adaptive immune response. BTK kinase interacts with MHC class II molecules through the co-stimulatory molecule CD40 in conjunction with the TLR signaling adapters myeloid differentiation primary response gene-88 (MyD88) and the TIR-domain-containing adapter-inducing interferon-ß (TRIF) to promote proinflammatory cytokine production.(56) As discussed in section 1.1.1.2, a common protease activation strategy in compartments where there is simultaneous antigen processing is an effective way to

link exogenous nucleic acid recognition to antigen presentation. In fact, several studies suggest that antigen loading is more efficient in the context of a TLR ligand.(57-60) BTK is also essential for co-localization of the B cell receptor (BCR) and TLR9; co-localization of these two receptors synergizes BCR signaling.(61)

Suppression of CpG DNA recognition is also accomplished through several proteins including human serum amyloid P (hSAP), serum mannan-binding protein (MBP), and the CD24/ siglec-10 axis. hSAP sequesters serum DNA and prevents binding by both high mobility box group 1 (HMGB1) and LL37, (discussed below) preventing immune recognition.(62) MBP, a C-type lectin, binds extracellular DNA from many sources and promotes clearance by phagocytosis to limit immune recognition.(63) CD24 binds to several promoters of TLR9 activation including HMGB1 and Hsp90.(64) This association blocks immune activation and the additional involvement of Siglec-10 helps to prevent nuclear factor κB (NF-κB) activation.

A few accessory proteins function in the context of physiological as well as pathological processes such as autoimmune disease progression. HMBG1 has been identified as having several functions related to DNA-protein interactions.(65) It is exported to the cytoplasm and excreted by immune cells stimulated with IFN-γ, IL-1, and TNF-α. HMBG1 interacts with CpG ODN internalized by macrophages and enhances their immune activating potential through TLR9. TLR9 and HMBG-1 associate and redistribute to EEA1 and LAMP-1 endosomes concurrently after ODN stimulation. Deficiencies of HMBG1 delay the redistribution of TLR9 to early endosomes to 30 minutes after stimulation and increase the effective concentration necessary for cytokine release. From these findings it is thought HMGB1 aids in the

recognition and or response to DNA through a mechanism dependent upon TLR9 association.

Another player in the recognition of nucleic acid is the receptor for advanced glycation end-products (RAGE).(66) RAGE recognizes a number of immunologically relevant ligands including HMGB1, Mac-1 and S100. A common attribute of all RAGE ligands is their ability to form multivalent structures. RAGE is hypothesized to form a hexameric receptor array that would preferentially bind larger multivalent ligands such as the interaction of DNA with HMBG1. Receptor ligation stimulates signaling through NF-κB and upregulates genes linked to inflammation. There may be a delicate balance in the recognition of RAGE ligands. In acute release, RAGE ligands remain monomeric and stimulate normal inflammatory response with healing. With chronic release, more multivalent forms of RAGE ligands may be present that stimulate strong inflammatory responses.

The binding of extra cellular DNA by HMBG1, interaction and internalization through RAGE, and activation of TLR9 may play an essential part in the improper activation of auto-reactive B cells in some autoimmune diseases. Tian et al showed that HMBG1 enhanced CpG-A DNA interaction with TLR.(67) Through immunoprecipitation experiments they showed RAGE interacted with TLR9 through HMBG1 complexed with DNA. HMBG1 promoted interaction of RAGE with TLR9 and enhanced IFN-α and TNF production. An interesting finding was CpG-B DNA did not bind to HMBG1 and some random DNA sequences indicating discretionary binding of DNA. They also determined that HMBG1 was present in chromatin immune complexes recognized by AM14 mice and HMBG1 was needed for the

interaction of the immune complexes and B cells. This shows a possible link between HMBG1 interaction with DNA containing immune complexes and pathological activation of TLR9, which promotes B cell proliferation, a key event in autoimmune disease.

A small (~4.5 kD), cationic, antimicrobial protein named LL37 was found to be a potent inducer of pDC IFN release and activation. The serum of psoriasis patients was examined for expressed proteins or factors that activate pDC's and cause production of IFN.(68) Psoriatic patients show highly elevated expression of LL37 with average epidermal tissue concentrations of 300 μM. Due to its cationic nature, LL37 was investigated for DNA interaction. LL37 induced condensation of DNA by size-exclusion chromatography and AFM. Human genomic DNA was not internalized by pDC's, however, DNA-protein complex internalization shows a dependence on LL37. The expression of cytokines was dependent upon TLR9 and the maturation of early endosomal compartments. Interestingly, these complexes were retained in early endosomal compartments, as was demonstrated for large DNA aggregates. LL37 is also highly upregulated in patients with lupus and is required for the FcγRIIa internalization of antibody-DNA complexes.(8) Preferential localization to the early endosomes would stimulate IFN-α production under the current model of TLR9 localization and activation, described in the next section, and required for promotion of autoimmune disease.

1.1.4 Physiological Response of Toll-like Receptor 9

TLR9, a transmembrane protein, is predominantly expressed within pDCs, B-cells, and neutrophils in humans.(69, 70) and belongs to the subgroup endosomal TLRs including 3, 7, 8, and 9 that share very similar sequence;(71) mice additionally express TLR9 in macrophages.(15) TLR9 activation involves a conformational alteration of receptor dimerization to assemble a signaling scaffold.(72) All TLRs have a cytoplasmic Toll-Il-1 receptor resistance (TIR) domain that recruits the MYD88 signaling scaffold complex.(73) The TLR9 signaling scaffold is comprised of the multi domain proteins MyD88, IRAK1 and 4, TRAF6, and TAK1.(74) The TIR domains of TLR9 and MyD88 associate and recruit IRAK 1 and 4 through MyD88-IRAK Death Domain (DD) interactions. Several ubiquitylation and phosphorylation events take place to recruit TRAF6. TRAF6 E3 ubiquitin ligase activity to form Lys63-linked polyubiquitin chains promotes the activation of TAK1, leading to the activation of p38 MAPK and Janus kinases, as well as NEMO ubiquitination for NF-κβ activation. The outcome is cytokine expression and an inflammatory response.(74, 75)

Three TLR crystal structures have been solved to date however, no structure has yet been determined for TLR9. The TLR3 structure, the first solved(23, 24, 76) exhibits an inner diameter of 42 Å, an outer diameter of 90 Å, and a thickness of 35 Å. The model, based on the crystal structure packing, is two solenoids which interact on their unglycosylated sides. The C-terminal end are directed away from one another and the N-terminal portions of the domain interact to bring the cytosolic TIR domains

(not seen in crystal structure) in close proximity making an "M" shaped dimer. It is this dimer and the specific interaction of the TIR domains that recruits the adapter proteins MyD88 (TLR9) or TRIF (TLR3) for intracellular signaling.(77)

The crystal structure of TLR3 was crystallized without a ligand, lacking structural information on activation. A detailed model has been put forth by Pirher et al(76) using the crystal data and known helical geometries of nucleic acids and they hypothesized that RNA would interact with the inner faces of the dimer and be parallel along the long axis. FRET and GFP reconstitution were used by Latz et al(72) to study the binding dynamics of TLR9 in endosomes. TLR9 appears to exist as a preformed dimer that upon binding of stimulatory DNA, changes conformation with closer association of the two solenoids. Work with other TLRs also suggests that the two solenoids exist as a pre-formed dimer and that signaling must involve structural changes with tighter association of the cytosolic TIR domains. TLR9 and all TLRs belong to the leucine-rich repeat family of proteins with significant sequence homology. Therefore, TLR9 should have a similar structure to TLR3 allowing prediction of how many receptors could be colocalized within a given surface area. The TLR8 structure was recently determined, largely agreeing with the TLR3 structures discussed above, and this structure is shown in Figure 1.2.(22) The TLR8 structure is in complex with the small molecule agonist CL097. Importantly, the cathepsin and furin cleavage event(20, 25, 78), now known to be necessary for activation, has occurred in this structure and shows both N- and C-terminal TLR8 fragments in association with each other in complex with the small molecule agonist. This structural information, although not of TLR9, minimally gives us a rough

estimation of the total number of TLR9 dimers which could be simultaneously engaged by a conjugate of known size.

The importance of supramolecular structure in the recognition and signal transduction of innate signals, is suggested by the role of the myeloid differentiation primary response protein 88 (MyD88),(75) in forming the MyD88-containing oligomeric signaling platform termed the MyD88some. Formation of the MyD88some, which leads to proinflammatory cytokine expression, begins with a conformational change in TLR dimers upon engagement of an innate ligand;(79) knock-out of MyD88 prevents activation of NF-κβ (necessary for cytokine expression) for multiple TLRs (including TLR9), while over expression of this protein leads to constitutive activation of NF-κβ.(75) The crystal structure of a TLR dimer/MyD88 complex demonstrates a specific MyD88:IRAK-4 (IL-1 receptor-associated kinase 4, involved in the signaling cascade) stoichiometric relationship of 7:4 and 8:4; it is hypothesized that these alternate stoichiometries relate to variable TLR supramolecular assemblies composing several activated dimers, which data presented in this thesis supports. In fact, cooperative TLR recognition has been demonstrated for *N. meningitides* (TLR2, TLR4, TLR9), *B. burgdorferi* (TLR2, TLR5, TLR9),(8) and *C. neoformans* (Mannose receptor, TLR2, TLR3, TLR9),(80) and is suggested to be critical for adequate response to *M. tuberculosis* and herpes simplex (TLR2 and TLR9).(81, 82)

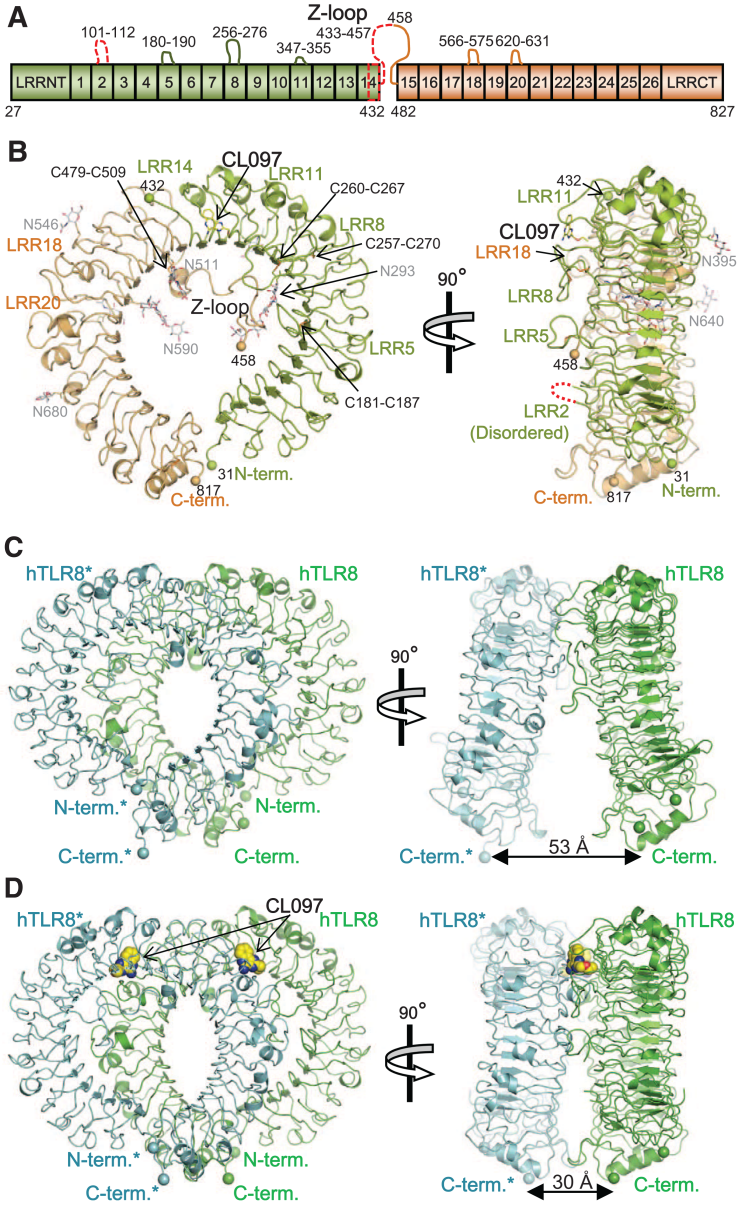

Figure 1.2 Structures of human TLR8. (A) Schematic representation of the domain organization of extracellular regions of TLR8 (hTLR8). (B) Monomer structure of the hTLR8-CL097 complex showing both lateral and convex face from N-terminal side. (C) Ligand induced state. (D) TLR8 and its dimerization partner TLR8* (green and cyan). CL097 molecules in activated dimer are illustrated by space filling representations.(22)

1.1.4.1 Toll-like Receptor 9 Ligand Specificities

ODN secondary structure and aggregation can alter TLR9 activation. There are now 4 classes of stimulatory ODN with differing propensities to aggregate.(83) The aggregation state alters the cellular response to CpG DNA with highly aggregated ODN, DNA condensed by immunomodulatory proteins, or DNA delivered with positively charge lipids or polymers inducing pDC to express high type I IFN.(68, 84-86) Stimulation with non-aggregating CpG DNA promotes expression of cytokines through the activation of NF-κß.(16, 83) To discern the molecular mechanism regulating differential cytokine release by stimulatory ODN, several novel approaches have been attempted to display DNA in an aggregated state. Protamine, a positively-charged peptide, was used to condense negatively charged CpG-ODN into protamine-DNA complexes.(87) Stimulation of IFN-α was as much as 20-fold greater without an apparent increase of internalization. Shimada et al used the polysaccharide schizophyllan to complex natural phosphodiester backbone ODN in an attempt to prevent enzymatic degradation by nucleases.(88) They isolated lengths of schizophyllan which could potentially complex 2, 11, or 200 CpG ODN; the nature of the complexes formed was not determined but did increase inflammatory response.

The effect of length on nucleic acid internalization to endosomal compartments and recognition well is defined. Roberts et al showed bacterial DNA is highly stimulatory to macrophages than shorter PD-ODN.(89) The importance of TLR9 receptor colocalization is suggested by oligonucleotide length influencing endocytosis

and activation of TLR9. In studies in which DNA concentration was normalized for the total number of bases, a minimal length of 22 bp was necessary to induce NO production and a 14 bp ODN showed no stimulatory activity. NO production increased upon exposure to a 44 bp ODN and was maximized upon exposure to a 250bp ODN. To distinguish the role of ODN length and CpG motif density, a 40 bp ODN containing two CG motifs demonstrated enhanced activity greater than any one motif alone at low concentrations. This was true where multivalent interactions would predominate at lower, but not higher, concentrations where monovalent interactions would be more prevalent. This and the preference for greater numbers of CpG motifs, suggests enhancements in recognition and or signaling through receptor clustering effects.

The use of either phospodiester (PD) backbone or phosphorothioate (PS) backbone ODN has significant effects on TLR9 binding and activation.(83, 90) Even before unmethylated CpG dinucleotides were identified as the TLR9 ligand, bacterial DNA was known as a potent stimulator of immune response. Vertebrate DNA contains fewer CpG motifs than bacterial DNA and are often methylated.(16) To improve the nuclease resistance of ODN, PS backbone linkages are employed. The chemically altered backbone confers resistance against nucleases that are ubiquitously present in the cellular environment and would enzymatically degrade free DNA. While determining the mechanism of B cell proliferation and Ig secretion by the combined stimulation of CpG ODN and antigen, Wang et al found all types of DNA were capable of this synergistic effect, including phosphodiester based and non-CpG DNA.(91) A series of experiments determined the CpG motif requirement was only

for PS-DNA and was not true for natural PD-DNA, when complexed with DOTAP.(92) Forcing the endosomal translocation of non-CpG PD DNA by DOTAP, a cationic lipid transfection reagent, induced TLR9 stimulation. However, CpG motifs are required for stimulation of dendritic cells by immune complexes.(93) Biacore analysis demonstrated TLR9 binds CpG PD-DNA three times greater than non-CpG PD-DNA. This work was furthered by Haas et al., reporting the major determinant of TLR9 binding is the 2' deoxyribose backbone. The addition of random bases to the backbone increased the activation of TLR9, even without CpG motifs.(94) PS backbone without bases or random bases not containing CpG motifs acts as an antagonist to TLR9 activation. This has implications for the development of TLR9 inhibitors.

Specifying the type and sequence of DNA used to activate TLR9 is essential. PS ODN's that are used in most studies termed A- and B-type, although other types exist which vary in aggregation potential.(83, 95) As shown in Table 1, both types have regions of PS linkage (upper case) while only A-type has some PD linked (lower case) bases.(95) The region directly surrounding the CpG motif impacts TLR9 activation. This "species-specific" DNA sequence requirement for the murine TLR9 has been described as PuPuCGPyPy where Pu=purine and Py=pyrimidine.(83, 96) The same group also determined the minimal activation motif for human TLR9 as being TCGXX where X can be any nucleotide. The source of sequence requirements is not clear, particularly with recent evidence that TLR9 recognizes DNA by the PD backbone and that sequence may play only a small role. It is perhaps a requirement of some accessory molecule or a receptor for endocytosis that imposes this requirement.

Table 1.1 Prototypical members of some TLR9-associated ODN classes

Name	Type	Sequence
D19	CpG-A	5'- GGtgcatcgatgcagGGGGG-3'
1018 ISS	CpG-B	5'- TCGTCGAACGTTCGAGATGAT-3'
C274	CpG-C	5'- TCGTCGAACGTTCGAGATGAT-3'
2088	INH-ODN	5'-TCC[1] TGG[2] CGGGG[3] AGT-3'

Upper case = phosphorothioate and lower case = phosphodiester

Superscripts refer to specific areas of INH-ODN explained in text in text

TLR9 antagonistic ODN have defined characteristics similar to the agonistic described above. TLR9 inhibitors were initially discovered by modifying agonist sequences. PS-ODN with poly(G) sequences could inhibit bacterial DNA-induced cytokine expression.(97) Further ODN sequence modifications showed specific regions with the ODN to be critical for stimulation or inhibition. Table 1 shows the sequence for inhibitory ODN (INH-ODN) 2088 with three regions labeled by superscripts 1, 2, and 3 and the corresponding nucleotides underlined.(97) The optimal region 1 sequence for inhibition is CCT and TCC for stimulation.(97, 98) Region 2 would be the placement of the CpG motif in a stimulatory ODN. Flipping of the CpG motif to GpC results in a non-stimulatory ODN while an exchange to GpG results in an inhibitory motif. The last region is pyrimidines in a stimulatory sequence; an exchange to three consecutive guanines promotes inhibition.(97, 98)

The aggregation potential CpG PS-DNA prompted the discovery that aggregation effects TLR9 activation. It was first noted that CpG-A was retained for longer periods in the early endosome in pDC's.(99) This long retention is not normally present in cDC's and CpG-A is rapidly transferred to LAMP-1 positive late endosomal compartments in these cells. Complexing CpG-A with the cationic lipid DOTAP localized CpG-A in cDC to the early endosomes and induced strong IFN production. CpG-B, which normally localizes to LAMP-1 staining late endosomes and does not induce IFN(100), can induce IFN when directed to early endosomes by DOTAP. Kerkmann et al. showed the strand-end poly(G) motifs of CpG A form tertiary structures resistant to denaturation through G-tetrads.(85) AFM showed that these structures were either globular and ~50x10 nm or more longitudinal and ~100x3 nm. Abolishing the ability to form the tetrads through substitution of the guanosines with 7'-deazaguanosine resulted in a nonstimulatory ODN. Polystyrene beads coated with the cationic initiator AIBI were used to adsorb CpG-B and the nonstimulatory CpG-A deaza to form ~180 nm structures. Both ODN became stimulatory when delivered as nano-particles showing a 300x increase in IFN production. Differences in internalization did not account for the increase in IFN production and both colocalized to early endosomes.

Other attempts to explain how structure impacts IFN expression used structures such as PMXB nanoparticles with sizes from 100 to 500 nm and Ficoll-CpG-B conjugates with diameters of approximately 20 nm complexed with CpG C PS-ODN(96, 100) All monodisperse PS-ODN localized to LAMP-1 late endosomes. This

correlates with the maturation of pDCs and the induction of cytokines like IL-6 through the MyD88-IF5 pathway. PS-ODN that formed larger structures were preferentially located in Transferrin staining early endosomes and stimulated IFN production through the MyD88-IRF7 pathway. CpG-C has the ability to both promote maturation and IFN production. Low pH -degradable liposomes were used to release ODN in only late endosomes. ODN delivered this way only promoted maturation with no IFN-α observed. The interpretation is the localization of the ODN causes maturation or cytokine release and that particle size enforces localization. They were not able, however, to determine whether promoting TLR9 clustering by a locally high concentration of ligand on a particulate carrier influences cellular activation. Any ODN, including non-CpG ODN, when complexed with DOTAP will localize to early endosomes and promote IFN expression. Interesting avenues of inquiry include whether ODN localization is regulated simply by particle size or through particulate induced receptor interactions. The greater stimulatory effect of longer ODN sequences, and much larger plasmid DNA, would suggest receptor effects play more of a role than size.

1.1.4.2 Current TLR9 Agonist Therapies in Development

CpG ODN are being investigated for use as both adjuvants for pathogen and anti-cancer vaccines as well as immunomodulatory agents in allergic response for their biased induction of T_H1 responses in the young and old.(101) The most clinically advanced CpG ODN therapy to date is a vaccine against Hepatitis B virus (HBV)

currently in phase III trials.(4, 102) This vaccine HEPLISAV®, developed by Dynavax, demonstrates faster protection with fewer doses(4); ideal properties to have greater patient compliance and reduced cost.(103) Dynavax and Idera Pharmaceuticals are currently evaluating CpG ODN currently in phase I trials for Hepatitis C virus (HCV) vaccination.(4) Also from Idera is a TLR9 agonist for cancer vaccination.(4) All of these applications use CpG ODN agonists to induce an effective adaptive immune response.

CpG ODN are also being evaluated as immunomodulators of the allergic response. TLR agonists strongly skew immune response to T_H1 type and CpG ODN conjugates with antigen were shown to be particularly effective in a murine asthma model to reduce allergenicity.(32) This finding was extended to a ragweed antigen conjugate.(29) There are several CpG ODN-based allergy therapies currently under investigation in Phase I and preclinical studies from Idera, Sanofi Aventis/ Coley Pharmaceuticals, and Astra Zeneca.(4) A TLR9 agonist from InDex Pharmaceuticals is being evaluated to treat ulcerative colitis by balancing the local inflammatory response. As these initial therapies are approved for use, CpG ODN will increase in use with their favorable stimulatory properties and ease of manufacture, therefore it is critical to determine how innate ligands induce an inflammatory response.

1.1.5 Pathological Response of Toll-like Receptor 9

How nucleic acids are distinguished from endogenous RNA and DNA is a critical question. Recognition of pathogen-associated nucleic acids is controlled by a

number of factors including: the localization of receptors, accessory proteins used for recognition, and the specific molecular and spatial recognition of nucleic acid chemical structure.(104, 105) Despite all of the safeguards in place to distinguish endogenous from exogenous nucleic acid, there are malfunctions of the system which result in the development of autoimmune disease.(104, 106, 107) Evidence now points to improper recognition of self nucleic acids as the source of many autoimmune disorders more prevalent in our aging society.(108, 109)

1.1.5.1 Autoimmunity

The link of nucleic acid recognition and autoimmune disorders can also offer some insight into the role of secondary and tertiary structure in this process. Autoimmune diseases are often associated with antibodies to DNA, RNA, or to DNA and RNA protein complexes.(104, 107, 110) Nucleo- or ribonucleo-protein complexes offer nuclease resistance and a structurally rich presentation of nucleic acid. Autoimmune diseases such as systemic lupus erythematosus (SLE), scleroderma, and Sjogren's syndrome are characterized by the presense of antibodies against U/G rich RNA's complexed with endogenous proteins.(107, 110) Another hallmark of autoimmune disease is high levels of IFNα, of which pDC's are the predominant source, and could be the result of large nucleoprotein complexes or enforced TLR9 colocalization by dense presentation of nucleic acid.(107, 111, 112) Extensive research has linked the recognition of endogenous nucleic acid with the progression of SLE, heart disease, psoriasis, Sjogren's syndrome and rheumatoid arthritis,

establishing pathological nucleic acid recognition as an important area of study.(113-116)

1.1.5.2 Aging

The reduced response to immunization by aged adults is well documented.(117) With aging, there is an increase in the rate of bacterial and viral infection, atypical infection due to reduced immune surveillance, and the recurrence of latent viral infection.(108, 109) The reduced innate response is likely due to several factors including reductions in the numbers of key cell types(108, 118), as well as altered cellular environment(119, 120), and intracellular signaling.(121) Recently, it was shown in a murine model that aged response to herpes simplex virus 2 by plasmacytoid dendritic cells (pDC) was due to impaired TLR9-dependent IRF7 signaling.(121) The role of nucleic acid sensing in the reduced immune response of the aged is not well understood.

Aging involves changes in immune function, known as immunosenescence, that impacts both innate and adaptive immunity.(108, 109, 112, 122) The implications of altered nucleic acid sensing in aging organisms includes improper recognition of self nucleic acid in autoimmune disease(108, 112, 122), reduced effectiveness of vaccines in the elderly(108, 123), and decreased immune response to infection.(108, 122) Improved vaccine response in the elderly will require a clear understanding of the molecular activation mechanisms of TLR9 and improved adjuvants. This insight could

also yield specific inhibitors of nucleic acid activation of DC's, B cells, and neutrophils leading to better therapies for autoimmune disease.

1.1.5.3 Current TLR9 Antagonistic Therapies in Development

Given the known links between autoimmune disease and TLR9 activation, TLR9 antagonists are currently in development for conditions such as SLE, rheumatoid arthritis, multiple sclerosis, and psoriasis.(4) Idera has TLR9 antagonists in Phase I and II trials for the treatment of psoriasis and lupus. Dynavax is currently investigating the TLR9 antagonist DV1179 for treatment of SLE.(4) Although these antagonists are in development, it is not clear if TLR9 antagonism is beneficial in the treatment of lupus; some studies have suggested a protective role for TLR9. TLR7 has also been implicated in the progression of autoimmune disease and the production of RNA nucleoprotein complexes.(124, 125) TLR7, 8, and 9 can all be inhibited by common ssDNA or mixed nucleic acid sequences.(126) For these reasons, TLR9 antagonists in development for ameliorating auto immune disease are also designed as antagonists for TLR7.(4)

1.2 Molecular Scale Investigations of Oligomeric Receptor Assemblies

Biological processes occur at a multitude of scales. Tissue organization occurs at length scales of 100 μm to several centimeters while individual cells are approximately 10 to 100 μm. Protein assemblies like the ribosome are 20 – 25 nm while individual proteins are roughly 5 nm. Within these size ranges are undefined

supramolecular protein complexes critical for biological function but not observable by current microscopy or crystallographic techniques.

Increasingly, it is clear most biological processes attributed to a known protein are not exclusive to the local environment. Membrane bound protein function and activity is often modified by the lipid content of the anchoring membrane.(127-129) Extra- or intracellular soluble proteins are often controlled by association with other proteins for allosteric control, recruitment of functional partners, or supramolecular scaffolds, which add an extra layer of control to biological function.(79, 130-132) In vitro assays of purified components are indispensible for determining biological activity of biomolecules, but by nature are simplified constructions lacking the complexity and possible additional players of cellular or in vivo conditions. This is even further complicated by membrane proteins, which must be extracted, often into artificial membranes lacking the sophistication of the cellular environment.(133, 134)

Microscopy is constantly evolving to bridge the gap between the nanometer resolution of electron microscopy and the inherent resolution limits of light microscopy. Advances in imaging probes and analysis techniques yield higher resolution light microscopy(135-137) while more robust methods and computer aided image analysis have allowed increased versatility in samples suitable for electron microscopy.(138, 139) Super-resolution methods (SRM) have been used the study receptor dynamics in systems as diverse as epidermal growth factor receptor clustering(140), chemotaxis networks in *E. coli*(141) and a cardiac signaling protein.(142)

Spatial orientation of macromolecules can be determined through electron microscopy or even x-ray crystallographic structures, but not within the context of the dynamic cellular environment. Well characterized and structurally complex probes can be developed which not only report microscopy-based location, but also how spatial presentation and orientation impact biological function. Tagged with an imaging agent, they show cellular localization, but also engage receptors through defined presentations of a biological ligand, providing specificities of how receptor clustering or orientation alters function.

The study and manipulation of innate immune signaling by controlled presentation of PRR ligands is of great general importance given evidence suggesting the role of supramolecular organization in the identification of PAMPs by a variety of TLRs. TLR2, TLR4 and TLR9 have all shown association with lipid microdomains known to be important in receptor organization and recruitment of signaling proteins.(38, 75) Recent SRM studies have shown the stimulatory potential of LPS is correlated to TLR4 receptor density;(143) these results highlight a direct link between receptor clustering and cellular response in the TLR family of receptors. It is also been demonstrated that ligand length or physical size influences cytokine profiles in TLR3, TLR2, and TLR9 signaling.(89, 138, 144) Although both electron microscopy and super-resolution microscopy allow study of events on macromolecular scales representing oligomeric assemblies (with significant limitations), several factors make synthetic multivalent probes particularly well suited for this work. These probes can be well characterized, synthesized to control ligand number, and can function within a cellular context to report receptor recognition and cellular activation.

1.2.2 Multivalent Probes

Multivalent presentations of biological ligands are often more accurate representations of how ligands are encountered. Signaling from larger oligomeric assemblies of proteins, either in the context of a membrane or free in the cytosol, allow differentiation of errant biding events from proper recognition of valid targets. An example is the engagement of the B cell receptor where cellular activation by single binding events would likely lead to premature activation and improper inflammatory response. Engagement of many receptors helps ensure the B cell receptor antigen is present in high amounts and indicative of an infection to which the ensuing inflammatory response would be appropriate.(145, 146)

Multivalent probes can be developed around known biomacromolecular structures such as viral capsids(147), DNA origami (148), or antibody-based structures.(149) They can also be developed around well-characterized polymers, allowing control over the specific chemical properties of the polymer and increased flexibility over the introduction of multiple binding ligands to study multivalent interactions. Examples of both approaches and the types of systems studies previously are given below.

1.2.2.1 Biomacromolecular-based probes of biological function

Biomacromolecular probes use the known supramolecular structures formed by nucleic acids, lipids, and proteins. These types of structures have the advantage of

monodisperse, template-driven subunits that self-assemble into supramolecular structures. Structures of this type are formed from synthesized single stranded DNA, proteins that oligomerize, or are antibody-based.

Single stranded DNA scaffolds use Watson-Crick base pairing to associate dimers into larger structures.(150) Common topologies are sheets, tetrahedra, cubic, or tubes.(148, 151-153) They were employed in the analysis of distance-dependent binding of aptamers to thrombin(148), which was subsequently used to design a highly selective inhibitor of thrombin.(154) DNA origami is also the primary vehicle used to deliver TLR9 CpG sequences with many shapes and sizes investigated; Y-shaped(155), tetrahedral(152), and dendritic or star shapes have been used to improve delivery but this function is independent of spatial display.(156, 157)

Proteins with defined oligomers or valencies have also been used as scaffolds to present ligands multivalently. Streptavidin, normally present as a tetramer and capable of strong association with biotinylated molecules, has been used to study T cell receptor dynamics(158) and how receptor clustering improved clathrin-coated pit maturation and lifetime.(159)

Antibodies, which have five classes with defined binding valency, are particularly well suited to investigate the role of valency in biological function. Anti-GalTase IgG (two binding sites) was used to cluster the GalTase receptor on sperm surface to induce the acrosome formation.(160) GalTase binds O-linked oligosaccharides on the egg surface; the antibody mimicked the condition, demonstrating the role of multivalency in acrosome activation. Anti-FLAG tag IgM (10 valent) in conjunction with a FLAG tagged soluble Fas ligand (sFasL) was able to

induce Fas signaling and apoptosis without the addition of ceramide to form lipid microdomains.(161) Antibody mimetics have also been engineered to modify cellular responses. Anti-CD3 IgG, although effective at targeting T cells, induces their activation through the Fc domain of the antibody. A novel system using a dihydrofolate reductase (DHFR) dimer-anti-CD3 fusion protein with a methotrexate dimer could oligomerize through DHFR binding of the folate mimic.(162) Oligomers with valencies similar to IgM, but lacking the Fc portion of the antibody could effectively deliver cargo to T cells using multivalent affinity, without inducing activation.

All of the systems described above benefit from the oligomerization properties of biomacromolecules and the defined presentations of biological ligands they can form. There are drawbacks to these systems, which include difficulty in modifying valency, difficulty or inability to include multiple ligands, inability to alter ligand density, and often fixed dimensions. Synthetic polymers overcome many of these limitations and their use is described below.

1.2.2.2 Polymer-based probes of biological function

Synthetic polymers offer the ability to easily tailor the physical properties of the scaffold, attachment chemistry, be synthesized in a wide rage of molecular weights and topologies and can allow alteration of ligand valency, density, or both. Many examples exist throughout the literature demonstrating the utility of synthetic polymer scaffolds to examine or control biological processes. Work in the laboratory of

Howard Dintzis used polyacrylamide conjugated to the hapten dintrophenol to examine the requirements of T cell-independent B cell receptor engagement for activation or tolerance.(163-165) Approximately 20 haptens, conjugated to a polymer of a molecular weight (MW) sufficient for activation, were required for B cell activation. A polymer below the activation MW was either an inhibitor or, at increasing hapten density, a toleragen. A polymeric scaffold above the activation MW and valence was an activator regardless of the values. These findings were shown to be applicable to other polymeric carriers and haptens.(166)

There are additional examples of polymeric scaffolds used to probe biological function. In examining the role of ADAM2 and -3 proteins in sperm and egg binding, ROMP polymerized monomers of the tripeptide ECD or QCD were used to study the role of each respective protein.(167) Both polymers inhibited the binding of sperm and egg, and were dependent on $ß_1$ integrin for function. Similarly, in the lab of Kenneth Jacobson, multivalent dendrimer conjugates of polyamidoamine (PAMAM) and G-protein coupled receptor (GPCR) adenosine agonists exploit the known homo- or heterodimerization, and even higher-order aggregation of GPCRs.(168) For instance, PAMAM conjugates of an adenosine agonist were shown to protect cardiomyocytes against H_2O_2 damage at 100-fold lower concentrations than the monomeric ligand.(169)

Lastly, there are many examples of ROMP-polymerized polymeric scaffolds used to examine the role of multivalency in several systems. Multivalent presentations of glucose were shown to stimulate bacterial chemotaxis in a valency dependent manner.(170) Dinitrophenol-bearing polymers likewise showed a valency dependent

increase in activity with the higher valency constructs inducing greater antibody production, calcium flux, and B cell receptor clustering in an in vitro B cell model.(171) These examples use multivalency to explore biological systems relying upon the binding of saccharides. Protein-saccharide or oligosaccharide interactions are weak and require either high concentrations or the high local concentrations provided by multivalent presentations to induce recognition or signal transduction.(172) The body of literature exploiting multivalent presentation of saccharides is large; a recent review from this group should be referenced for readers interested in this area.(173)

Nucleic Acids have been covalently attached to surfaces and other molecules for a large number of purposes including hybridization microarrays, new nucleic acid sequencing technologies, probes of protein activities and specificities and novel nano-construction purposes.(174-178) As mentioned before, covalent modification of antigen by ODN has been used to enhance presentation of the antigen by MHC II and the T_H1 response for overall better vaccine efficacy.(27, 28, 33) In fact, some of the work that supports the hypothesis of multivalent presentation of DNA affecting cytokine release profiles involves the covalent attachment of stimulatory DNA to the polysaccharide ficoll(96) or microparticle embedment or attachment.(86, 100) The systematic design of a series of DNA-polymer conjugates, not previously accomplished, is presented in this work. It is clearly shown how nucleic acid-polymer conjugation not only alters their physical and biological properties, but most importantly, allows control over cellular responses originating from recognition of CpG oligonucleotides.

Chapter 2

DNA-POLYMER CONJUGATES FOR IMMUNE STIMULATION THROUGH TOLL-LIKE RECEPTOR 9 MEDIATED PATHWAYS

2.1 Introduction

Early detection of pathogens in humans and other jawed vertebrates relies largely on identification of non endogenous chemical structure by four protein families called the pattern recognition receptors (PRRs).(8, 106, 179) Unlike the adaptive immune systems' T cell (TCR) and B cell receptors (BCR), the germ line-encoded PRRs allow broad, quick, and nonspecific recognition of most pathogens that is a hallmark of the innate immune system. Innate pathogen recognition is necessary for a competent adaptive immune system function, and is critical for the response to most pathogens and vaccine efficacy, but has also been implicated in the development of autoimmune disorders.(3, 113, 116) The Toll-like receptor (TLR) family, characterized by the presence of leucine-rich repeat (LRR) sequences, are the most well studied of the PRRs.(106) Toll-like receptor 9, which is expressed in humans in the intracellular compartments of B-cells, plasmacytoid dendritic cells (pDC), and neutrophils, (15) is responsible for the recognition of unmethylated CpG dinucleotides predominant in the DNA of viruses and bacteria.(16, 17)

Pathogens often contain multiple pathogen associated molecular patterns (PAMPs) that are recognized by the PRRs, and PAMPs have thus been of considerable interest in understanding the mechanisms of immunity, as well as in the more practical considerations of vaccine design.(8, 77, 103) Oligodeoxynucleotides (ODN) containing unmethylated CpG dinucleotides have been investigated as adjuvants for vaccines for their ability to activate the innate immune system through Toll-like receptor 9 (TLR9).(180) Four classes of ODN (A, B, C, and P) all contain unmethylated CG dinucleotides, but have different flanking nucleic acid sequences that mediate differences in their propensity to form structures through Watson-Crick base pairing,(83) have been identified. The differences in structure and aggregation of the ODNs alter not only the subset of immune cells activated by the ODNs, but also the profile of elicited cytokines.(83) These differences in activation have also been linked to expression of cellular receptors, accessory proteins, and the site of TLR9 localization; however, no definitive answer explains how DNA structure potentiates this differential response.(42, 44, 83, 181) Elucidating the relationship between DNA presentation and the biological response to these different classes of ODN could lead to improved adjuvants as well as the ability to control immune response.

The response of TLR 9 to CpG-containing ODN is influenced by the number of CpG motifs, the backbone linkage used (phosphate or phosphorothioate), and the tendency of the sequence to form secondary (intramolecular) or aggregated (intermolecular) structures. Studies directed at explaining the structural sources of this differential response have included the conjugation of CpG ODN motifs with

polystyrene(85, 182) or into protamine nanoparticles(87). Other delivery vehicles for CpG ODN include positively charged lipids such as DOTAP(100), the polysaccharide schizophyllan(88), gold nanoparticles(183), carbon nanotubes(184) and a number of Watson-crick base-paired structures.(152, 153, 157, 185, 186) A recent report using silicon nanoparticles demonstrates that 3' ODN conjugation promotes type I cytokines while electrostatic association promotes IFN-α secretion, providing significant insight into the role of ODN presentation on observed immunological response.(86) All of these systems permit manipulation of the spatial display of ODN, and have shown some enhancements in cytokine expression through enhanced delivery or protection from nucleases, but fail to inform how changes in DNA valency can alter activation of TLR9 by CpG ODN.

Polymeric conjugates offer an attractive alternative to such investigations. While ODN-based polymer conjugates have not previously been explored, polymeric conjugates have been used previously to study immune system processes such as B-cell signaling through the defined presentation of dinitrophenol groups(171), lectin binding by mannose-functionalized poly(HEMA)(187), and complement activation through BSA- and mannose-functionalized (poly methacrylate).(188) Nucleic acids have been covalently attached to polymers for diagnostic and micro-array applications(177, 178) as well as to improve the stability and delivery of siRNA.(189-192) To study the role of CpG ODN valency and size in TLR9 activation, synthetic polymer scaffolds afford interesting tools where both valency of the ligand and size of the complex can be controlled. Here, we report the synthesis of novel, soluble ODN-

poly(acrylic acid) (PAA) conjugates of controlled valency to study the activation of TLR9 in murine macrophages. Biotinylated conjugates were also produced to allow for detection by flow cytometry and confocal and transmission electron microscopy. Polymers and conjugates were analyzed by UV-VIS spectroscopy, NMR, GPC, and DLS to characterize their chemical identity and size. Flow cytometry and confocal and transmission electron (TEM) microscopy were used to analyze polymer uptake and cellular localization. The cytokine responses (TNF-alpha and IL-6) of the RAW264.7 murine macrophage-like cell line were examined by ELISA. We also demonstrate, through siRNA gene silencing, that the immune-stimulating properties of these novel CpG ODN-polymer conjugates are mediated by TLR9. Data indicate the high activity of these conjugates for TLR9 activation, with variations in cellular responses that correlate with macromolecular structure.

2.2 Experimental

2.2.1 Materials

Poly(acrylic acid) of 118 kDa M_w and a PDI of 1.13 was purchased from Polymer Source (Dorval, Quebec) and purified precipitation in 0.1 M HCl, dissolution in H_2O , filtration through a 0.22μm PES membrane, lyophilization, and then precipitation in ether from an acetone/isopropanol 50/50 solution. Gamma-irradiated 10K MWCO dialysis cassettes were purchased from Pierce Biotechnology (Rockford, IL) and washed with sterile filtered 30% ethanol and then hydrated with molecular

grade water from Mediatech (Manassas, VA) before use. Centrifugal filtration units with a 30K MWCO were purchased from Millipore (Bilerica, MA) and washed with sterile filtered 30% ethanol before use. All other reagents were used without further purification or treatment. N-(2-aminoethyl)maleimide trifluoroacetate salt (NEAM) (>95%), N-(3-dimethylaminopropyl)-N'-ethylcarbodiimide hydrochloride (EDC) (>99%), 1-hydroxybenzotriazole hydrate (HOBT) (97%), triethylamine (TEA) (≥99%), Dimethyl sulfoxide (≥99%), 4-mercaptophenol (97%), molecular grade sodium chloride, and anhydrous sodium phosphate were purchased from Sigma Aldrich (St. Louis, MO). 2-(N-morpholino)ethanesulfonic acid sodium salt (MES) (>99%) was purchased from Fisher Scientific (Pittsburgh, PA). O-(Benzotriazol-1-yl)-N,N,N',N'-tetramethyluronium hexafluoro phosphate (≥99%) (HBTU) was purchased from Chem-Impex (Wood Dale, IL). Biotin hydrazide was purchased from Proteochem (Denver, CO). Oligodeoxyribonucleotide (ODN) 1668AT CG (5'-TCCATGA**CG**TTCCTGATGCTAT) and the negative control sequence ODN 1668AT GC (5'-TCCATGA**GC**TTCCTGATGCTAT), both thiolated at the 3' end, and control sequences without the 3' C_6 thiol linker, were purchased from Integrated DNA Technologies (Coralville, IA). Sequences deviate from the published ODN 1668 sequence by the addition of an AT dinucleotide on the 3' end as a small spacer between the 1668 sequence and the C_6 thiol linker. DMEM, β-mercaptoethanol, antibiotic/antimycotic (100X), sodium pyruvate (100X), ethidium homodimer, and HEPES were purchased from Invitrogen (Grand Island, NY). Fetal bovine serum was purchased from Denville Scientific (South Plainfield, NJ) and heat inactivated.

2.2.2 ^{1}H NMR spectroscopy

All spectra were collected on a Bruker AV-400 spectrometer with a cryogenic QNP probe. NMR was performed at room temperature on samples dissolved in deuterium oxide (D_2O) or deuterated dimethylsulfoxide (DMSO-d6), purchased from Cambridge Isotopes. For all polymer samples, 128 or 256 scans were used, with a D1 of 10 seconds and a 90° pulse program.

2.2.3 Synthesis of biotin-functionalized poly(acrylic acid)

PAA was dissolved at 20mg ml^{-1} in DMSO. To this solution, with constant stirring, both biotin hydrazide and HBTU, dissolved at 10mg ml^{-1}, were added to the PAA solution to yield a final molar ratio of 1:4 (biotin: HBTU). Triethylamine was added at a 10:1 molar ratio over biotin. Biotin to PAA molar ratios was 35:1 for conjugates described. After 24 hours, the reaction mixture was dialyzed twice, in a 10K MWCO dialysis cassette, against H_2O. The solution was then dialyzed twice against a 500mM NaCl solution and then a final time (twice) against H_2O. All dialysates were prepared with 18MΩ H_2O and filtered through a 0.22μm membrane and were employed at a 1:1000 volume ratio. ^{1}H NMR (D_2O): δ= 4.48 (bm, (C3)-C**H**, biotin) δ= 4.31 (bm, (C3)-C**H**, biotin), δ=3.23 (bm, C-C**H**-S, biotin), δ=2.86 (d, N**H**, biotin), δ=2.64 (d, N**H**, biotin), δ=2.29 (b, C-C**H2**-C, biotin), δ=2.09 (bp, C-C**H**-C, PAA), δ=1.46-1.62 (bp, C-C**H2**-C, PAA).

2.2.4 Synthesis of maleimide-functionalized poly(acrylic acid)

All glassware, plastic, and reagents were treated to maintain sterility to limit product contamination by LPS. All reagents were dissolved in a 75mM MES solution buffered at pH 6.05 and filter sterilized. Poly(acrylic acid), EDC, HOBT, and NEAM were all dissolved at a concentration of 10 mg ml^{-1}, and the EDC, HOBT, and NEAM were added immediately at a ratio of 1:3:4 respectively. EDC was used (6% for **118K-10** and **118K-3** and 3% for **118K-1**) of the total acid groups on the polymer respectively. The reaction was conducted under nitrogen, and purified/transferred via dialysis to the DNA reaction buffer (50 mM sodium phosphate, 11 mM citrate, 5 mM EDTA at pH 6.6 (degassed)). 4-mercaptophenol (4-MP) was reacted with maleimide groups to provide a probe for NMR analysis of the extent of maleimide functionalization of the polymers. Dialyzed polymer was lyophilized and then dissolved in D_2O for analysis via ^1H NMR spectroscopy. The extent of functionalization of the polymer with maleimide was determined by comparing the ratio of the three polymer backbone peaks δ=2.09 (bp, C-C**H**-C, PAA), δ=1.46-1.62 (bp, C-C**H2**-C, PAA) to the 4 protons of the 4-MP phenyl ring δ=6.76 (d, Ph-**H(2)**, 4-MP), δ=7.29 (d, Ph-**H(2)**, 4-MP) . ^1H NMR (D_2O): δ= ^1H NMR (D_2O): δ=6.76 (d, Ph-**H(2)**, 4-MP), δ=7.29 (d, Ph-**H(2)**, 4-MP), δ=2.09 (bp, C-C**H**-C, PAA), δ=1.46-1.62 (bp, C-C**H2**-C, PAA).

2.2.5 Synthesis of ODN-functionalized poly(acrylic acid)

All apparatus and materials were treated as stated above. Oligodeoxynucleotides and DTT were dissolved in 125 mM phosphate buffer at pH 7.5 to yield an excess of DTT to ODN at a ratio of 10:1; the ODN and DTT were incubated for one hour. This ODN was then filtered, under gravity, via size exclusion chromatography using sterilized G 15 resin equilibrated in a 50mM phosphate, 13mM citrate, and 5mM EDTA ~pH 7.05 buffer, at a resin volume 10 times greater than that of the ODN solution. The eluate was fractionated and fractions tested for the presence of DNA by UV absorbance. DNA-positive fractions were combined with maleimide-functionalized polymer from centrifugal filter exchange in 50mM phosphate, 13mM citrate, 5mM EDTA ~pH 6.9 buffer. This reaction mixture of the ODN and maleimide-functional polymer components was placed in a ported bell jar, vacuum purged 3 times with nitrogen with constant stirring, and incubated under nitrogen for 5 days. The polymer control samples (PAA) were prepared from a fraction of the total synthesis, which was diluted 2-fold into 200mM pH 8 phosphate buffer and incubated for 24 hours to remove any residual maleimide via formation of the 3-hydroxyl succinimide or ring-opened derivatives of the maleimide-functionalized polymer. This control polymer, **118K**, was purified and prepared as above, without addition of ODN.

2.2.6 UV characterization of ODN-poly(acrylic acid) conjugates

All solutions were made from molecular grade water from Mediatech (Manassas, VA) and filter-sterilized before use. Reaction mixtures (from above) were diluted with 50 mM phosphate pH 8 buffer. This solution was filter-sterilized and passed through a centrifugal filter. After filtration, the volume was brought back to 4 ml with molecular grade water and again passed through a centrifugal filter. This process was repeated until absorbance at 260 nm was stable and then the concentrated fraction was removed from the centrifugal filter unit, the unit washed with molecular grade water, and the volume brought to 2 to 4ml depending upon the concentration of DNA (to remain in linear absorbance region. The 260nm absorbance values allow determination of DNA concentration by the calculated extinction coefficient ($201{,}800 cm^{-1}mol^{-1}$ and $200{,}400 cm^{-1}mol^{-1}$ for the CG and GC sequences respectively (193, 194)); the DNA functionality of the polymer was determined by comparison of the DNA concentration (determined by UV-Vis) to the polymer concentration (determined gravimetrically). The DNA concentration in the low-MW fractions was also monitored; the amount of DNA in all fractions was calculated and corresponded to the total ODN employed during the reaction. The solution was concentrated one last time and brought to a volume sufficient to yield a stock solution of 100μM DNA. UV-Vis absorption spectra were measured on an Agilent 8452 spectrophotometer or a Thermo Nanodrop 2000.

2.2.7 NMR characterization of ODN-poly (acrylic acid) conjugates

Conjugate **118K-1.5** was purified in the same manner as above and then exchanged in D_2O using three, 1:80 sample dilutions. The sample was concentrated to a volume of 600μL and characterized via ^1H NMR spectroscopy (Figure 2.1). The ODN 1668 CG has 22 base pairs with 32 nucleobase protons and 22 anomeric protons from the ribose. Since the ribose anomeric proton overlaps with peaks from the maleimide groups, the nucleobase protons were used for quantitation relative to the PAA backbone protons.

2.2.7.1 Calculation of ODN functionality by NMR

The following number of protons are found on each 1668 AT oligonucleotide:

Ring Protons
T – 8 = 8
C – 6 = 12
G – 4 = 4
A – 4 = 8
32 Total

Anomeric Protons
22 Bases = 22 Protons

Non Anomeric Deoxyribose Protons
22 Bases = 88 Protons

Using the nucleobase region, which does not overlap the maleimide region with a total of 32 protons per ODN as calculated above.

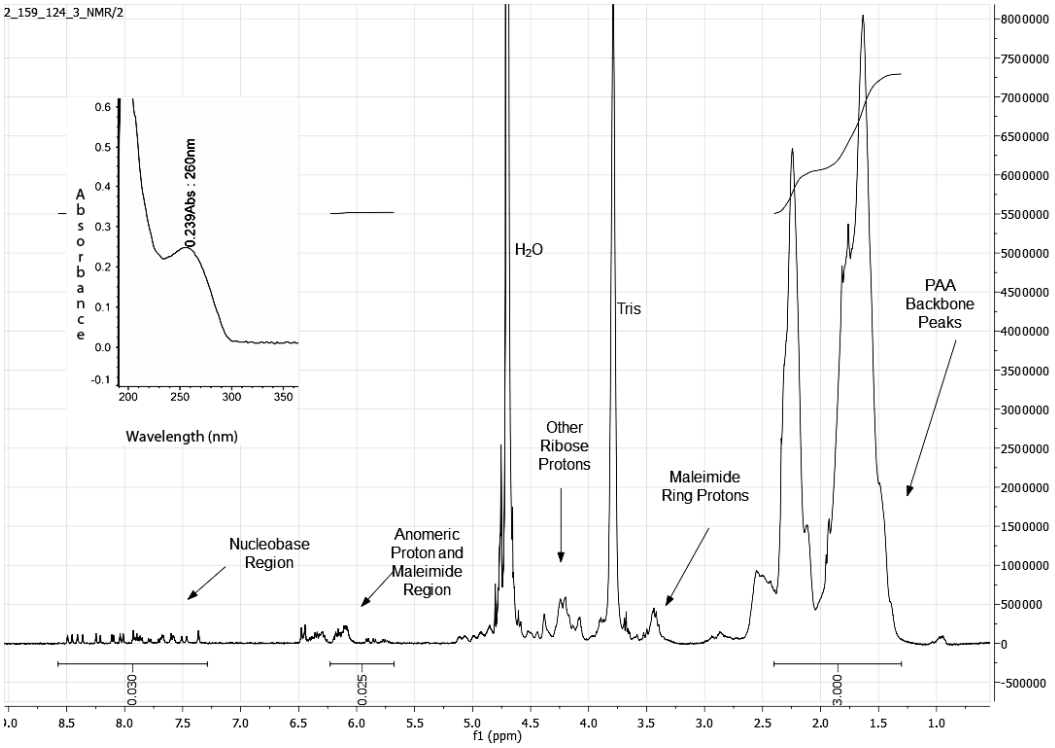

Figure 2.1 NMR spectra of conjugate 118K-1.5. ODN functionality was calculated from the areas of the nucleobase and PAA backbone regions. The inset shows the UV trace of the same conjugate at 11.8µM showing the characteristic 260 nm absorbance of the oligo is not masked by the low wavelength absorbance of the polymer.

The area calculated for nucleobase protons on the NMR spectra scaled to the three backbone protons of one monomer is:

(0.03 nucleobase protons/monomer)*(1722 monomers/polymer) =

51.6 nucleobase protons/polymer

To calculate the number of ODN per polymer:

(51.6 nucleobase protons/ polymer)/(32 nucleobase protons/ODN) = 1.6 ODN/polymer

2.2.8 Gel permeation chromatography

Spectra were obtained on a Waters GPC (Milford, MA) system with a 2414 refractive index detector. Phosphate-buffered saline (PBS) at pH 7.0, filtered through a 0.22μm PES filter, was used as the mobile phase and the flow rate was maintained at 1 ml/min. Stock solutions of the polymers or conjugates were dissolved in PBS pH 7.0. Conjugates were heated to 95°C for 5 minutes to eliminate any annealing of DNA and were then flash cooled before dilution and analysis.

2.2.9 Dynamic light scattering

Data were obtained on a Malvern Nanoseries Zetasizer (Worcestershire, UK) and from samples in a 3mm pathlength quartz cuvette. Control samples were diluted into filtered PBS (0.22 μm PES membrane, pH 7.0) at a gravimetrically determined concentration of 0.5μM. Samples were maintained at 20°C and equilibrated at least 5 minutes before measurement. The reported size in nm was calculated as the Z-average from the fit to the correlation function using the cumulant method with the software provided by the manufacturer. Average values from three separate samples of a given polymer are reported in Figure 2.2.

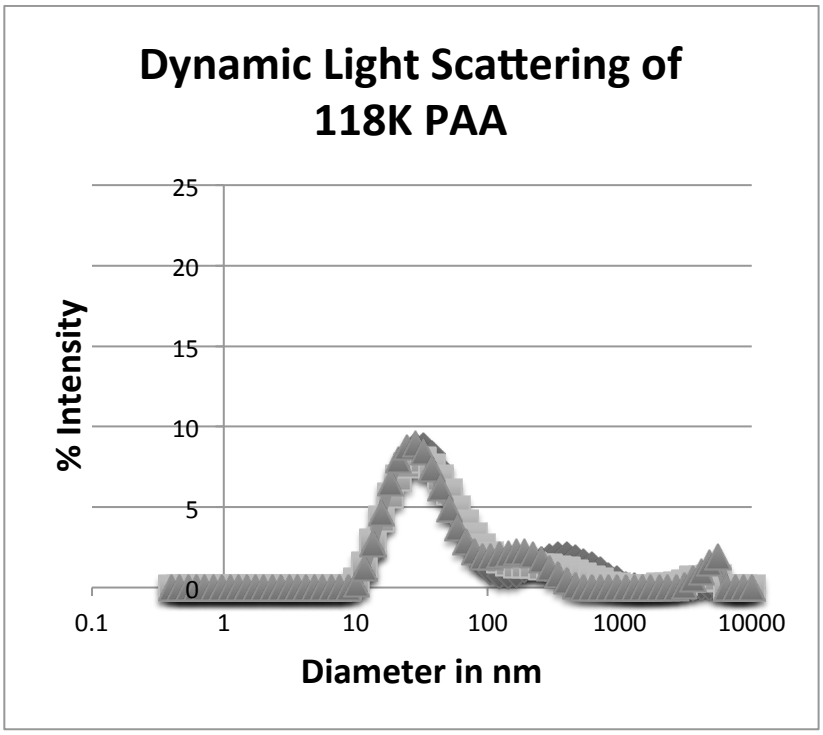

Figure 2.2 Dynamic light scattering of three separate samples of 118K PAA plotted as % intensity vs. diameter in nm. The three samples are in close agreement with Z-average diameters calculated as 35 nm (grey diamonds), 36 nm (light grey squares), and 35 nm (grey triangles). Percent intensity favors larger particles and demonstrates the low abundance of any larger species.

2.2.10 Cell titer blue assay

RAW264.7 cells were plated the night before the assay, in a 96-well tissue culture polystyrene plate, at 75000 cells per well. Cells were washed once with PBS and the solutions of the polymer samples were applied (at various concentrations, at a total volume of 200 μL). Samples included conjugates **118K-1**, **118K -3**, and **118K-10** as well as control wells containing the conjugate at the tested concentration but no

cells. Untreated cells were plated as above and tested in the same manner without the addition of any conjugate. At 8 hours the cell titer blue reagent (Promega Madison, WI)) was added to all wells for testing and incubated for 2 hours at 37° C. The supernatant was removed from the wells and placed in a 96–well plate. Samples were characterized at a fluorescence emission wavelength of 600nm using a Perkin Elmer VICTOR^{3}V multilabel counter (Perkin Elmer; Waltham, MA).

2.2.11 Cell culture

RAW264.7 cells were cultured on tissue culture polystyrene plates (Cell Treat; Shirley, MA) in DMEM supplemented with 10 mM HEPES, 55μM β-mercaptoethanol, antibiotic/antimycotic, and sodium pyruvate (Invitrogen), and 10% fetal bovine serum in an environment containing 5% CO2. Cells were used up to passage 8 and maintained at between 20 and 90% confluence. Cells were washed with calcium- and magnesium-free PBS and scraped for passage.

2.2.12 Bone Marrow Derived Macrophages (BMDM)

BMDM were prepared as previously described(195) and isolated from femurs of BALB/C mice and cultured in RPMI 1640 medium, supplemented with 10% heat-inactivated FCS, 2 mM GlutaMax-1, 100 U/ml penicillin, and 100 μg/ml streptomycin in the presence of murine GM-CSF (5 ng/ml). At day 4, nonadherent cells were

collected and cultured for a further 3 d in GM-CSF (5 ng/ml). On day 7, adherent cells were harvested and plated in cell culture 96-well plates at 200,000 cells/ml (50,000 cells/well).

2.2.13 Flow cytometry

For Figure 2.8 all samples were treated as follows. RAW264.7 cells were lifted, counted, and divided into 15 ml conical tubes at 750,000 cells/ml per tube in 500 µL of HBSS containing 4µM ethidium homodimer, and then incubated for 10 min at 37° C. Cells were centrifuged (180 x *g*), resuspended, and then incubated at 4° or 37° for 15 min in media. Cells were again centrifuged in 300µL HBSS (at either 4° or 37° C) containing either conjugate **118K Biotin-10** or **118K Biotin-1**, at a normalized ODN concentration of 100nM. Cells were incubated at either 4° or 37° C for 25 min, centrifuged, washed once with HBSS, and centrifuged and resuspended in PBS with 4% formaldehyde at 4 or 37° C respectively. Cells were fixed for 15 min. and the previous wash procedure was followed. The 37° C and 4° C samples were then permeablized with 0.25% Triton X-100 for 15 minutes and washed twice at room temperature, via the previous protocol. The samples were then centrifuged and resuspended in PBS with 10% FBS and blocked by treatment with 6% BSA for 1 hour. The samples were again centrifuged and resuspended in 200µL of PBS containing 10nM Qdot 525 streptavidin conjugate (Invitrogen Grand Island, NY) / 6% BSA and incubated for 1 hour. Cells were washed with PBS, resuspended and centrifuged 3 times, and finally suspended in 500µL PBS and placed in Falcon flow

cytometry tubes (BD biosciences; San Jose, CA) on ice. For Figure S7, the two samples are normalized to scaffold concentration of 16.6 nM and the 37° C samples were split in half to yield two samples, one of which was permeabilized, the other which was not. No permeablization does not allow entrance of the quantum dot into the cell and only allows surface labeling. The non-permeabilized samples were resuspended in 0.5ml PBS and stored on ice. Positive control samples for dead cells comprised cells that were separately treated with 0.1% Triton X-100 for 15 minutes, washed, and then treated with 4μM ethidium homodimer. Cells treated with 500nM conjugate **118K-10 Biotin** at 37° C were used as a positive control. Both positive controls (Triton-X treated cells for ethidium homodimer and 500nM conjugate **118K Biotin-10** for the Qdot 525 streptavidin conjugate) were used for calculation of the compensation coefficient using the manufacturers software. Cell analysis was conducted on a BD LSR II cell analyzer (BDbiosciences; San Jose, CA) with gates set by untreated cells; a total of 10,000 events were recorded. Flow analysis was conducted using FlowJo software (Tree Star; Ashland, OR) with cells positive for ethidium homodimer (dead) not included in analysis.

2.2.14 Confocal microscopy

RAW264.7 cells were seeded at 150,000 cells per chamber in Nunc 8-chamber microscopy slides (Nunc ; Rochester, NY). Cells were washed once with PBS prior to use and then treated with 200μL of a 2 μM solution of FM 4–64 FX (Invitrogen; Grand Island, NY) in HBSS for 4 min at 37°C. Cells were washed once with PBS

prior to use and then treated with 200µL of a 2 µM solution of FM 4–64 FX (Invitrogen; Grand Island, NY) in HBSS for 4 min at 37°C. Cells were then aspirated and treated with 200 µL of either polymer **118K Biotin** or conjugate **118K Biotin-10** for 12 min at 37°C for active endocytosis in the presence of the plasma membrane localizing FM4-64. Cells were aspirated and immediately fixed with 4% formaldehyde in PBS for 15 min at room temperature (RT) and all remaining steps were completed at RT. Cells were washed twice with PBS and permeabilized with 0.25% Triton in PBS for 15 min. Cells were washed 3 times with PBS and treated with PBS containing 10% FBS and 6% BSA for one hour. Cells were again aspirated and then treated with PBS containing a 10nM solution of the Qdot 525 streptavidin conjugate with 6% BSA for one hour. Cells were washed 3 times with PBS and treated with a 2.5µM concentration of DRAQ5 (Biostatus Limited; Leicestershire, UK). Cells were aspirated and placed in PBS for imaging. Imaging was conducted using a 780 Zeiss confocal microscope (Carl Zeiss Microscopy; Thornwood, NY) with a 40 X water lens (1.2 NA) with all images 1056x1056 pixels**.** The image in Figure 2.10 a 2-dimensional representation of a 30 image Z-stack with the image LUTs adjusted to min/max and interpolated by Zen (Zeiss Oberkochen, Germany). Image analysis was conducted by colocalization mask analysis using pixel overlap intensity thresholds to limit colocalization counts to only spots manually identified as positive to generate an image mask (Figure 2.3, Zen). The total number of colocalization spots for each mask was then counted using the Velocity software package (Perkin Elmer; Waltham, MA).

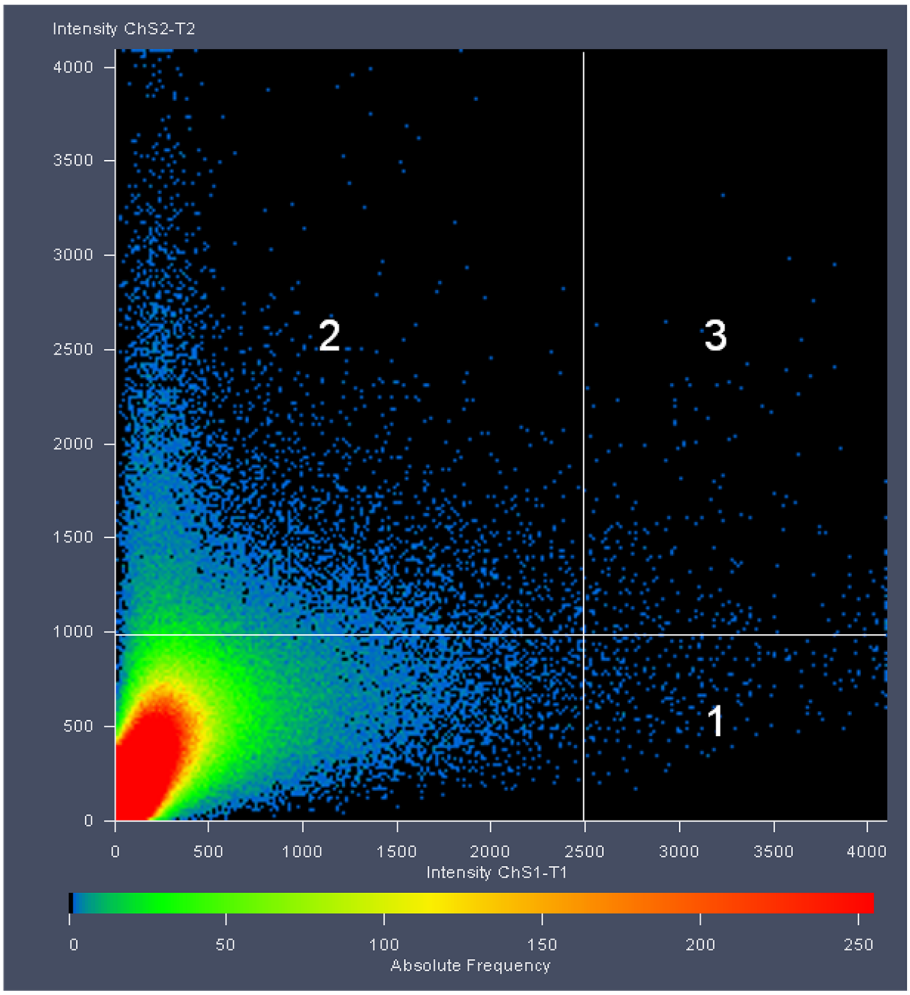

Figure 2.3 The colocalization intensity thresholds used to generate the image mask identifying areas of colocalization. All spots on this intensity map show colocalization. Areas 1 and 2 have high greyscale intensity for the FM4-64 and Q Dot 525 channels respectively, however, only area 3 has areas of colocalization with high intensity in both channels. Only areas of pixel overlap in area 3 were used for analysis and were confirmed by manual inspection. The image mask generated from these boundary conditions was then analyzed with the Velocity software package for the number of colocalization events.

2.2.15 Transmission electron microscopy

RAW264.7 cells were lifted, counted, and divided into 15 ml conical tubes at 375,000 cells/ml per tube in 500 μL of DMEM containing 50 nM biotinylated polymer conjugate **118K Biotin-10** or non-biotinylated polymer conjugate **118K-10** prehybridized for 10 minutes with 0.5 nM streptavidin conjugated 10nm gold nanoparticles (Electron Microscopy Sciences; Hatfield, PA). Cells and streptavidin gold-biotinylated polymer conjugate and control were incubated for 1 hour at 37° C and 5% CO_2 with occasional shaking to keep cells suspended. Cells were centrifuged (180xg), resuspended with 3 ml PBS (Mediatech; Manassas, VA), centrifuged again, and the supernatant removed three times as washing cycles. After the third wash, cells were again centrifuged and resuspended in 100mM sodium cacodylate, 2% glutaraldehyde, and 2% paraformaldehyde pH 7.4 (Electron Microscopy Sciences; Hatfield, PA) and fixed for 1 hour at room temperature to begin the sample prep and staining protocol below. The cells are additionally fixed in osmium tetroxide, resin embeded with Embed-812 (Electron Microscopy Sciences, Hatfield, PA), and uranyl acetate stained with protocols shown below. TEM images were collected with A Zeiss LIBRA 120 transmission electron microscope (TEM) is an energy filtering TEM equipped with a Gatan Ultrascan 1000 2k x 2k CCD camera.

2.2.15.1 Transmission Electron Microscopy Sample Preparation

1. Fix cells in 2% glutaraldehyde/2% paraformaldehyde in 0.1M Na cacodylate buffer pH 7.4.
2. Pellet cells by centrifugation, remove supernatant and replace with 4% low temperature Agar.
3. Once cooled, remove pellet in Agar and cut into 2 mm x 2 mm x 2 mm cubes.
4. Wash 3x, 15 min in 0.1M Na cacodylate buffer pH 7.4
5. Fix 2 h in 1% osmium tetroxide in 0.1M Na cacodylate buffer pH 7.4
6. Wash 2x, 15 min in 0.1M Na cacodylate buffer pH 7.4
7. Wash 2x, 15 min in dd-water
8. Dehydrate in ascending ETOH (25, 50, 75, 95%), 15 min each, and store in 95% ETOH 4°C overnight.
9. Dehydrate 2x, 15 min in 100% anhydrous ETOH
10. Infiltrate with Embed-812 resin, 1 hr each, as follows:
    a. 1 part Embed-812 (without DMP-30): 3 parts 100% anhydrous ETOH
    b. 1 part Embed-812 (without DMP-30): 2 parts 100% anhydrous ETOH
    c. 1 part Embed-812 (without DMP-30): 1 part 100% anhydrous ETOH
    d. 2 parts Embed-812 (without DMP-30): 1 part 100% anhydrous ETOH
    e. 3 parts Embed-812 (without DMP-30): 1 part 100% anhydrous ETOH
    f. 100% Embed-812 (without DMP-30)
    g. 100% Embed-812 (with DMP-30)
    h. 100% Embed-812 (with DMP-30) overnight

11. Infiltrate with fresh 100% Embed-812 (with DMP-30) 1 hr
12. Replace with fresh resin and polymerize in BEEM capsules at 60°C for 48 hr.
13. Obtain thin sections of sample with Microtome and place sections onto copper TEM grids.
14. Stain grids with uranyl acetate + Reynolds lead citrate method.

2.2.15.2 Staining Grids with Uranyl Acetate and Lead Citrate

1. Fill an Erlenmyer flask half-full with water and heat to a boil in microwave (~3-4min) with lid placed on top but not screwed down.
2. Place in ice-bath to cool.
3. In hood, fill large Petri dish with methanol.
4. Place smaller Petri dish into a larger one (to catch spills) and fill with 9ml filtered uranyl acetate solution.
5. Rinse Haruka plate with water and dry briefly.
6. Situate Haruka plate onto Haruka plate holder, and insert grids on Haruka plate.
7. Carefully remove Haruka plate from holder and set on hot plate at low heat for 5min. to flatten.
8. Place Haruka plate upside-down in uranyl acetate and allow to stain for 5min.
    a. Note: Manipulate placement of Haruka plate to avoid air bubbles which will dry out grids. Careful not to ram grids into dish.
9. Rinse grids in methanol by placing Haruka plate rightside-up and “swishing” it around using forceps.
10. Place Haruka plate right-side up in a Petri dish with filter paper, and wick away excess methanol.

11. Allow to dry for ~20min. at RT or 5min. under heat lamp.

12. Transfer Haruka plate into Petri dish lined with sodium hydroxide pellets (used to get rid of any residual CO_2). Let sit 5min.

13. Use Pasteur pipette to fill 5ml syringe approx. 1ml full with lead citrate solution.
    a. Note: Pipette from middle of container and do not scrape sides.

14. Catch first couple drops in syringe filter cap and dispense 1ml onto Haruka plate, avoiding air pockets.

15. Stain for 5min. and rinse with copious amounts of cooled CO_2-free water.

16. Wick away excess water using filter paper.

    Allow to dry for 1hr. under heat lamp prior to imaging..

2.2.16 Response of RAW264.7 macrophages to stimulatory ODN-poly(acrylic acid) conjugates

RAW264.7 cells were seeded the night before the experiment, at 75,000 cells/well in a 96-well tissue culture plate. Media was removed from plates and the wells washed with sterile PBS before addition of the solutions containing the conjugates. Conjugates were heated, directly before addition to the cells, to 95°C for 5 minutes, flash cooled, and diluted into media as described above at various concentrations and a final volume of 200 μL per well. Conjugates were added to the cultured cells, and after 8 hours, the supernatant was removed and frozen.

2.2.17 Enzyme-linked immunosorbent assay (ELISA)

ELISA was performed by analysis of supernatants collected from experiments described above, diluted with 10% FBS in PBS. Monoclonal antibody sets for murine IL-6 and TNF-α were purchased from Becton Dickinson (BDbiosciences; San Jose, CA), and used with adherence to the provided protocol. Independent values are from two independent measurements at two different concentrations within the linear range of the standard curve. ELISA measurements were measured using a Perkin Elmer VICTOR^{3}V multilabel counter (Perkin Elmer; Waltham, MA).

2.2.18 siRNA transfection

Transfection was accomplished using the Qiagen HiPerFect reagent and protocol. Briefly, RAW264.7 cells (75 μL) were plated in a Costar 48-well cell culture plate with a cell concentration of 2,000,000 cells/ ml (150,000 cells per well) in culturing media before transfection. TLR9-specific siRNA sc-40271 or control siRNA sc-37007 (Santa Cruz Biotechnology Santa Cruz, CA) was diluted to a concentration of 100 nM in 75 μL Optimem (Gibco), with addition of 3 μL HiPerFect and mixing by vortexing. Samples were incubated for 5-10 minutes at room temperature. After incubation, the siRNA mixture was added onto cells and mixed by pipetting 3 times. Samples were incubated for 5 hours under cell culturing conditions and then were supplemented with 300 μL culturing media. Stimulation, as described above, was started 24 hours later.

2.2.19 RT-PCR

Media was aspirated from the well at 6 hours post treatment and 600 µL of RNA lysis buffer from the Quick-RNA Miniprep kit added (Zymo Research Irvine, CA). The cells were freeze/thawed, scraped, and transferred to a Zymo-Spin IIICG column and processed according to the manufacturer's protocol. RNA was eluted in 35 µL and characterized for quality and concentration by 260/280 on a Nanodrop spectrophotometer (Thermo Scientific Waltham, MA), all with ratios > 1.9. 1.5 µg of RNA was then reverse transcribed using the High-Capacity cDNA Reverse Transcription Kit (Applied Biosystems Foster City, CA) supplemented with 10 units (0.5 µL) Ribolock RNase Inhibitor (Thermo Scientific Waltham, MA) in a 20µL reaction volume with the manufacturer's recommended thermal program. After completion, this reaction was then diluted directly with MB grade water to 100 µL total volume (15 ng/µL) for PCR analysis assuming 1.5 µg RNA = 1.5 µg cDNA after RT. The Power SYBR Green PCR master mix (Applied Biosystems Foster City, CA) was used in a 25 µL reaction volume. PCR conditions were 30 ng template, 0.25 µM PCR primers, 60°C extension, 40 cycles, and the remainder according to master mix specifications. The fold change in mRNA is calculated using $\Delta\Delta C_t$ with β-Actin as control. PCR primer sequences are for TLR9 (Accession # NM_031178; forward 5'-GCACTTCTCTTGCCACATGA-3', reverse 5'-TTCCCGTCCATGAAGAGAAC-3') and β-Actin (forward 5'- TCACCCACACTGTGCCCATCTACGA-3', reverse 5'-GGATGCCACAGGATTCCATACCCA-3').(196) Efficiency was determined by the equation efficiency (E) = (10^(-1/slope))-1 where the slope equals the slope of the line

for log(mass) vs. C_t value. This efficiency plots for TLR9 and ß-Actin are shown in the supporting info (Figures 2.S1 and 2.S2 respectively). The reaction was run on an ABI PRISM 7200 system (Applied Biosystems Foster City, CA) with the additional melting temperature cycle to analyze product homogeneity. The PCR product was also analyzed by gel electrophoresis and shows the expected product (data not shown).

2.2.20 4'-hydroxyazobenzene-2-carboxylic acid (HABA) assay

The amount of biotin on polymer conjuates was determined via HABA displacement by the Pierce (Rockford, IL) Biotin Quantitation Kit according to the manufacturer's instructions. Polymers were diluted into Tris-buffered saline for analysis until $Abs_{500} \leq 1$. The UV absorbance was measured on a Beckman Coulter DU 730 UV/VIS spectrophotometer.

2.2.21 Limulus amoebocyte assay

The chromogenic limulus amoebocyte assay (Lonza; Allendale, NJ) was conducted on all materials in accordance with the manufacturer-provided protocol. Conjugates, as well as purified polymer and ODN, were tested for endotoxin and found to be lower than 0.02 EU/ml. Conjugates containing the control sequence 1668 GC were also characterized and were confirmed to not promote cytokine release.

2.2.22 Statistical analysis

Statistical analyses were calculated using Kaleidagraph (Synergy Software; Reading, PA); statistical significance was calculated with one-way ANOVA with a post hoc Tukey's analysis at the 99% confidence level. A minimum of three independent samples were used for analysis.

2.3 Results and Discussion

2.3.1 Design and synthesis of poly(acrylic acid)-DNA conjugates

It is known that differential cytokine responses are demonstrated by ODNs with differing aggregation, which offers opportunities to tailor the responses of cells of the immune system. The use of polymer scaffolds, in particular, allows the design of novel materials with greater control over presentation and number of ODN ligands than that previously possible with ODN aggregates or complexes. Because TLR association with lipid rafts(52, 128) and receptor colocalization are important for the formation of cytosolic signaling protein scaffolds,(79) we postulated that control of the number and density of ODN ligands available for interaction with TLR9, in particular, would be a good target for affecting cytokine response. The design of polymeric carriers for such differential display of ODN ligands was based on several considerations. Although positively charged polymers such as poly(ethylene amine) have been widely used as nucleic acid carriers, in order to promote condensation and

protection of the nucleic acid, the passage of the nucleic acids through cellular membranes into the cytosolic space is mediated at least in part through the interactions of the positively charged polyplex with the negatively charged cellular membrane.(197-199) Such nonspecific interaction of the conjugates with cellular membranes is undesirable in the current studies, as the goal is to probe the role of ODN display in the TLR9-mediated activation of immune cells without complications of interactions with the polymer scaffold. Poly(acrylic acid) (PAA) was thus chosen as the scaffold owing to its high negative charge at physiological pH, as well as the fact that low-PDI polymers are available over a large range of molecular weights. The high negative charge density of both the polymer and the nucleic acid also serves to prevent macromolecular interaction or aggregation of the ligand and polymer. PAA polymers of a molecular mass of 124kDa were employed in these studies; these polymers exhibit a hydrodynamic diameter of approximately 35nm under physiological conditions, as assessed via dynamic light scattering (Figure 2.2), providing an intermediate size scaffold (between monomeric ODN and other aggregate-based particles) for investigation, and dimensions that are sufficiently large that engagement of multiple TLR receptors is possible.(14, 24, 138)

PRRs can detect very low concentrations of PAMPs(200, 201) so a sensitive imaging strategy was necessary in the present work to ensure detection of synthesized PAA conjugates by flow cytometry and confocal microscopy. Multiple biotin labels were thus employed to enhance the binding capacity of the PAA conjugate for streptavidin-labeled fluorophores. Biotin was chosen for its versatility for labeling of the polymer with any streptavidin-functionalized detection agent, as well as for its

small size, which minimizes any steric impact on the binding of the conjugate to TLR9. Similar strategies have been employed in other work to provide high avidity binding of DNA to solid substrates for DNA hybridization,(202) as well as enhancing uptake of PAMAM-biotin conjugates in an ovarian cell cancer line.(203) Biotinylation was accomplished through the chemical protocols detailed in the experimental section and shown in Figure 2.5, the extent of biotinylation determined via H^1 NMR, and functional streptavidin binding by HABA displacement assay (Supporting Information). The effect of biotinylation on the activation of RAW264.7 cells (via

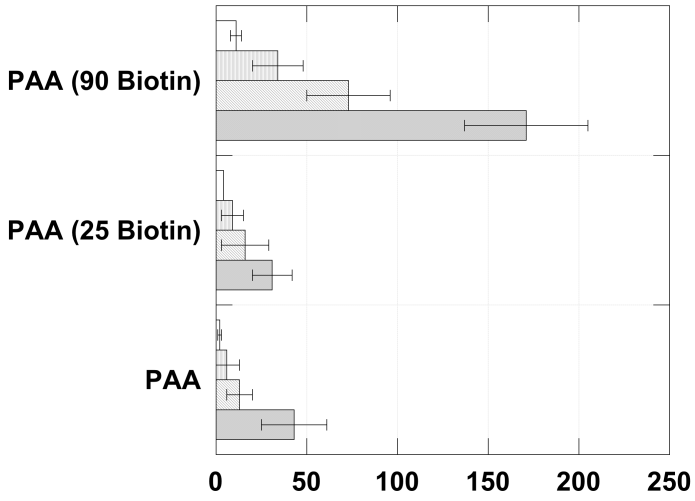

Figure 2.4 RAW264.7 cell 8 hour TNF-α response to PAA and two biotin modified PAA scaffolds. The concentrations of polymer used are 5μM (closed bar), 1μM (cross hatched bar), 0.5μM (horizontal hatched bar), and 0.1μM (open bar). The standard deviation of 3 independent measurements is shown. Concentrations of 5μM, 1μM, and 0.5μM are all well above those used in other experiments, and the low response demonstrates the low immunogenicity of the scaffolds.

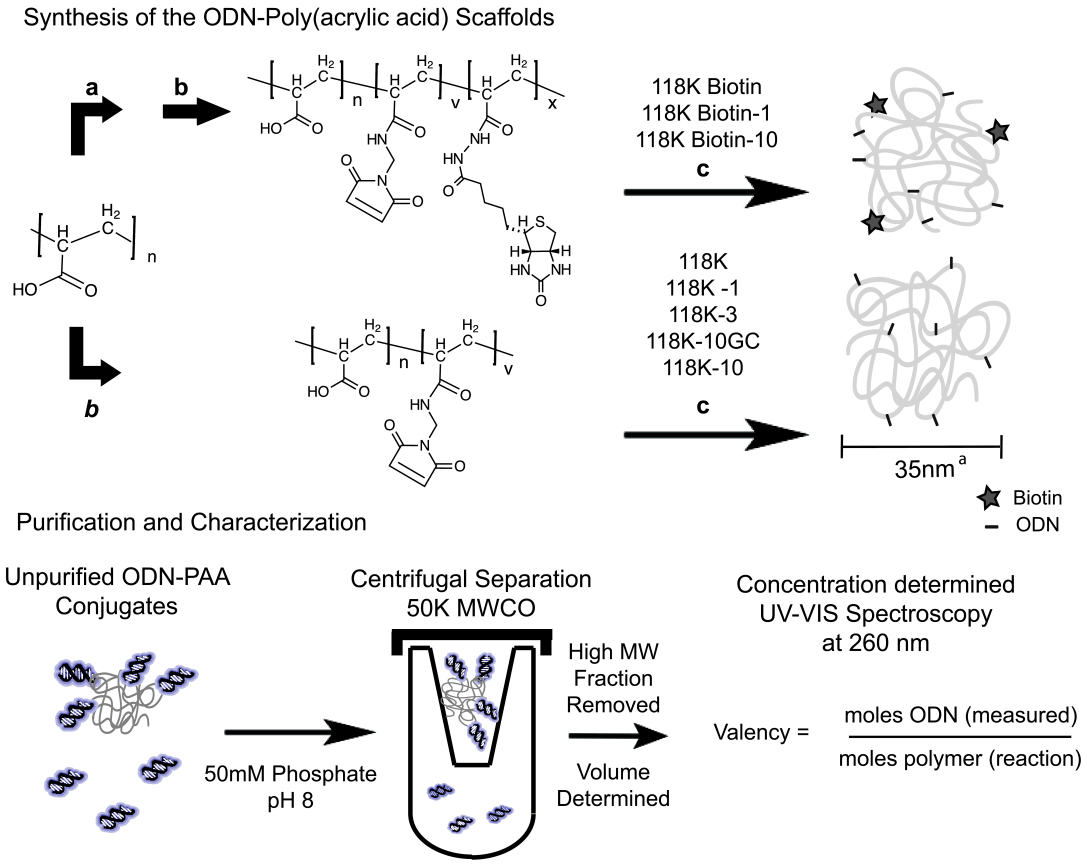

Figure 2.5 Reagents and conditions: (a) 118K PAA, biotin hydrazide , HBTU, and TEA (all 10mg ml^{-1}) except TEA added as liquid) in DMSO; (b) 118K PAA with EDC, HOBT, and NEAM (all 10mg ml^{-1}) in 75mM MES pH 6.05 under nitrogen; (c) maleimide polymer and reduced DNA in 50mM phosphate, 13mM citrate, 5mM EDTA ~pH 6.9 under nitrogen; *a.* Size of 35nm determined by DLS; all conjugates shown to co-elute via GPC.

assessment of TNF-α expression) was monitored to ensure that the modification of the polymer did not complicate interpretation of cellular uptake and activation. Based on these activation results (Figure 2.4), a biotin functionality of approximately 30 showed

minimal activation with full binding accessibility, and was thus chosen for labeling and detection in flow cytometry and confocal microscopy experiments.

Synthesis of the ODN-PAA conjugates required a robust and efficient bioconjugation strategy compatible with available chemical end-functionalities available for synthetic ODN. We chose to functionalize PAA with N-(2-aminoethyl)maleimide (NEAM) through the chemical protocols outlined in Figure 2.5 and subsequent reaction with a 3' thiol-functionalized ODN. Similar chemical approaches were employed by Lifland and colleagues for the synthesis of poly(ethyleneglycol)-ODN hybridization probes.(190) ODN must be conjugated through the 3' end for proper interaction with TLR9(204) and thus ODN with a 3' C6-thiol linker were employed in these studies. Synthesis of the PAA-ODN conjugates described in Table 2.1 was accomplished by varying the molar ratio of 3'-thiol ODN to maleimide-functionalized PAA synthesized as described in **Figure 2.5**

Table 2.1. Polymers Prepared

Conjugate	Maleimide # (NMR)	Number Biotin	Theoretical Valency	Actual Valency (UV)
118K	10	0	0	0
118K-1	10	0	1	0.8
118K-1.5	10	0	2	1.5*
118K -3	43	0	4.5	3
118K -10	43	0	14	10.5
118K -10GC	43	0	14	10.5
118K Biotin	10	33	0	0
118K Biotin-1	10	33	1	0.8
118K Biotin-10	48	33	14	10

* NMR characterization was used to validate this functionality and UV characterization method (Figure 2.1).

(lower pathway **b**). The buffers used for both the column purification of the reduced 3'-thiol ODN and for the maleimide-functionalized PAA were optimized to reduce hydrolysis of the maleimide group and maintain the nucleophilicity of the thiol group. Small changes in pH or ionic strength resulted in drastic changes in observed reaction efficiency, often with no observed product. Both TCEP and DTT were examined as reductants for the 3' thiol-functionalized ODN. Only DTT, with subsequent purification via SEC with a Sephadex G 15 column and 50mM phosphate, 13mM citrate, 5mM EDTA ~pH 7.05 buffer, yielded efficient conjugation. Table 2.1 indicates the maleimide functionalities of the conjugates used in these studies, which ranged from 10 to 45 and yielded 1 to 10 ODNs per polymer. Polymer conjugates **118K Biotin-1** and **118K Biotin-10** were synthesized with both biotin and maleimide functionality, for visualization of these polymer conjugates during flow cytometry and microscopy, while **118K-1, 118K-1.5, 118K-3, 118K-10GC,** and **118K-10** were synthesized (without biotin) for cellular activation studies**,** as shown in **Figure 2.5**. Polymer conjugates **118K Biotin-1**, **118K-1.5,** and **118K-1** were synthesized with a lower maleimide functionality of approximately 10 (Table 2.1) owing to the fact that higher maleimide functionalities introduced slight absorbance at 260nm that interfered with the spectrophotometric determination of ODN functionality for the PAA-ODN conjugates equipped with a single ODN (data not shown). The higher functionality polymer conjugates **118K Biotin-10, 118K-10**, and **118K-3** were synthesized from a

PAA equipped with a higher maleimide functionality of approximately 45 (Table 2.1) for more efficient conjugation and higher ODN functionality.

Purification methods were also optimized to allow complete removal of unreacted ODN from any HMW species (>118K). Purification buffer with an elevated pH (8) was employed to ionize all phosphates and carboxylic acids, thus maximizing electrostatic repulsion of the ODN from the polymer scaffold. In addition, the expected covalent bond formation was validated (in part) by examining several buffer conditions (over several different syntheses) that would disrupt noncovalent association of ODN with the PAA polymers and conjugates. Various solutions (1M NaCl (ionic forces), 18 MΩ H_2O (hydrophobic forces), and 5% DMSO (also hydrophobic forces)) were tested as eluents; there was no decrease, after five washes under these various conditions, in the observed ODN absorbance at 260 nm of the high molecular-weight fractions. Analysis of all reactions and fractions during the synthesis confirmed that all ODN was accounted for during the synthesis, and that there was no alteration of the expected UV absorbance properties. Thus, the ODN absorbance at 260nm was employed to indicate the concentration of ODN in a given sample, and the functionality of the polymer determined by using the absorbance value and the pre-measured mass of polymer in a given sample.

To validate that these protocols accurately represented the ODN functionality of product given conjugate, ^{1}H NMR was employed. The polymer 118K-1.5 was used to compare ODN functionalities determined via UV-Vis and ^{1}H NMR. The low ODN:polymer ratio of this sample provided the most stringent test case as samples with low numbers of ODN pendant ligands are the most susceptible to interference in

the UV spectra. The functionality value determined by both methods was shown to be in very close agreement, with UV-Vis analysis yielding a valency of 1.5 and ^{1}H NMR analysis yielding a valency of 1.6. Also, the NMR spectra (Figure 2.1) shows peak broadening not only for the polymer proton peaks, but also for the ODN peaks (when compared to unreacted ODN (not shown)) as a result of slower tumbling, and an indication of the conjugation of the ODN to the polymer. The inset of Figure 2.1 shows the UV trace of this conjugate demonstrating the characteristic peak in absorbance at 260nm.

In addition, all raw materials and final polymers and conjugates were tested, via LAL assays, for lipopolysaccharide (LPS), a ubiquitous environmental contaminant from Gram (-) bacteria, to confirm that there would be no activation of the RAW264.7 cell line owing to contamination of the ODN or polymer samples. All synthesis protocols were designed specifically to prevent LPS contamination and all conjugates were measured to be <0.02 EU/ml; these values are well below levels capable of activation (data not shown).

2.3.2 Characterization of ODN-PAA conjugates

Gel permeation chromatography (GPC) analysis was used to determine if the ODN and polymer co-eluted, which would further indicate covalent association and indicate the absence of monomeric ODN in any polymer conjugates. We anticipated that the small size of the ODN (~2 nm)(205) would not significantly modify the hydrodynamic volume of the much larger polymer (~ 35 nm). Figure 2.6 shows that the separate

peaks (detection at 260nm) resulting from the free ODN (open circles) and the polymer-ODN conjugates **118K Biotin-10** (light grey crosses), **118K-1** (black

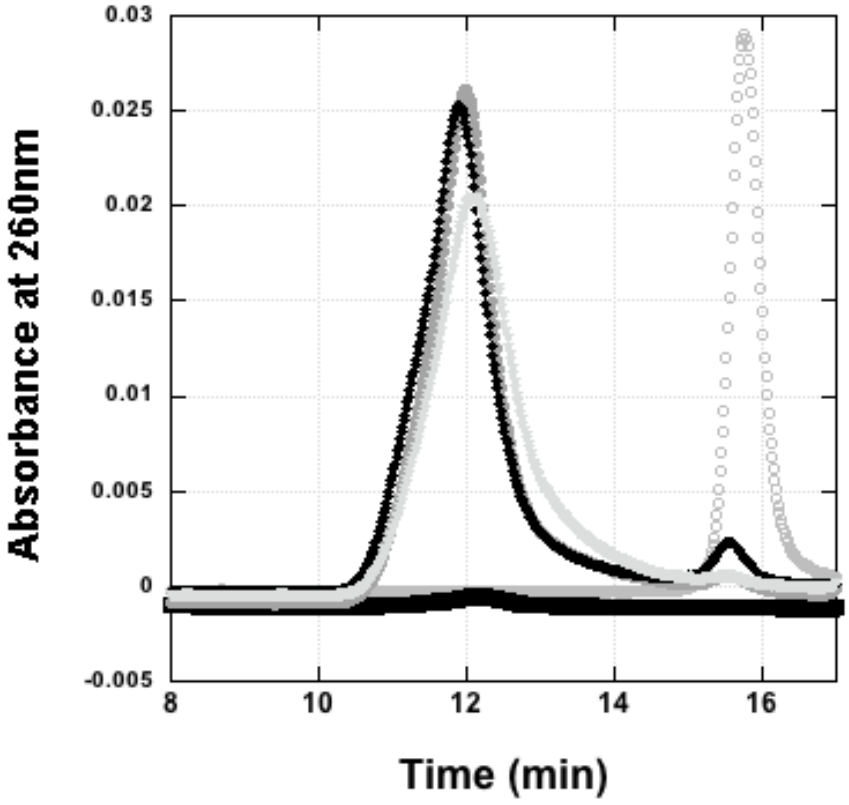

Figure 2.6. Gel permeation chromatography of polymers and ODN samples in PBS pH 7.0, monitored at a wavelength of 260nm. Samples are ODN 1668 (5µM DNA) (open circles), **118K Biotin** (black line) (0.5µM polymer), **118K-10 Biotin** (light grey crosses) (5µM DNA and 0.5µM polymer conjugate), **118K-1** (black diamonds) (5µM DNA and 5µM conjugate), and **118K-10** (closed circles) (5µM DNA and 0.5µM conjugate).

diamonds), and **118K-10** (closed circles) are clearly discernible, supporting that any absorbance of the high molecular mass peak at the polymer elution time arises from

ODN that is covalently conjugated to the polymer backbone. A slight contamination of free ODN in sample **118K-10** (ca. 2%) is observed; this low concentration of monomeric ODN was separately determined to be nonactivating to the macrophage-like cell line, and the 118K-10 sample was thus employed in cellular assays without further purification. Solutions of conjugates **118K Biotin-10**, **118K-1**, and **118K-10** were prepared gravimetrially to yield solutions with similar ODN concentration; the similar observed intensity of the absorbance from these samples thus further confirms UV-Vis analysis accuracy. The results of this GPC analysis, when taken together with the results of the DLS (Figure 2.2), suggest that all of the PAA-ODN conjugates are approximately 35 nm in diameter.

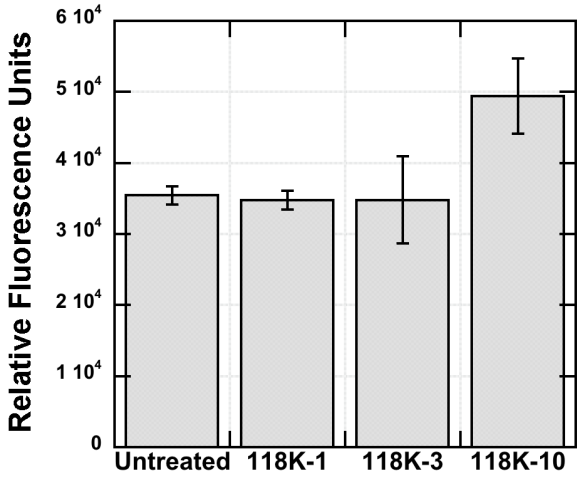

Figure 2.7. Cell titer blue viability assay of RAW264.7 cells at 8 hours. Untreated cells were monitored, as well as cells treated with conjugates **118K-1** (200nM DNA), **118K-3** (200nM DNA), and **118K-10** (200nM DNA). Standard deviation calculated from the average of 3 independent measurements. A)* indicates statistically significant differences at $p \leq 0.014$.

The cytotoxicity of conjugates **118K-1**, **118K-3**, and **118K-10** was monitored using the cell titer blue reagent, which measures the reductive capacity of metabolically active cells, and thus indirectly measures cell viability. The data in Figure 2.7 present results for RAW264.7 cells exposed to the highest concentration of conjugate tested (normalized to 200nM DNA), and illustrate that the metabolic activity of each sample is at or above the level of the control sample. Thus, no cytotoxicity was observed for any of the conjugates tested; a slight increase in metabolic activity measured for the cells exposed to **118K-10** is likely a result of innate cellular activation of TLR9 by the conjugate.(152)

2.3.3 Flow cytometry and microscopy analysis of uptake and localization

Flow cytometry, as well as confocal and transmission electron microscopy, were used to study the uptake and cellular distribution of conjugates, respectively. The flow cytometry studies were designed to determine whether the cellular uptake was an active process and the microscopy studies to assess if the localization within the cell was defined and in membrane-bound vesicles. To this end, we employed **118K**

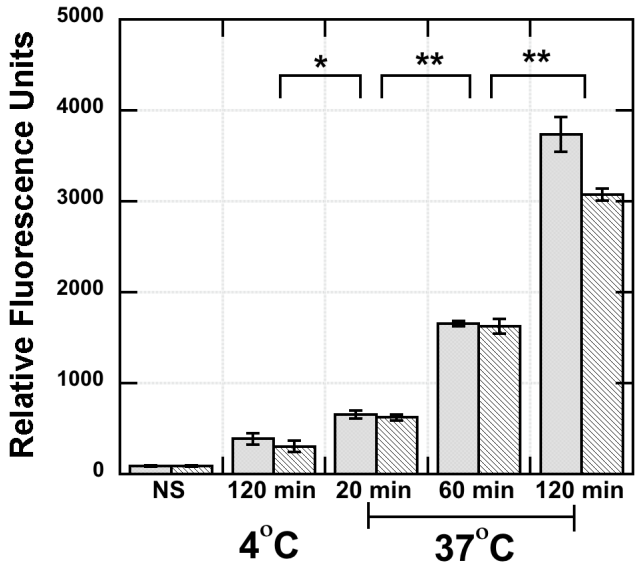

Figure 2.8 Flow cytometry of RAW264.7 cells exposed to conjugates 118K Biotin-1 (light grey) and 118K Biotin-10 (hashed) normalized to 100 nM ODN concentration at 37° for 20 min, 60 min, and 120 min and 4°C for 120 min. NS = No Stain. The results presented are the MFI average of the geometric mean of 10,000 cells, n=3 samples, with error bars representing standard deviation and are representative of greater than three independent trials. Statistics between time points of each condition, * $p<0.001$ and ** $p<0.0001$.

Biotin-10 and **118K Biotin-1** conjugates, which allowed detection via the fluorescence of streptavidin-labeled quantum dots. The flow cytometry data are shown in Figure 2.8, and the data illustrate the levels of cellular internalization of **118K Biotin-1** and **118K Biotin-10** at 37°C over a time course of 20, 60, and 120 min, and at 4°C after 120 min, in order to assess if uptake is an active or passive process. There is clearly an increase in the mean fluorescence intensity (MFI) over time for both **118K Biotin-1** and **118K Biotin-10** ($p<0.001$) at 37°C with only a small detectable increase in MFI at 4°C over 120 min ($p<0.0001$). With the increase in MFI observed by flow cytometry only for samples incubated at physiological temperature, we conclude that internalization of these conjugates is an active process. We also employed a separate flow cytometry experiment (Figure 2.9) in which permeablization conditions were altered to permit labeling only of the surface of the cell. Specifically, the fluorescence of permeabilized and non-permeabilized cell populations (at 37°C) were compared, and the fluorescence of the non-permeabilized cells at 37°C was compared to that of permeabilized cells at 4°C. If uptake is an active process, the permeabilized cells incubated at 37°C should show an elevated fluorescence relative to the other two conditions. The data in Figure 2.9 clearly illustrate this, and also illustrate that the histograms for **118K-1** and **118K-10** for the permeabilized 4°C and non-permeabilized 37°C conditions overlay, thus indicating that any fluorescence observed at 4°C is a result of surface labeling. Taken together, these two flow cytometry experiments clearly confirm the active internalization of the PAA-ODN conjugates.

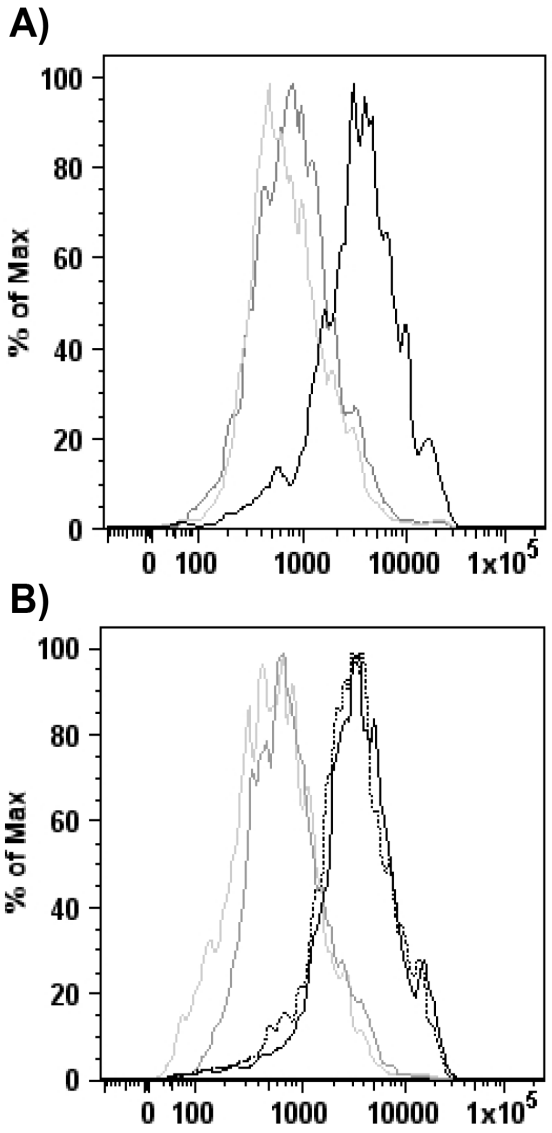

Figure 2.9 Flow cytometry of RAW264.7 cells exposed to conjugates 118K-1 Biotin (a) (100 nM polymer and 100nM ODN) and 118K-10 Biotin (b) (8 nM polymer and 100 nM ODN) at 37° and 4°C. Conditions shown are at 37°C with no permeabilization of cells highlighting only surface binding (light grey) (1186 (a) and 863 (b)), 4°C (medium grey) (1111 (a) and 1106 (b), and 37°C (black line and dotted black line of replicate) (4841 (a) and 4828±313 (b). The results presented are representative of three independent trials.

Confocal microscopy (Figure 2.10a) was used to corroborate the flow cytometry data (that the conjugates were internalized and not simply associated with the plasma membrane), but more importantly, to show that conjugates had defined distribution throughout the cell and were localized within membranous structures and not dispersed in the cytosol. The dye FM4-64 was used by Lande et al. to determine endosomal colocalization of DNA complexed by the cathelicidin LL_37.(68) Similarly, the fixable analogue FM4-64FX was used in the present study to mark membrane-mediated endocytic events and internalization of the polymer conjugate **118K Biotin-10** (or polymer **118K Biotin**). Intracellular colocalization of the dye with quantum dots would indicate that the dye and conjugate were concurrently endocytosed from the plasma membrane. Figure 2.10 shows a representative confocal image with the green indicating the Qdot 595-complexed **118K Biotin-10**, the red indicating the FM4-64, and the blue indicating DRAQ5-stained nuclei. The distribution of **118K Biotin-10** is limited to localized regions of 150-500nm, which corresponds to the expected size of endocytotic vesicles.(206, 207) This colocalization was further analyzed via intensity-based analysis of image masks (example Figure 2.3) on Velocity software, to estimate the number of colocalization events (Table 2.2). The scaffold **118K Biotin** exhibited 2 ½ times the number of colocalization events of **118K Biotin-10,** perhaps from greater accessibility of the pendant biotin or a difference in receptor-mediated endocytosis. Although these data show that the biotin-streptavidin detection method is likely only qualitative, they unequivocally demonstrate colocalization of the Qdot-labeled conjugates with the

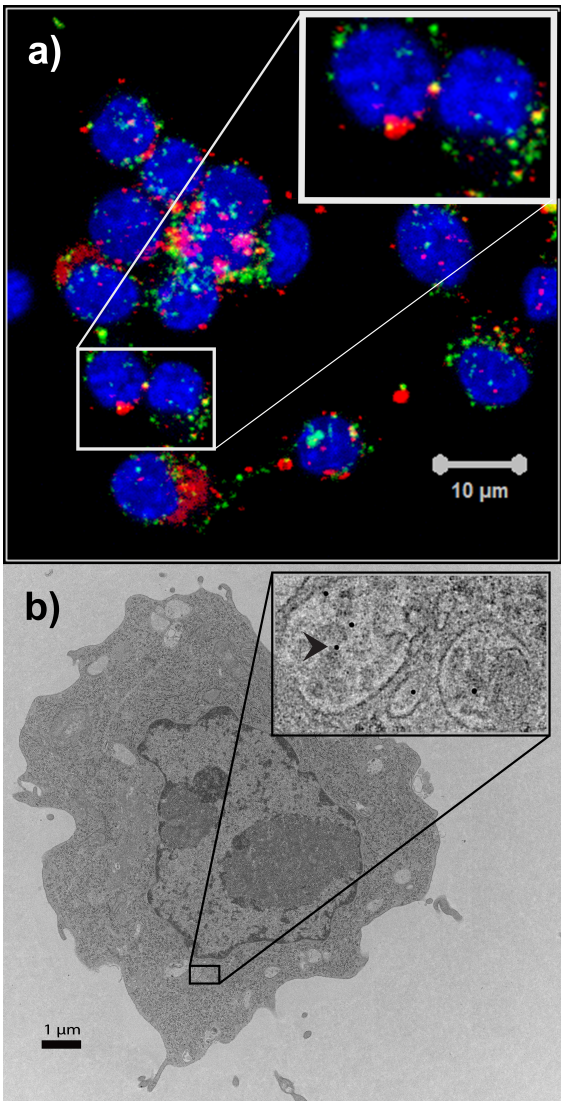

Figure 2.10 Microscopy of polymer conjugate subcellular localization. Confocal image **(a)** is a two dimensional rendering of a 32 image z-stack of RAW264.7 cells exposed to conjugate **118K Biotin-10** (20nM conjugate/ 200nM ODN) labeled by streptavidin conjugate Qdot 525 (green), endocytosed vesicles by FM4-64FX (red), and nuclei by DRAQ5 (blue) with sites of colocalization visible as yellow (white scale bar 10 µm). Transmission electron microscopy **(b)** of RAW264.7 cells exposed to polymer conjugate **118K Biotin-10** complexed with 10nm streptavidin-gold particles (black scale bar 100 nm).

plasma membrane-localized FM4-64 and thus demonstrates that the scaffold is endocytosed from the plasma membrane.

Table 2.2. Confocal analysis

Sample[a]	Number spots colocalized	Total Brightness	Average spot brightness
118K Biotin	42±5	38930±7100	956±320
118K-10 Biotin[b]	17±11	11567±9700	523±210

(a) three independent trials were conducted and images selected were representative examples from each trial. (b) one of these samples showed no colocalization spots so the standard deviation given is for the two positive samples.

Transmission electron microscopy (TEM) was used to corroborate that the polymer conjugates were indeed localized within endocytotic vesicles. Biotinylated **118K Biotin-10** (or the non-biotinylated **118K-10**) was mixed with streptavidin-gold nanoparticles (at a 100:1 polymer:particle mixing ratio in order to limit labeling of the polymer scaffolds to a single (or a very low number of) gold nanoparticle(s)) prior to addition to cells. Figure 2.10b shows a representative image of a cell from the **118K Biotin-10** samples and clearly shows the gold-labeled **118K Biotin-10** within two distinct membrane-bound endocytic compartments with sizes appropriate for early or late endosomes and matching those in Figure 2.10a. Twelve independently selected cells were imaged for both sample and control, and the number of endocytosed gold particles counted. Analysis demonstrates the number of endocytosed gold particles in the cells treated with the biotinylated **118K Biotin-10** (28±20) is statistically different ($p=0.00071$) from the number of nanoparticles in cells treated with the non-

biotinylated **118K-10** control (5±5), indicating that the uptake of the gold nanoparticles is mediated by uptake of the biotinylated, ODN-modified polymer, rather than by aggregates of free gold nanoparticles. The conclusion that gold nanoparticle uptake is mediated by the polymer scaffold is further substantiated by the fact that in the **118K Biotin-10** samples, which can bind to the gold particles through the biotin-streptavidin interaction, no gold nanoparticle aggregates were observed. In contrast, aggregates were common in **118K-10** samples in the absence of biotin-streptavidin interactions, owing to the high aggregation propensity of free gold nanoparticles (data not shown). The combination of the flow cytometry, confocal microscopy, and TEM data clearly illustrate that the ODN-modified scaffold is actively internalized and that endocytotic events localize conjugate within vesicular compartments. The microscopy images also show that the conjugates are localized in defined, vesicular-sized areas within the cell; the lack of diffuse cytoplasmic distribution indicates the lack of endosmolytic breakage.

2.3.4 RAW264.7 cell-line response to ODN-PAA conjugates

Murine-derived RAW264.7 cells are the standard cell-line for TLR9 studies due to their expression of TLR9 and their macrophage-like characteristics.(155, 157, 183) These cells were cultured and exposed to ODN–PAA conjugates of multiple valencies and the cell supernatants were analyzed by ELISA for murine TNF-α and IL-6. These two cytokines are both type I inflammatory cytokines and are secreted by cells in response to TLR9 activation by CpG motifs in pathogen DNA.(16)

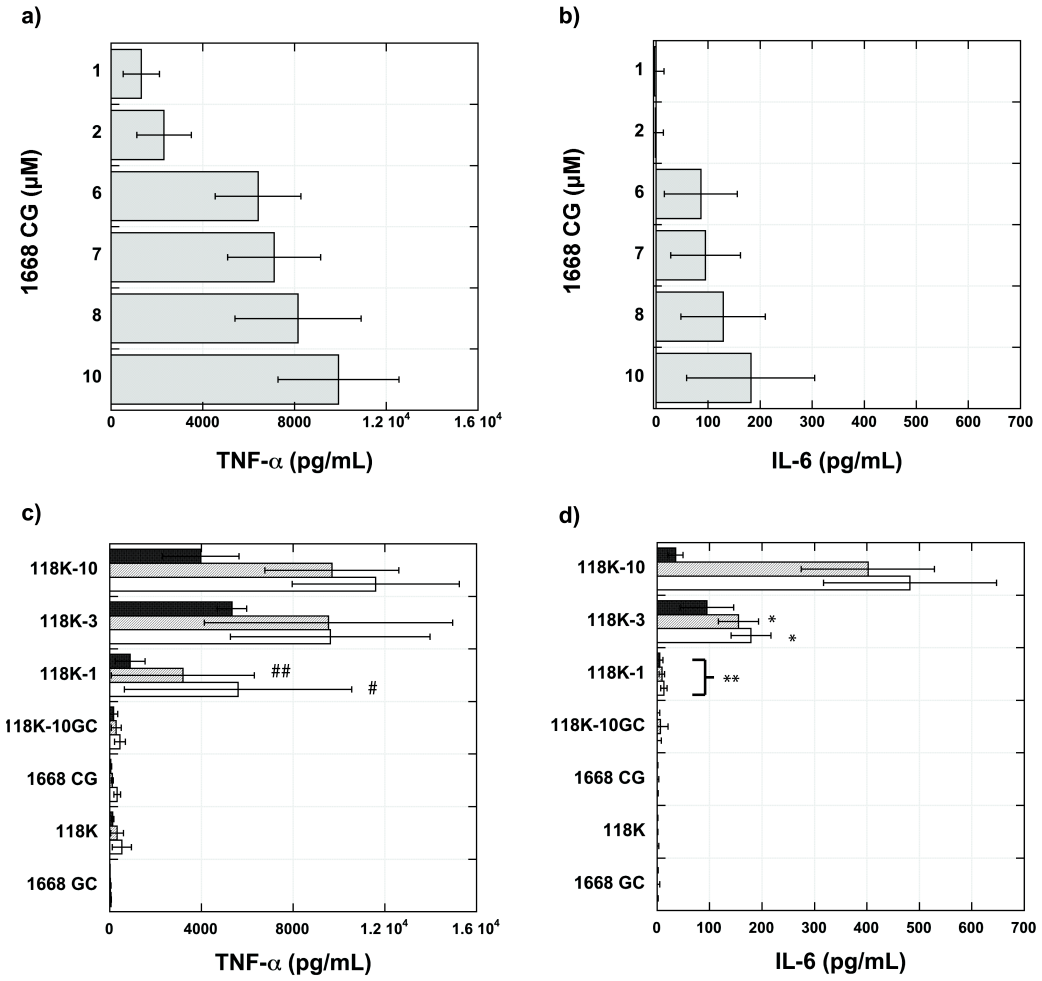

Figure 2.11 Cytokine release at 8 hours from RAW264.7 cells by ODN 1668 (a and b) and DNA conjugates (c and d). Comparison of TNF-α (a and c) and IL-6 (b and d) release for ODN 1668 in μM DNA and conjugates or controls by normalized concentration DNA at 16.6nM (closed bar), 100nM (crosshatched bar), and 200nM (open bar). Concentration of 118K is the PAA concentration for conjugate 118K-1 (200nM, 100nM, or 16.6nM). Error bars represent the standard deviation from the average of three independent experimental trials and ≥6 independent measurements. # statistically different from the 118K-10 conjugate ($p=0.02$). ## statistically different from the 118K-10 and 118K-3 conjugates ($p\leq0.003$). * statistically different from the 118K-10 conjugate ($p<0.0001$). ** Statistically different from conjugate 118K-10 ($p<0.0001$) and statistically different from conjugate 118K-3 ($p\leq0.0148$).

Figure 2.11 shows the TNF-α and IL-6 responses, at 8 hours, to free ODN (Figures 11a and 11b respectively) compared on the same scale to the cytokine responses to polymer conjugates **118K-1**, **118K-3**, **118K-10** (all normalized to ODN concentration), and controls (PAA, monomeric ODN, monomeric GC-ODN, and a GC-ODN-containing PAA) (Figures 11c and 11d). The controls include the polymer conjugate **118K-10GC** (comparable in construction to **118K-10**), equipped with the control ODN sequence 1668GC that is not competent for TLR9 activation; this conjugate shows no cytokine expression above the PAA controls. Both Figure 2.11a and 11b show the expected increased cytokine excretion with increasing free ODN concentrations (1μM, 2μM, 6μM, 7μM, 8μM, and 10μM). Figures 11c and 11d show the cell response to conjugates **118K-10**, **118K-3**, and **118K-1** (at ODN concentrations of 16.6nM, 100nM, and 200nM), and illustrate the lack of cytokine secretion from cells exposed to the negative ODN-PAA control (GC motif), the unmodified PAA, or the monomeric ODNs at these concentrations.

The TNF-α response (Figure 2.11c) shows an increase in cytokine secretion with increasing conjugate concentration for all samples in this concentration range, indicating the sensitivity of the cells to the polymer-bound ODN. The data also show that the conjugate **118K-1** (with a single polymer-bound ODN) elicits greater TNF-α production relative to that elicited by the free 1668 CG ODN. This could result from higher resistance to exonucleases activity for the polymer-bound ODN conjugate, consistent with the fact that exonucleases degrade DNA from the 3' terminus(83), and that this terminus was used for conjugation of the ODN to the PAA scaffold. Increased cellular uptake could also be the source of this enhancement, however, the labeling

strategy used here does not allow direct comparison to single ODN in flow cytometry and confocal analysis. A modified detection strategy is currently being used to address the origin of increased TNF-α production in response to the **118K-1** conjugate. Both the **118K-10** and **118K-3** polymer conjugates show statistically significant increases in TNF-α production over **118K-1** at ODN concentrations of 100nM ($p \leq 0.003$). The **118K-10** polymer conjugate also shows a statistically significant increase in cytokine release (TNF-a) compared to that of **118K-1** at an ODN concentration of 200nM (11605±3650 pg/ml vs. 5599±4960 pg/ml; $p=0.02$), indicating that higher valencies elicit increased cytokine responses normalized for ODN concentration. Although the detection method employed here is not quantitative, it is likely that the higher-valency scaffolds have lower intracellular concentrations than the low-valency scaffolds, given the necessary differences in the scaffold concentrations required to normalize ODN concentration. Thus, the higher valency scaffolds may be more potent activators of TNF-a production than indicated by these data. Current studies are focused on determining relative intracellular concentrations for conjugates of differing valency. Regardless, comparison of the DNA concentrations required to elicit similar cytokine responses (for the conjugates versus the free ODN) suggests that the conjugates are at least 100-fold more potent for cytokine production and that this potency is related to valency.

Comparisons of Figures 11b and 11d illustrate that the enhancement in IL-6 expression for the conjugates relative to the free ODN is perhaps even more striking. Here, enhancement in cytokine production by the polymer conjugates is highly dependent on the ODN valency (all samples are normalized to ODN concentration)

and both **118K-3** and **118K-10** show significant increases in immunostimulation as indicated by IL-6 production. Conjugate **118K-10** (482±165pg/ml) shows statistical significance over **118K-3** (179±38pg/ml) and **118K-1** (13±6pg/ml) ($p<0.0001$) and **118K-3** shows significance over **118K-1** ($p\leq0.0148$). Comparisons of the IL-6 production between the free ODN and conjugates (Figures 11b and 11d) show that conjugates **118K-3** and **118L-10** elicit the same (or even 2-fold greater) IL-6 response as a free ODN at 100-fold lower concentrations (100nM vs. 10μM). We are currently exploring the biological implications of this altered cytokine profile.

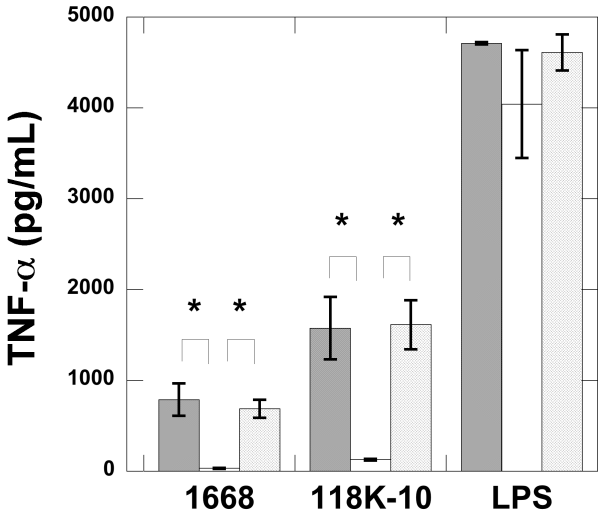

Figure 2.12 The effect of TLR9 siRNA knockdown on stimulation of untreated, TLR9 knockdown, or mock transfected RAW264.7 cells. Figure shows the TNF-α (pg/ ml) measured by ELISA of untreated (dark grey), TLR9 knockdown (white), or mock transfected (light grey) RAW264.7 cells by ODN 1668 (2.5 μM), conjugate 118K-10 (200 nM), and LPS (100 ng/ml). Error bars represent the standard deviation from the average of three independent samples. ** Indicates statistically relevant difference ($p<0.003$).

To ensure that the enhanced immunostimulation of these novel ODN-polymer conjugates is indeed mediated through TLR9 and not other PRRs, we employed siRNA to silence TLR9 mRNA and evaluate the effect of knockdown on RAW264.7 stimulation (Figure 12). The TNF-α concentrations in the media were analyzed via ELISA for untreated (dark grey), TLR siRNA-treated (white), and mock siRNA-treated (light grey) cells exposed to ODN 1668 (2.5 μM), conjugate 118K-10 (200 nM in ODN), and LPS (100 ng/ml) (Figure 12). As is illustrated in the data, treatment of the cells with TLR9-silencing siRNA results in an over 90% decrease of the observed TNF-α response versus that observed for untreated cells, for both ODN 1668 and **118K-10** ($p<0.01$); no such decrease in TNF-α response was observed for the mock samples. We also monitored knockdown by RT-PCR, confirming that siRNA treatment also significantly lowered TLR9 mRNA levels in stimulated cells (Figure 13). These data pinpoint TLR9 as the immunological target of these novel ODN-PAA conjugates.

As a further test of the utility of these PAA-ODN conjugates, we have confirmed the immunostimulatory impact of these novel ODN-PAA conjugates on GM-CSF-matured, murine bone marrow-derived macrophages (BMDM). A titration of the ODN 1668 (panel a) was used to compare the levels of IL-6 expression in BMDM treated with monomeric ODN to that of cells treated with the conjugate **118K-10** (Figure 14). Panel (a) illustrates the levels of IL-6 production for GM-CSF

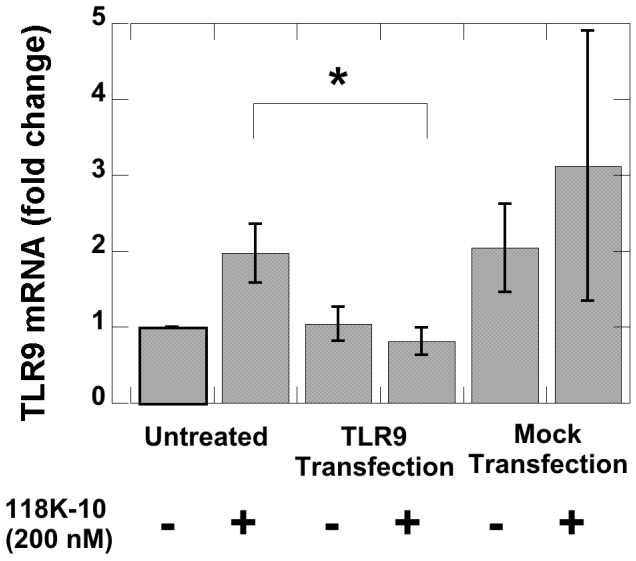

Figure 2.13 The effect of TLR9 siRNA knockdown on TLR9 mRNA levels. Figure shows the relative change in the amount of TLR9 mRNA for untreated, TLR9-transfected, or mock-transfected RAW264.7 cells with or without stimulation by 200 nM conjugate 118K-10. * Statistically different ($p<0.01$).

maturated macrophages exposed to various ODN concentrations (1 to 10 μM), as assayed by ELISA. Panel (b) shows the concentrations of IL-6 produced by GM-CSF maturated macrophages exposed to conjugate **118K-10** (dark grey), ODN 1668 (light grey), and the control ODN 1668 GC (white) at ODN concentrations of 200 nM, 100 nM, and 6.3 nM. As illustrated via comparisons of the IL-6 production, conjugate **118K-10** elicits similar IL-6 expression at a concentration approximately 10-fold lower than the monovalent ODN 1668 (Panel b). These results validate, in primary macrophages, the enhanced immunostimulation of the multivalent ODN-PAA conjugates suggested by results in the RAW264.7 cell line.

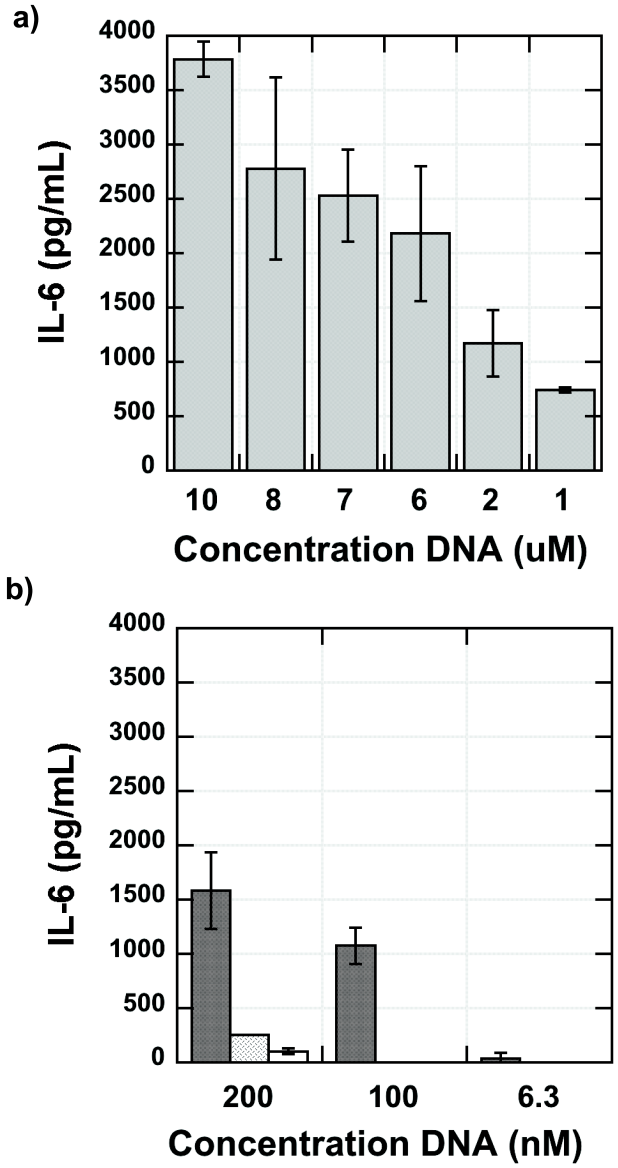

Figure 2.14 ODN 1668 titration **(a)** and response to conjugate 118K-10, ODN 1668, and ODN 1668 GC **(b)** for GM-CSF matured murine macrophages as determined by IL-6 ELISA 8 hours post treatment. Panel **(a)** shows the IL-6 response at 8 hours for primary macrophages at the specified concentration of ODN 1668 in μM. Panel **(b)** is the IL-6 (pg/ml) at 8 hours for conjugate 118K-10 (dark grey), ODN 1668 (light grey), and ODN 1668 GC (white). Error bars represent the standard deviation from the average of three independent samples.

When comparing the activity of these ODN-PAA conjugates to that of other complex displays of DNA described in the literature, conjugates **118K-3** and **118K-10** elicit a greater fold increase over monomeric ODN of TNF-α, than any other complex of comparable concentration. Rattanakiat et al. demonstrate a 15- to 20-fold increase in TNF-α (at 8 hours) for a 12-functional hybridized DNA dendritic structure,(157) while **118K-10** shows an 35-fold increase at comparable concentrations. Nishikawa et al. and Li et al. observed 6- and 15-fold increases for 3-functional Y or tetrahedral-structured displays,(152, 155) while **118K-3** demonstrates a 85-fold increase at comparable concentrations. It is also important to note that the relative increases of TNF-α production in our studies are greater than those of other reports, despite the fact that the ODN employed in our studies is significantly less potent that those used in the above reports (which contain multiple CG motifs).(89) Taken together, comparison of our data with these previous studies illustrates the substantially enhanced potency of these simple ODN-PAA conjugates versus any other multivalent ODN displays yet reported.

The IL-6 results from our studies (8 hours) are difficult to compare directly with other published results, due to the fact that IL-6 is commonly assayed at later time points (24 or 36 hours) because its ODN-induced expression is kinetically slower compared to that induced by other PRR stimuli.(26) Despite the earlier time point utilized in our studies (8 hours), we observe 100-fold increases in IL-6 expression (multivalent vs. monomeric) for the conjugate **118K-10** compared to the previously reported 5-fold increase observed for a 12-functional dendritic structure.(157) Conjugate **118K-3** shows a 30-fold increase, compared to a 10-fold observed by

Nishikawa et al. and an approximately 20-fold increase observed by Li et al. for ODNs at comparable concentrations.(152, 155) We have preliminary data (not shown) suggesting that the production of IL-6 at 24 hours is increased over 1000-fold for both **118K-3** and **118K-10** at 100nM, values much greater than those of any previously reported immunostimulatory complexes. The most critical point of comparison is the change in IL-6 expression observed with increasing valency for the ODN-PAA conjugates. The IL-6 concentrations elicited by **118K-3** are at least 13-fold greater those elicited by **118K-1** at all ODN concentrations, while enhancements reported previously by Li et al. for a 3-functional structure are only 1.5 fold greater than the monofunctional structure.(152) We observe IL-6 concentrations 2.5-fold greater for cells stimulated with **118K-10** versus **118K-3** (even at normalized ODN concentrations), further highlighting the importance of ODN valency. Taken together with previously reported studies, the data reported here illustrate that, at the very least, expression of IL-6 occurs more rapidly in cells exposed to PAA-ODN conjugates of multiple valency than is commonly reported for other multivalent DNA displays.

These PAA-ODN conjugates represent useful probes of biological function that may inform the design of potential therapeutics. As introduced above, no non-aggregated, polymer-based ligands have been previously used to study TLR9 ligand recognition. A significant advantage of the polymer-based approaches versus those based on aggregation or DNA-origami (in addition to the demonstrated increased immunostimulation that the polymer carriers provide), is the substantially enhanced versatility to control both carrier size and valency; this versatility is likely to offer highly attractive routes to finely tune and understand immunostimulatory responses.

Should their use as therapeutics be recommended in the future, the scaffolds could be easily modified to contain degradable esters or other hydrolyzable bonds that would promote decomposition to below the renal filtration threshold (ca. 30-40kDa). Increasing the response to ODN by cells of the innate immune system may aid current efforts to expand vaccine supplies, and the reduction in the quantity of ODN required to elicit an immune response will ensure lower cytotoxicity and cost.(103)

2.4 Conclusion

We have described the synthesis of a novel poly(acrylic acid)-oligodeoxynucleotide conjugate that can control the presentation of ODN by variations in valency or polymer size. By monitoring the in vitro response of the macrophage-like RAW264.7 cell line to these polymers, we have demonstrated that increasing the valency of the ODN conjugates increases the potency of these scaffolds, for eliciting cytokine responses, that are up to 350-fold greater than that of monomeric ODN. We also show that the quality of the activation increases with increasing valency, eliciting high TNF-α and much higher IL-6 production compared to that of the free ODN and polymers bearing a single ODN. TLR9 silencing by siRNA confirms that the immunological properties of these conjugates are mediated by TLR9. Current and future studies include the elucidation of the rules governing cytokine secretion profiles for ODN–PAA conjugates of differing sizes and valences, the role of these factors in inhibition of cytokine secretion, and detailed comparative analysis of intracellular concentrations.

2.5 Acknowledgments

This work was supported in part by the Center for Neutron Science at UD under award (U.S. Department of Commerce) #70NANB7H6178, as well as by the National Institutes of Health (1-RO1-EB006006). Eric A. Levenson was supported (in part) by NIH/NIGMS CBI Training Grant 5T32 GM 08550-15. Its contents are solely the responsibility of the authors and do not necessarily represent the official views NIH or the Department of Commerce. We also acknowledge the kind gift of the RAW264.7 murine macrophage cell-line from Prof. Michele Parent, the confocal imaging expertise of Dr. Jeffrey Caplan, and the TEM expertise of Dr. Shannon Modla (University of Delaware). We would also like to thank Prof. Laurence Eisenlohr (Thomas Jefferson University) for assistance with experimental design.

2.6 Supplementary Information

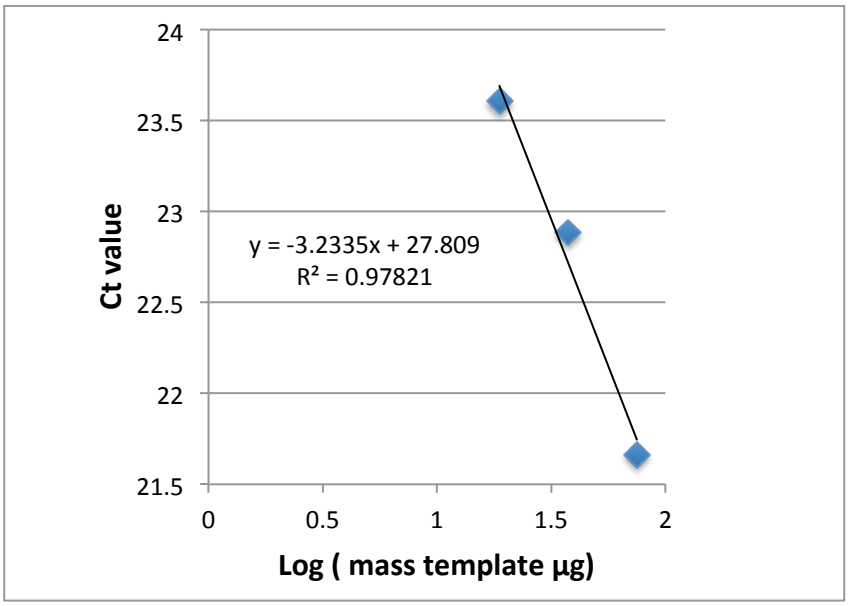

Figure 2.15 Plot of log (mass template) vs, Ct value for TLR9. Slope used for efficiency determination.

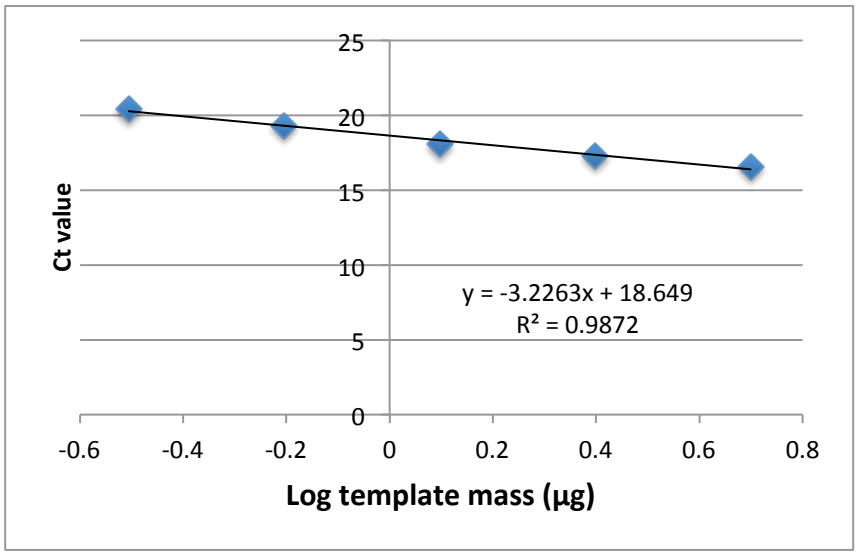

Figure 2.16 Plot of log (mass template) vs, Ct value for ß-Actin. Slope used for efficiency determination.

Chapter 3

DIVERGENT TOLL-LIKE RECEPTOR 9-MEDIATED CYTOKINE PROFILES ARE MODULATED BY CPG OLIGONUCLEOTIDE LIGAND DENSITY

3.1 Introduction

Toll-like receptor 9 is a member of the leucine-rich repeat and toll-like receptor families which is responsible for the immunological detection of bacterial DNA and CpG oligonucleotides (ODN).(71, 208, 209) TLR9 transits from the endoplasmic reticulum to endolysosomal compartments, aided by the chaperones UNC93B1 and heat shock protein gp96, where it colocalizes with and signals activation by DNA or ODN possessing unmethylated CpG motifs.(40, 43, 210) TLR9 activation promotes antigen presentation and T_H1 skewed inflammatory processes.(16, 35, 57-60) However, improper activation or disregulation has been implicated in autoimmune diseases such as systemic lupus erythematosus, psoriasis, heart disease, Sjogren's syndrome, and rheumatoid arthritis.(97, 113, 114, 116) TLR-9 agonist CpG oligonucleotides (ODN) are currently under investigation as vaccine adjuvants for Hepatitis B and C, allergy immunotherapy, and cancer immunotherapy.(4)

TLR9 agonists currently under investigation are 18-24 base pair, single stranded oligonucleotides comprising, at least partially, of a phosphorothioate (PS) backbone.(4) PS modification of ODN increases the strength of hydrophobic protein interactions, significantly increases nuclease resistance and alters biological properties such as enforcing the need of a CpG motif (not strictly necessary for natural phosphodiester DNA).(93, 94, 211) There are currently four classes of ODN, all with different aggregation potentials and secondary structure.(83) These classes originate from the observations that CpG ODN containing poly(guanosine) segments selectively stimulated plasmacytoid dendritic cells (pDC) to express very high quantities of type I interferon (IFN).(45) These ODN did not elicit IFN from B cells, the other major TLR9-expressing human cell subset, which required non-aggregating sequences, and promoted cell maturation for both B cells and pDC.(212) Several other observations have indicated that differences in aggregation or spatial presentation influence TLR9 ligand recognition, including length-dependent responses.(89) A recent report suggests that bacterial DNA and ODN have unique receptors responsible for endocytosis.(54) For these reasons, we choose to examine the role of spatial presentation and number of ODN in TLR9 engagement and activation.

Recognition of multivalent displays of a ligand is a common biological strategy to increase specificity and meet signaling thresholds of a required minimum of receptor interactions, and is commonly employed in carbohydrate-protein interactions.(173, 213, 214) Synthetic or engineered probes have been previously used to elucidate multivalent interactions in bacterial chemotaxis(215), B-cell activation(171), B-cell tolerance(166), sperm binding(167), clathrin-coated pit

formation(159), and T cell receptor signal transduction.(158) Previously we reported the design of multivalent scaffolds of ODN to probe the specificities of TLR9 ligand recognition; these approaches were employed to discern any role of receptor clustering or organization and to determine if significant increases in cytokine expression could be triggered by multivalent displays of ODN on a polymeric scaffold.(216)

Here, we report a systematic investigation of the role of valency on the observed inflammatory response by RAW264.7 macrophages to multivalent ODN-poly(acrylic acid) (PAA) conjugates. We utilized quantitative fluorescent labeling of the scaffold and flow cytometry to determine relative intracellular concentration to correlate those concentrations with cytokine expression induced by the conjugates (ELISA). Cellular responses to TLR9 activation show that there is a critical valency for significant induction of IL-6, TNF-α and IL-10, and that this threshold is related to only valency, not endocytosis or scaffold intracellular concentration. We additionally demonstrate a linear relationship between the density of ODN displayed on the PAA scaffold and IL-10 expression. In contrast, TNF-α shows an inverse relationship between density and expression, but only for higher molecular weight scaffolds. High TNF-α correlates with low density and concomitant IL-10 expression. This defines two key parameters, valency and density, as critical when considering the development of CpG ODN-based therapies.

3.2 Experimental

3.2.1 Materials

Poly(acrylic acid) of 44 kDa and 124 kDa molecular weight (MW), with PDI of 1.08 and 1.24 respectively, was purchased from Polymer Source (Dorval, Quebec) and purified via precipitation in 0.1 M HCl, dissolution in H2O, filtration through a 0.22 μm PES membrane, lyophilization, and then precipitation in ether from an acetone/isopropanol 50/50 solution. Centrifugal filtration units (30 kDa molecular weight cutoff) were purchased from Millipore (Bilerica, MA) and washed with sterile filtered 30% ethanol before use. Fetal bovine serum was purchased from MP Biomedical (Santa Ana, CA) and heat inactivated. All other reagents were used without further modification. The following were purchased from Sigma Aldrich (St. Louis, MO): molecular grade sodium chloride, N-(2-aminoethyl)maleimide trifluoroacetate salt (NEAM) (>95%), dimethyl sulfoxide (≥99%), Ultra TMB HRP substrate, anhydrous sodium phosphate, 1-hydroxybenzotriazole hydrate (HOBT) (97%), triethylamine (TEA) (≥99%) and N-(3-dimethylaminopropyl)-N'-ethylcarbodiimide hydrochloride (EDC) (>99%). SYBR II and Alexa Fluor 647 hydrazide were purchased from Invitrogen (Grand Island, NY). O-(Benzotriazol-1-yl)-N,N,N',N'-tetramethyluronium hexafluoro phosphate (≥99%) (HBTU) was purchased from Chem-Impex (Wood Dale, IL). From Fisher Scientific, (Pittsburgh, PA): 2-(N-

morpholino)ethanesulfonic acid sodium salt (MES) (>99%), high melting temperature agarose, and NUNC maxisorp 96-well ELISA plates. All oligodeoxyribonucleotide (ODN), (sequences 1668AT CG (5'-TCCATGACGTTCCTGATGCTAT), negative control sequence ODN 1668AT GC (5'-TCCATGAGCTTCCTGATGCT AT), 3'-thiolated 1668AT and 3'- Alexa Fluor 647 or 594 (HPLC purified)) were purchased from Integrated DNA Technologies (Coralville, IA).

3.2.2 Proton nuclear magnetic resonance spectroscopy (^{1}H NMR)

All spectra were collected on a Bruker AVIII-600 spectrometer with a 5mm Bruker SMART probe. NMR was performed at room temperature on samples dissolved in deuterium oxide (D_2O) purchased from Cambridge Isotopes. For all polymer samples, 128 or 256 scans were used, with a D1 of 10 s and a 90° pulse program.

3.2.3 Synthesis of Alexa Fluor 647-functionalized PAA

Precipitated and lyophilized PAA (above) was dissolved at 10 mg ml^{-1} in DMSO. To this solution, Alexa Fluor 647 hydrazide (AF647) and HBTU dissolved at 10 mg ml^{-1}, were added to yield a final molar ratio of 1:12 (AF647: HBTU). AF647 to PAA molar ratios were 1.5:1 or 2:1 for conjugates described. Triethylamine was added at a 75:1 molar ratio in excess to AF647. After 24 hours, the mixture was purified/transferred by centrifugal filtration in the following conditions (#washes/

solvent): 3X or until 650 nm absorbance stable/ H_2O, 3X/ 250 mM NaCl and 50 mM phosphate pH 8 and then a final 2 washes against H_2O or D_2O for proton NMR analysis. Before reaction with maleimide (section 3.2.4), the AF647-PAA was washed as above (3X with 75 mM MES pH 6.05). All solutions were prepared with molecular grade water and employed at a 1:50 volume ratio for each spin under sterile conditions. AF647 functionality determined by ^{1}H NMR spectroscopy; patent applications allow chemical structure determination so that 6 unambiguous downfield protons from AF647 can be identified with quantitation (Figs. 4.S1 and 4.S2).(217-219) To determine functionality, the fraction (area of downfield Alexa Fluor protons/ area of PAA backbone protons) was multiplied by the average number (1720 124 kDa PAA or 610 44 kDa PAA) of acrylic acid monomers per polymer. ^{1}H NMR analysis was validated by UV-VIS spectroscopy, using ε=247000 $cm^{-1}mol^{-1}$ to determine the concentration of AF647. The functionality was calculated by dividing the moles of AF647 (UV-Vis) by the number of moles (determined gravimetrically); both the NMR and UV-Vis methods were in agreement. ^{1}H NMR (D_2O): δ= 7.8 (m, 4H, Alexa Fluor), δ=7.3 (m, 2H, Alexa Fluor), δ=1.7-2.25 (bp, C-C**H**-C, PAA), δ=1.1-1.7 (bp, C-C**H2**-C, PAA).

3.2.4 Synthesis of maleimide-functionalized PAA

Maleimide-functional polymer was synthesized as described previously.(216) Briefly, AF647 labeled poly(acrylic acid), EDC, HOBT, and NEAM at a concentration of 10 mg ml^{-1}, were all transferred/dissolved separately into a 75 mM MES solution

buffered at pH 6.05. All solutions were filter sterilized. The EDC, HOBT, and NEAM were added immediately at a molar ratio of 1:3:4 respectively. The amount of EDC employed , as a molar % of all acid, was 8% for **124K-30**, **124K-11** and **124K-5** and 6.5% for **44K-12**, **44K-7, 44K-5**, **44K-4**, **44K-3 44K-2** and **44K-1**. The reaction was conducted under nitrogen, and purified/ transferred via centrifugal filtration to the DNA reaction buffer (50 mM sodium phosphate, 11 mM citrate, 5 mM EDTA at pH 6.6 (degassed)). This maleimide functional polymer was used immediately for synthesis of ODN-PAA.

3.2.5 Synthesis of ODN-functionalized PAA

ODN-PAA synthesis was described previously.(216) Briefly, 3' thiol-modified ODN and DTT were added to a 125 mM phosphate buffer at pH 7.5 to achieve a molar ratio of 25:10:1 (Phosphate:DTT:ODN); the ODN and DTT were incubated for one hour. After incubation, this solution was gravity filtered, via size exclusion chromatography, using sterilized G 15 resin (10X resin to solution volume). The eluate was fractionated and fractions tested for the presence of DNA by UV absorbance (NanoDrop 2000 Wilmington, DE). DNA-positive fractions were combined with maleimide-functionalized polymer from dialysis at ODN:PAA ratios (theoretical yield at 100% reaction) listed in Fig 3.1c. This reaction mixture was placed in a ported bell jar, vacuum purged 3 times with nitrogen with constant stirring, and incubated under nitrogen for 5 days. The polymer control samples (PAA) were diluted 2X into 200 mM pH 8 phosphate buffer and incubated for 24 hours to remove

any residual maleimide. This ODN-free control polymer (**44K** or **124K**) was purified as stated in section 3.2.6.

3.2.6 UV characterization of ODN-PAA conjugates

Reaction mixtures (from above) were diluted with 50 mM phosphate pH 8 buffer made with molecular grade water (Mediatech, Manassas, VA). This solution was filter-sterilized and passed through a centrifugal filter. After filtration, the volume was brought back to 4 ml with molecular grade water and with passage again through a centrifugal filter. This process was repeated until the absorbance at 260 nm was stable. The residual high molecular weight conjugates were analyzed by UV-Vis spectroscopy on a NanoDrop 2000 (Wilmington, DE). The 260 nm absorbance values allow determination of DNA concentration by the calculated extinction coefficient (201,800$cm^{-1}mol^{-1}$ and 200,400$cm^{-1}mol^{-1}$ for the CG and GC sequences respectively (193, 194)); for each synthesis the DNA functionality of the polymer is equal to the DNA concentration of the HMW fraction divided by the polymer concentration. The polymer concentration (UV-Vis) was determined by diving the AF647 concentration (Alexa Fluor 647 ε=247000 $cm^{-1}mol^{-1}$) determined via UV-Vis by the number of AF647 per PAA determined via NMR described above. The DNA concentration in the low-MW fractions was also monitored; the total amount of DNA recoved in all fractions corresponded to the total ODN initially employed during the reaction.

3.2.7 Cell culture

RAW264.7 cells (ATCC, Manassas, VA) were cultured on tissue culture polystyrene plates (Cell Treat; Shirley, MA) in DMEM supplemented with 10 mM HEPES, 55 μM β-mercaptoethanol, antibiotic/ antimycotic, and sodium pyruvate (Invitrogen, Grand Island, NY)), and 10% fetal bovine serum (Mediatech, Manassas, VA). Cells were not cultured past passage 8 and were maintained at between 20 and 90% confluence. Passage was accomplished by a wash with calcium- and magnesium-free PBS and scraping.

3.2.8 Stimulation of RAW264.7 macrophages by ODN-PAA conjugates

RAW264.7 cells were seeded the night before the experiment, at 75,000 cells $well^{-1}$, in a 96-well tissue culture plate. Media was removed from plates and the wells were washed with sterile PBS before addition of the solutions containing the conjugates. ODN and conjugates were heated to 95°C and flash cooled to 4°C before addition to media to remove secondary structure.(220) Conjugates, ODN 1668, and controls were diluted into media at a concentration of 150 nM (or as specified) at a final volume of 200 μL per well. Conjugates were added to the cultured cells, and after 6, 12 or 24 hours, the supernatant was removed and frozen for later ELISA analysis.

3.2.9 Enzyme-linked immunosorbent assay (ELISA)

Analysis of supernatants collected from experiments described above was performed by ELISA on samples diluted with 10% FBS in PBS to measure concentrations within the assays liner range. Monoclonal antibody sets for murine IL-6, IL-10 and TNF-α were purchased from Becton Dickinson (BDbiosciences; San Jose, CA), and used with adherence to the provided protocol. Values represent two independent measurements at two different concentrations for 3 or 4 separate biological repeats. Absorbance measurements were measured using a Perkin Elmer VICTOR^{3}V multilabel counter (Perkin Elmer; Waltham, MA).

3.2.10 Nuclease degradation assay

Kinetic nuclease degradation was measured for both monomeric and conjugated ODN via Exonuclease T (3' exonuclease) and Exonuclease V (5' exonuclease and endonuclease) (New England Biolabs, Ipswich, MA). Reactions were assembled to include 9.9E-11 moles of ODN (oligo and conjugate) and the components (specified below) for nuclease activity to a final volume of 10 µL. Enzyme used was diluted 1:19 (Exo T) and 1:44 (Exo V) in supplied reaction buffer (#4). 2 µL of the dilution was used to provide 0.50 and 0.44 activity units per reaction for Exonuclease T and V respectively. Immediately after dissolution, reactions were conducted at room temperature (Exonuclease T) or 37°C (Exonuclease V) and at the indicated time, quenched by addition of 2 µL stop buffer (275 mM EDTA, 1.5 wt% SDS pH 7) and boiled for 10 minutes. From this inactivated reaction, 2 µL was removed and combined with 6X loading buffer, 0.5 µL SYBR II stain (Invitrogen,

Grand Island, NY) and brought to 12 μL final volume with PCR grade water (BioExpress, Kaysville, UT). This solution was loaded on an 0.8% agarose gel and run for 45 minutes at 60 mV. Gels were immediately imaged for fluorescence on a Typhoon 9410 (GE Healthcare Biosciences, Pittsburgh, PA); excitation 457 nm (laser) and emission 520 nm. Images were saved as *.tiff flies, look-up tables reversed, and bands measured using Image J64 (area kept static). Time 0 is the 0% degradation value. Each time point (0, 0.5, 2, 5 and 8 hours) represents 3 independent replicates.

3.2.11 Endocytosis Analysis

Flow cytometry was used for analysis of the relative intracellular concentration of ODN and ODN-PAA, in addition analysis of the kinetics of endocytosis of the ODN and ODN-PAA conjugates. RAW264.7 cells were cultured as described above. The day of the experiment, cells were washed with phosphate buffered saline (PBS) (no calcium or magnesium), with a second wash for 5 minutes followed by cell scrapping. Live cells were counted using trypan blue and control cells treated with ethidium homodimer (Invitrogen; Grand Island, NY) for 5 minutes to mark dead cell forward scatter/ side scatter (FSC/SSC) parameters for exclusion from flow cytometry analysis (<2%). Treated cells were aliquoted at a concentration of 500,000 cells per tube (Falcon 352054). These cells were centrifuged (300*g* for 5 minutes room temperature) and resuspended in 500 μL 37°C DMEM containing 250 nM conjugate (normalized by ODN) or Alexa Fluor 647 ODN and polymers **44K** or **124K** at 250 nM. To ensure fluorescence values represent only endocytosis values, three replicates

were prepared in 4°C DMEM, and maintained at 4°C for 90 minutes to mark cell surface labeling. Treated cells were incubated at 37°C for 90 minutes, three centrifugation and wash cycles at 4°C, resuspended in 300 μL 4°C flow buffer (phosphate buffered saline, 1% BSA, and 2.5 mM EDTA pH 7), and incubated on wet ice until measurement. The intracellular fraction is the difference in the mean fluorescence values at 37°C and 4°C; this difference is the number reported.

3.2.12 Inhibition of endocytosis

The mechanism of endocytosis was analyzed using the drug monodansylcadaverine, which inhibits clathrin-mediated endocytosis. RAW264.7 cells were cultured as described above. The day of the experiment, cells were washed with PBS (no calcium or magnesium), with a second wash for 5 minutes followed by cell scraping. Live cells were counted using trypan blue. Treated cells were aliquoted at a concentration of 500,000 cells per tube (Falcon 352054). These cells were centrifuged (300*g* for 5 minutes room temperature) and resuspended in 250 μl 37°C DMEM containing the drug monodansylcadaverine (MDC) at the concentration specified (or just in DMEM for control cells) and were incubated at 37°C for 30 minutes to pretreat cells. After 30 minutes pre-warmed DMEM (250 ml) containing MDC at the concentration specified (and two times the working concentration of Alexa Fluor 647 conjugate or ODN), was added to cells; working concentrations employed were 250 nM conjugate (normalized by ODN), polymers **44K** or **124K** at 250 nM or 1.75 μM fluorescent 1668. After 30 minutes, cells were processed with

three centrifugation/ PBS wash cycles at 4°C, resuspended in 300 μL 4°C flow buffer (phosphate buffered saline, 1% BSA, and 2.5 mM EDTA pH 7), and incubated on wet ice until measurement. The percent inhibition reported is the percent reduction in the geometric mean fluorescence compared to that of untreated cells. Cell detection was conducted on a BD LSR II cell analyzer (BDbiosciences, San Jose, CA); a total of 10,000 events were collected within a gate set using FSC/ SSC parameters determined above. Each sample (replicates of three) was analyzed (FlowJo software, Tree Star; Ashland, OR) to determine the geometric mean fluorescence intensity.

3.2.13 Conjugate endocytosis and subcellular localization

Confocal microscopy and immunocytochemistry were used to probe the colocalization of endocytosed conjugates and ODN with the endosomal markers early endosomal antigen 1 (EEA-1) and lysosomal-associated membrane protein 1 (LAMP-1). RAW264.7 cells were seeded at 300,000 cells per coverslip on super resolution quality coverslips (Schott, Germany) placed in the bottom of a standard 12-well plate (Corning, Tewksbury, MA) the day before the experiment. This seeding density gave a confluence of approximately 80-90% for the experiment. Cells were carefully washed once with PBS prior to use. Either **44K-2** or Alexa Fluor 594 ODN 1668 (brighter and more stable than Alexa Fluor 647) were applied to cells in the 12-well plate at 1 μM and 4 μM, respectively. After the time indicated, media was aspirated and cells were washed twice with 2 ml 4°C PBS. Cells were then immediately fixed for 10 minutes using 4% recently depolymerized paraformaldehyde and washed 2 times using PBS

with 0.05% Tween 20 (PBS-T). Permeabilization was accomplished using 0.4% Triton X-100 for 10 minutes, and cells were washed twice with 2 ml PBS. Cells were blocked by treatment with 100mM glycine in PBS-T for 20 minutes and aspirated, and then were treated for 1 hour with 2% bovine serum albumin (BSA), 5% Donkey Serum (Invitrogen), 0.1% Triton X-100 in PBS-T at room temperature (or overnight at 4°C). EEA-1 and LAMP-1 were labeled using Santa Cruz antibodies E-8 and E-5, respectively, at a dilution of 1:40 in 1% BSA, 1% Donkey Serum, and 0.25% Triton X-100 overnight at 4°C. Cells were washed twice with 2 ml PBS for 15 minutes each wash. Secondary Alexa 488 donkey anti mouse (Jackson Immunolabs) was diluted at 1:150 into PBS-T, applied for 1 hour, and again washed twice for 15 minutes with 2 ml PBS-T (PBB-Tween 20) at room temperature. Coverslips were removed from the 12-well plate, dried by blotting the edge with adsorbent paper, and applied to microscopy slides (Fisher Scientific) with prolong gold (Invitrogen). Slides were allowed to dry for two days in the dark and were then stored at 4°C until imaged. Imaging was conducted using a 780 Zeiss confocal microscope with 32 channel ultra sensitive GaAsP detectors (Carl Zeiss Microscopy; Thornwood, NY) with a 40 X water lens (1.2 NA) with all images at 1056x1056 pixels. Z-stacks used for colocalization analysis are comprised of the 25-28 images with identical imaging settings. Four imaging locations were chosen randomly to prevent bias. The images were imported into Volocity (Perkin Elmer; Waltham, MA) and each Z-stack analyzed for pixel colocalization from the EEA-1 or LAMP-1 Alexa Fluor 488 channel with the **44K-2** or Alexa Fluor 594 ODN 1668 channel. Colocalization detection parameters were limited to sizes of 300 nm to 500 nm and a brightness empirically determined to

yield only events detectable upon manual inspection. These parameters, once set, were used for all images of the same primary antibody.

3.2.14 siRNA transfection

Transfection was accomplished using the Qiagen HiPerFect reagent and protocol. Briefly, RAW264.7 cells (75 μL) were plated in a Costar 48-well cell culture plated at 150,000 cells well^{-1} in culturing media before transfection. TLR9-specific siRNA sc-40271 or control siRNA sc-37007 (Santa Cruz Biotechnology Santa Cruz, CA) was diluted to a concentration of 100 nM in 75 μL OptiMEM (Gibco), with addition of 3 μL HiPerFect and mixing by vortexing. Samples were incubated for 10 minutes at room temperature. After incubation, the siRNA mixture was added dropwise to media containing cells and mixed by pipetting 3 times. Samples were incubated for 5 hours under cell culturing conditions and then supplemented with 300 μL culturing media. Stimulation with 150 nM **44K** or **44K-12**, or with 1.5 μM ODN 1668, was started 24 hours later. Supernatants were collected 24 hours after the start of stimulation and were assayed for TNF-α via ELISA.

3.2.15 Limulus amoebocyte assay

The fluorogenic limulus amoebocyte assay (Lonza, Allendale, NJ) was conducted on all materials in accordance with the manufacturer-provided protocol. Conjugates, purified polymer and ODN were tested for endotoxin and found to be <

0.1 endotoxin units ml^{-1} or 10 pg ml^{-1} at concentrations used in this work. The data is displayed in Fig. 3.14.

3.2.16 Data analysis and statistics

Statistical analysis was calculated on Kaleidagraph (Synergy Software, Reading, PA); statistical significance (p) was calculated via one-way ANOVA with post hoc Tukey's analysis at the 99% confidence level. A minimum of three independent samples were used for analysis. All experiments were repeated a minimum of three times for validation.

3.3 Results

3.3.1 ODN-PAA conjugate design

Poly(acrylic acid) of 44 kDa or124 kDa was employed as a negatively charged and highly water soluble scaffold for the presentation of single-stranded CpG oligonucleotides. The synthesis scheme, relying upon the Michael-type addition of a 3' thiolated ODN to maleimide-functional PAA, is shown in Fig. 3.1a. This synthesis scheme was previously employed by us, demonstrating high efficiency, to develop a series of multivalent ODN-PAA conjugates.(221) A deviation from that reported synthesis is the conjugation of the fluorescent dye Alexa Fluor 647 (AF647) to the scaffold with the extent of labeling determined by proton nuclear magnetic resonance

spectroscopy (NMR). This internal molecular standard allowed more accurate determination of functionality via the characteristic UV-Vis absorbance

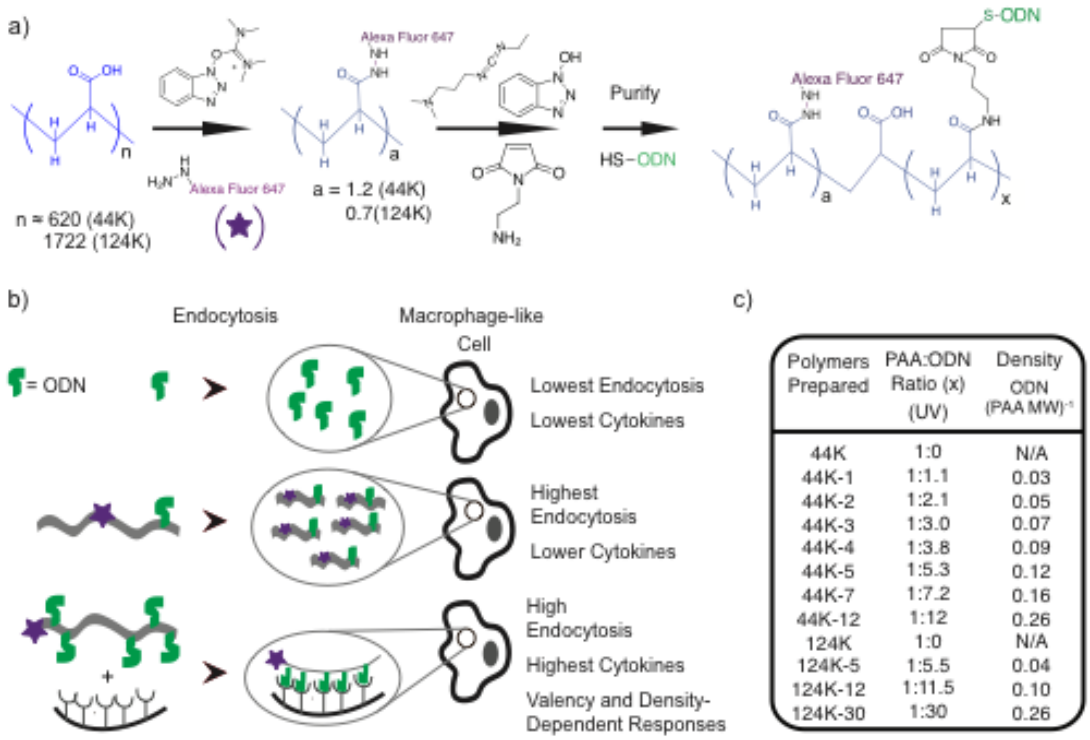

Polymers Prepared	PAA:ODN Ratio (x) (UV)	Density ODN (PAA MW)$^{-1}$
44K	1:0	N/A
44K-1	1:1.1	0.03
44K-2	1:2.1	0.05
44K-3	1:3.0	0.07
44K-4	1:3.8	0.09
44K-5	1:5.3	0.12
44K-7	1:7.2	0.16
44K-12	1:12	0.26
124K	1:0	N/A
124K-5	1:5.5	0.04
124K-12	1:11.5	0.10
124K-30	1:30	0.26

Figure 3.1 The chemical synthesis scheme and molecular compositions, observed activities, and physical properties of ODN-PAA conjugates prepared for this work. A schematic representation of the synthesis scheme, a), showing the number of monomer units (n), fluorescent label (a), and ODN (x). The observed biological properties for ODN, monovalent conjugate and multivalent conjugates is shown in b). The value of (x) and the corresponding density for each conjugate is shown in c).

values of ODN 1668 (260 nm) and Alexa Fluor 647 (650 nm). The extent of AF647 labeling by ^{1}H NMR allowed calculation of the number of moles of polymer and the ODN functionality via division of the ODN concentration by the polymer

concentration (UV-Vis). The polymers prepared for this work, their ODN functionality and resulting density, are given in Fig. 3.1c.

3.3.2 Competent TLR9 activation requires a minimal valency

We had previously shown an IL-6 expression enhancement of 37-fold, much greater than the 2-fold TNF-α by increasing ODN-PAA conjugate valency from 1 to 10. We hypothesized that there was potentially a critical valency necessary for competent activation of TLR9, and thus used IL-6 expression as a measure. RAW264.7 macrophages were exposed to conjugates **44K-1**, **44K-2**, **44K-4**, **44K-5**, **44K-7** (normalized to 150 nM ODN), ODN 1668AT (150 nM), polymer **44K** and LPS (10 ng ml^{-1}) for 12 (dark grey) and 24 hours (light grey), results are shown in Fig. 3.2. There is a steady increase in IL-6 expression with increasing valency from **44K-1** to **44K-7**. However, there is a statistically significant difference between **44K-4** and **44K-5** at 12 hours with 6 ±1 and 13 ± 0.5 pg ml^{-1} respectively ($p = 0.0079$) and at 24 hours with 8 ± 2 and 17 ± 2 pg ml^{-1} respectively ($p = 0.0203$). These values are two-fold different despite very similar valencies and identical ODN concentrations. Between **44K-2** and **44K-4** and between **44K-5** and **44K-7** there are no significant differences (^).

Cytokine expression is proportional to intracellular concentration, so to determine if this was the source of the statistically relevant increase, we examined the relationship between IL-6 expression and intracellular quantity of scaffold, and therefore, ODN. Using the relative scaffold concentrations and the known

functionality of the conjugates, the relative ODN concentrations can also be calculated. RAW264.7 cells were exposed to conjugates **44K-1**, **44K-4**, **44K-5** and the high valency **44K-12** (normalized to 150 nM ODN) along with AF647-labeled ODN 1668AT (150 nM) for 90 minutes at 4°C or 37°C conditions. Subtraction of the 4°C values from the 37°C values provides a measure of the intracellular quantity of the scaffold by removing the surfaced labeled component. Intracellular scaffold (dark grey) and ODN (blue) values are shown in Fig 3.3. The difference in ODN and conjugate endocytosis is striking with ODN 1668AT endocytosed 29-fold less than **44K-1** ($p < 0.0001$). Among the conjugates, **44K-1** has the highest relative scaffold endocytosis ($p < 0.0001$), with the trend of decreasing internalization with increasing valency. Importantly, **44K-4** and **44K-5** are not significantly different in intracellular scaffold concentration. **44K-4** and **44K-**5 do have relevant differences in delivered ODN ($p < 0.0001$), however, the higher valency **44K-7** (and **44K-12** data not shown) shows no discernable increase in observed IL-6 expression despite the higher valency and greater intracellular ODN concentration. These data demonstrate that the statistically significant increase in IL-6 expression for **44K-5** is due to the increase in valency from 3.8 (**44K-4)** to 5.3 (**44K-5**) and suggests maximal activation for a given scaffold, is achieved by an ODN valency which provides an optimal number of ligands for receptor complex activation.

3.3.3 IL-10 expression is directly proportional to ODN density, not valency

With the observation that IL-6 expression was sensitive to an ODN threshold, we sought to determine if this also applied to other cytokines. Initial experiments indicated IL-10 expression induced by ODN-PAA conjugates were different

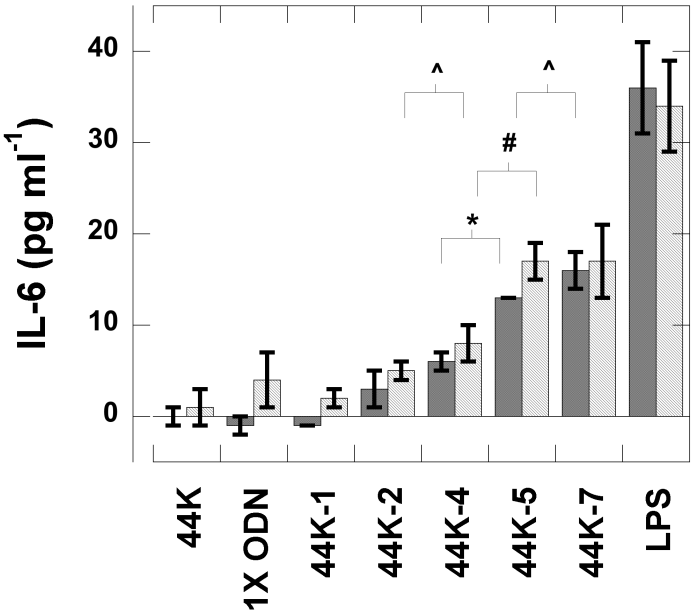

Figure 3.2 Expression of IL-6 in response to ODN-PAA conjugates of increasing valency. RAW264.7 macrophages were exposed to polymer **44K** (150 nM), ODN 1668 (150 nM), **44K-1**, **44K-2**, **44K-4**, **44K-5**, **44K-7** (normalized to 150 nM ODN) or LPS (10 ng ml^{-1}). Cell supernatants were collected after 12 (dark grey) or 24 (light grey) hours and assayed for IL-6 concentration by ELISA. A significant difference in IL-6 expression was only observed between **44K-4** and **44K-5** with p = 0.0079 for 12 hours (*) and p = 0.0203 for 24 hours (#). No significant differences exist between conjugates of similar valencies (^). Error bars represent the standard deviation of the average of three independent samples.

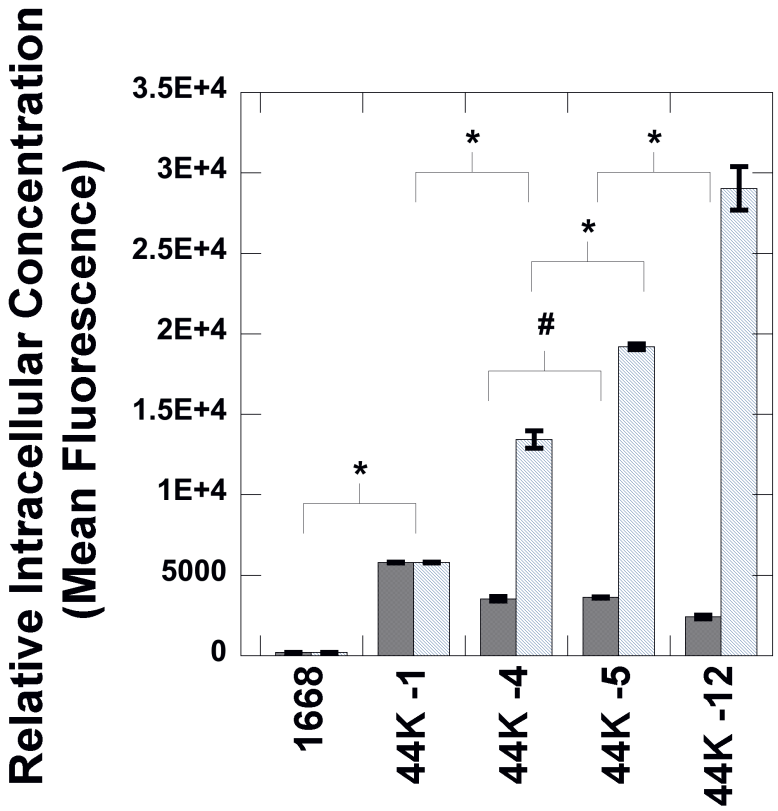

Figure 3.3 The relative intracellular scaffold and ODN concentrations (Scaffold* ODN functionality) measured through fluorescence emission by flow cytometery. RAW264.7 macrophages were exposed to AF647 labeled ODN 1668 (150 nM), **44K-1**, **44K-4**, **44K-5** and **44K-12** (normalized to 150 nM ODN) for 90 minutes. Values displayed are mean fluorescence intensity for cells treated at 37°C (intracellular), less cells treated at 4°C (surface labeling) for true intracellular concentration. Both the relative scaffold (dark grey) and ODN (scaffold * functionality) (blue crosshatched) quantities are displayed. No significant difference exists between **44K-4** and **44K-5** scaffold values (#). Significant difference $p < 0.0001$ (*). Error bars represent the standard deviation of the average of three independent samples.

than that observed for IL-6. We assayed IL-10 expression in response to an expanded set of conjugates using scaffold of two molecular weights (44 kDa and 124 kDa). The 124kDa-based conjugates were synthesized to match valency (**44K-5** with **124K-5** and **44K-12** with **124K-12**) as well as ODN density (**44K-12** with **124K-30**) to determine if any observed responses were from specific valencies or density of ODN, not specific polymer scaffold effects. The inflammatory response of RAW264.7 macrophages exposed to ODN 1668AT and a series of conjugates, measured as IL-10 concentration determined by ELISA, is shown in Fig. 3.4. The full data set including all positive and negative controls in in Fig. 3.15. This response was monitored over the course of 24 hours with measurements at 6 (dark grey), 12 (light grey), and 24 hours (open bar). Similar to the results for IL-6, there is an increase in cytokine expression with increasing valency and with increasing time for conjugates of both scaffolds. However, conjugates of the same valency did not elicit the same response; IL-10 concentrations were significantly different at 24 hours between **44K-5** and **124K-5** (283 ± 18 and 102 ± 5, $p < 0.005$) and between **44K-12** and **124K-12** (537 ± 32 and 233 ± 6, $p < 0.0001$). This data suggested the smaller 44 kDa scaffold was more potent for Il-10 expression.

We then further analyzed the recorded IL-10 concentrations of Fig. 3.4 against the ODN density of each conjugate, a measure of the spatial density of presentation; results are reported in Fig. 3.5. Remarkably, the concentrations at 6 (circles), 12 (squares) and 24 hours (triangles) are linear with respect to ODN density, regardless of the scaffold. A linear fit of the values for 6, 12 and 24 hours have coefficients of determination of 0.981, 0.990 and 0.977 respectively, demonstrating the high degree

of linearity. This data suggests ODN density, more than valency, of ODN-PAA conjugates has a profound impact on TLR-9 induced expression of IL-10.

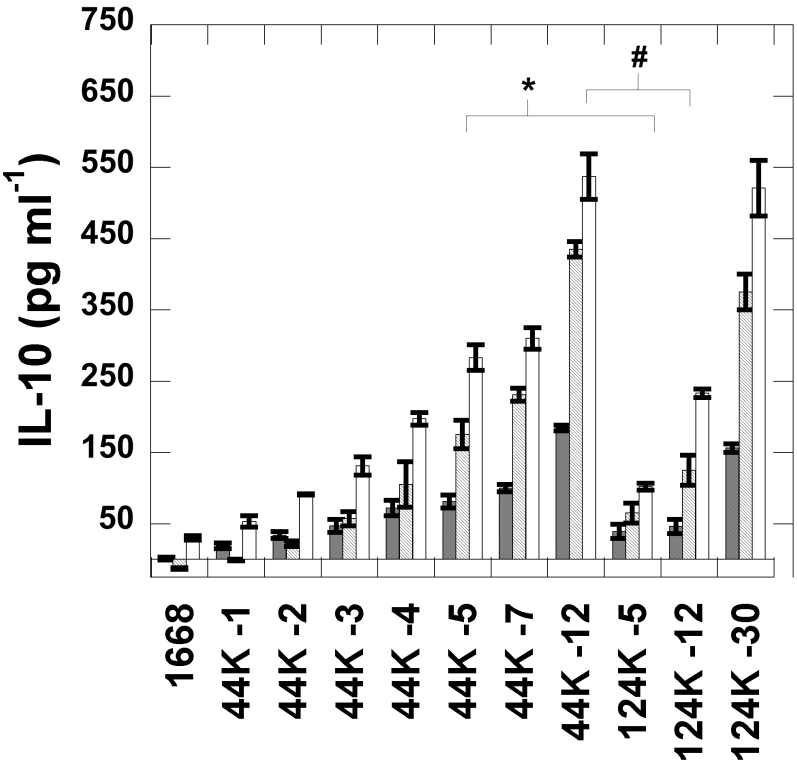

Figure 3.4 The IL-10 expression of RAW264.7 cells exposed to to ODN-PAA conjugates of increasing valency. RAW264.7 macrophages were exposed to polymer ODN 1668 (150 nM) and **44K** or **124K**-based conjugates (normalized to 150 nM ODN). Cell supernatants were collected after 6 (dark grey), 12 (light grey) or 24 hours (open bar) and assayed for IL-10 concentration by ELISA. Significant differences highlighted are $p < 0.005$ (*) and $p < 0.0001$ (#). Error bars represent the standard deviation of the average of four independent samples.

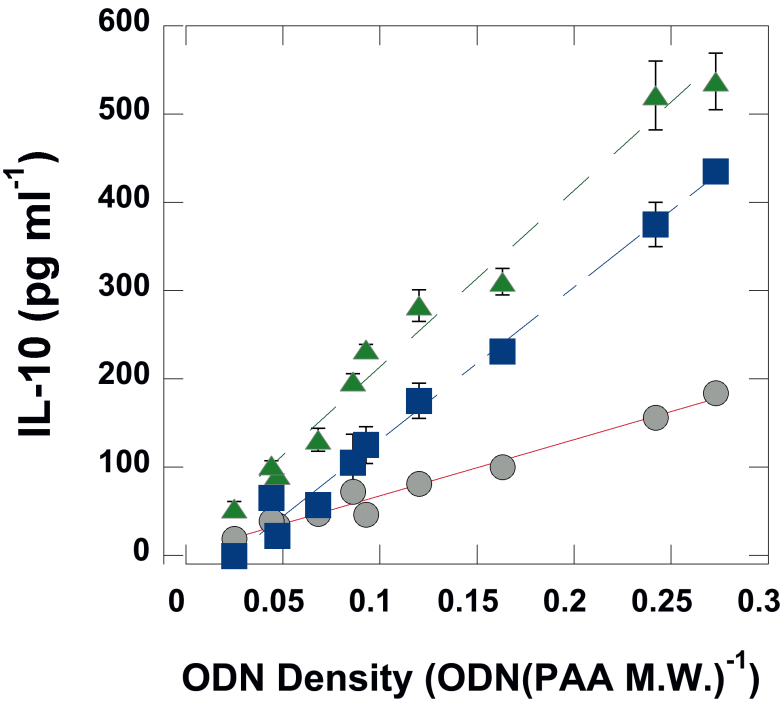

Figure 3.5 The inflammatory response to ODN-PAA conjugates of increasing valency shown in Fig.3.4 (IL-10), and graphed against the ODN density (Fig 1c). Values for 6 hour (circles), 12 hour (squares), or 24 hour (triangles) time points were fit to a linear equation with corrected R^2 values of 0.981 (solid), 0.990 (long dash), and 0.977 (short dash), respectively. Error bars represent the standard deviation of the average of four independent samples.

3.3.4 TNF-α expression is scaffold-dependent and inversely proportional to density

We had previously observed a correlation between TNF-α expression and valency but a less significant role in increased valency as compared to that observed for IL-6.(216) We again used the expanded set of set of conjugates and assayed RAW264.7 macrophage inflammatory response, as indicated by TNF-α concentration,

with the results in Fig. 3.6. The full data set, including all positive and negative controls is shown in Fig 3.16. We again observed an increase in TNF-α concentration with increasing valency for the **44K** scaffold conjugates, but a distinct expression profile for the **124K** scaffold conjugates. **124K-5** elicits the greatest 24 hour TNF-α concentration of 2646 ± 74. This value is 5-fold higher than the isovalent **44K-5** (522 ± 39) and 30-fold higher than the similar density **44K-2** (89 ± 5) ($p < 0.0001$). **124K-12** (1112.3 ± 124) is not significantly different from **44K-12** but is 2 to 3.5-fold greater than similar density **44K-4** (322 ± 9) and **44K-5** (522 ± 39).

We again compared the observed TNF-α concentrations reported in Fig. 3.6 and plotted them against the ODN density (Fig. 3.7). We observe a less linear correlation between TNF-α concentration and density at 6 hours ($R^2 = 0.933$, red line) (circles) than that observed for IL-10, but then quickly lose linearity with time at 12 ($R^2 = 0.533$, blue dash) and 24 hours ($R^2 = 0$, not shown). This data suggests the TLR9 receptor complex can differentially identify ligands of high and low valency with distinct associated cytokine expression profiles.

3.3.5 Intracellular ODN concentration is dosage dependent

Given the significant differences in response between the isovalent **44K-5** and **124K-5**, we assayed the relative intracellular concentrations of both to determine if differences in intracellular concentration could explain these distinct cytokine expression profiles. We exposed RAW264.7 macrophages to conjugates **44K-1** (triangles), **44K-5** (open diamond), **124K-5** (blue diamond, blue line) and **124K-30**

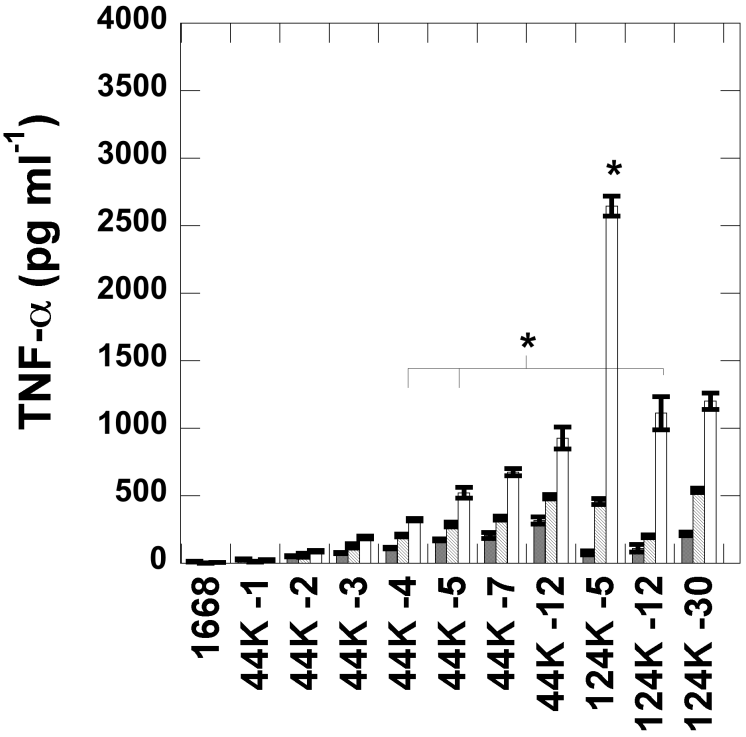

Figure 3.6 The TNF-α expression of RAW264.7 macrophages exposed to ODN-PAA conjugates of increasing valency. RAW264.7 macrophages were exposed to polymer ODN 1668 (1X ODN) and **44K** or **124K**-based conjugates (normalized to 150 nM ODN). Cell supernatants were collected after 6 (dark grey), 12 (light grey) or 24 hours (open bar) and assayed for TNF-α concentration by ELISA. Significant differences highlighted are $p < 0.0001$ (*). Error bars represent the standard deviation of the average of four independent samples.

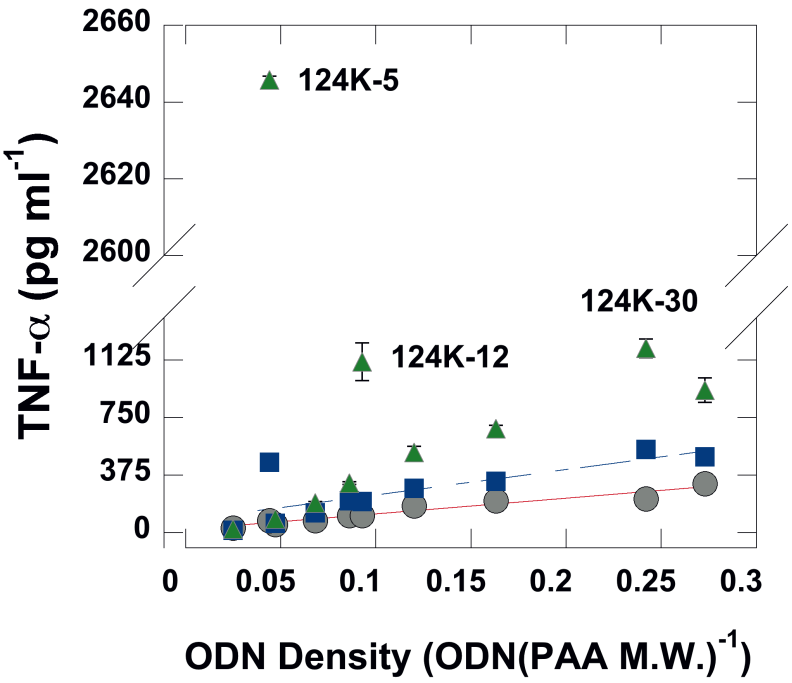

Figure 3.7 The inflammatory response to ODN-PAA conjugates of increasing valency shown in Fig.3.6 (TNF-α), and graphed against the ODN density (Fig 1c). Values for 6 hour (circles), 12 hour (squares), or 24 hour (triangles) time points were fit to a linear equation with corrected R^2 values of 0.933 (red), 0.533 (blue dashed), and 0 (not shown), respectively. **124K**-based scaffolds are labeled. Error bars represent the standard deviation of the average of four independent samples.

(closed circle, blue line), normalized to 150 nM ODN, in addition to the two scaffolds **44K** (cross) and **124K** (cross, blue line), used at a scaffold concentration identical to that of **44K-5** and **124K-5** (30 nM) over 2 hours and measured intracellular quantity at 20, 60, and 120 min was measured via mean fluorescence intensity by flow cytometry (Fig. 3.8). Most importantly, there was no observed difference in the intracellular scaffold or ODN concentrations of **44K-5** and **124K-5** (ODN quantity Fig. 3.9). This highlights the distinct cytokine profiles observed for **44K-5** and **124K-5** for IL-10 and

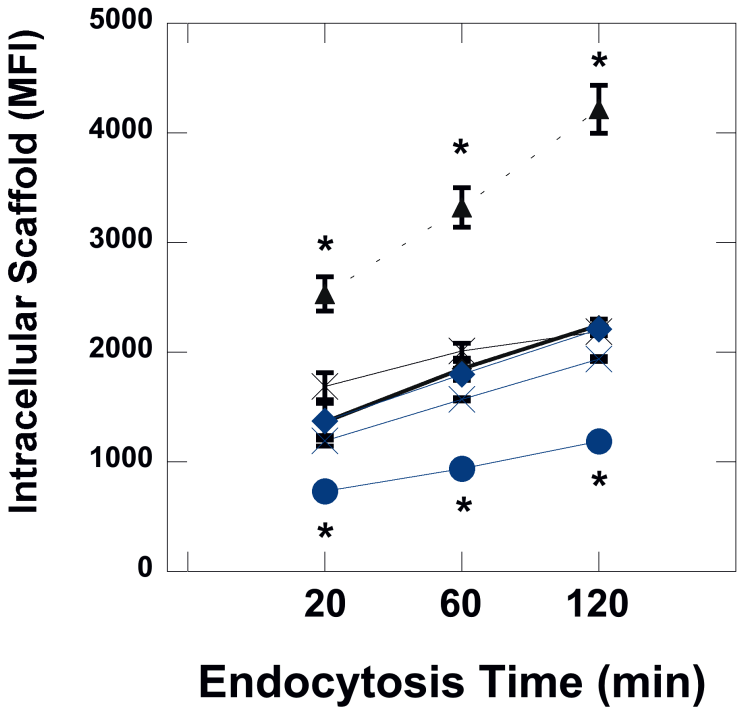

Figure 3.8 Kinetics of endocytosis for selected conjugates displayed as relative intracellular scaffold concentration. RAW264.7 cells were exposed to polymers **44K** (black cross) and **124K** (blue cross) (30 nM) and conjugates **44K-1** (triangles), **44K-5** (open diamond), **124K-5** (blue diamond) and **124K-30** (blue circle) (normalized to 150 nM ODN) for the time indicated and measured for mean fluorescent intensity by flow cytometry. Values displayed are mean fluorescence intensity for cells treated at 37°C (intracellular), less cells treated for 90 minutes at 4°C (surface labeling) for true intracellular concentration. No significant difference exists between **44K-4** and **44K-5** scaffold values. Significant difference $p < 0.0001$ (*) from **44K, 124K, 44K-5 and 124K-5**. Error bars represent standard the deviation of the average of three independent samples.

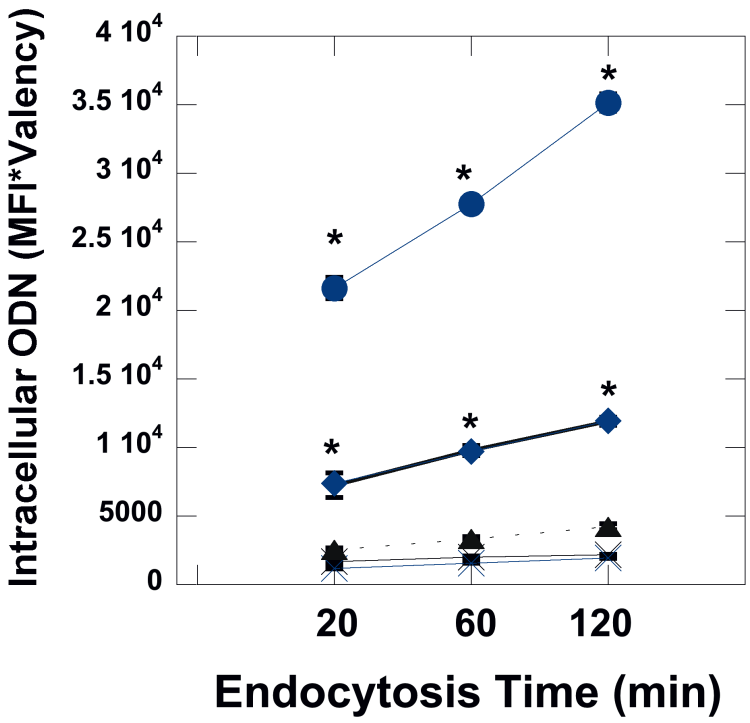

Figure 3.9 Kinetics of endocytosis for conjugates from Fig. 3.8 displayed as relative ODN concentration (scaffold * ODN valency). Samples shown are **44K** (black cross) and **124K** (blue cross) (30 nM) and conjugates **44K-1** (triangles), **44K-5** (open diamond), **124K-5** (blue diamond) and **124K-30** (blue circle) for the time indicated and measured for mean fluorescent intensity by flow cytometry (scaffold concentration) multiplied by the conjugate ODN functionality. No significant difference exists between **44K-4** and **44K-5** ODN values. Significant difference $p < 0.0001$ (*) from **44K, 124K and 44K-1**. Error bars represent the standard deviation of the average of three independent samples.

TNF-α expression are not the result of differences in delivery, but of the ODN density. We observe, in agreement with Fig. 3.3, that the conjugates of lowest functionality (**44K-1**), applied at the highest scaffold concentration, have the greatest intracellular concentration; this was true at all time points (2531 ± 157, 3320 ± 179, 4217 ± 219, p

< 0.0001). **124K-30**, with the lowest applied scaffold concentration had the lowest intracellular scaffold concentration and this was also true across all time points (731 ± 27, 938 ± 9, 1188 ± 22, $p < 0.0001$).

3.3.6 ODN-PAA endocytosis is clathrin-mediated

Given the striking difference in intracellular quantity of ODN 1668 and **44K-1** in Fig. 3.3 and the equivalent endocytosis of scaffold and conjugate shown in Fig. 3.8 we wanted to determine if the mechanism of endocytosis for ODN-PAA conjugates was the same for PAA and ODN. We employed monodansylcadaverine (MDC), an inhibitor of transglutaminase, a enzyme which is necessary for clathrin-dependent receptor-mediated endocytosis via protein cross-linking.(222, 223) ODN endocytosis is receptor mediated(51, 54, 67), thus we focused on this pathway. We examined whether endocytosis of AF647-labeled ODN 1668AT (blue square), scaffold **44K** (cross), **44K-1** and **44K-5** was inhibited in RAW264.7 macrophages treated by a titration of monodansylcadaverine from 100 to 400 μM. Inhibition is indicated by a reduction of mean fluorescence as measured by flow cytometry. The mean fluorescence was converted to percent conjugate endocytosed. The untreated (no drug) samples were normalized to 100% endocytosed and data are shown in Fig. 3.10. All samples showed a reduction in mean fluorescence intensity at the lowest drug concentration of 100 μM. **44K**, **44K-1** and **44K-5** continued to show reduction in endocytosis with 31 ± 4, 34 ± 3 and 11 ± 1 respectively with increasing drug concentration. The crucial finding is endocytosis of the multivalent **44K**-5 can be

inhibited ~ 90% and is significantly different from other samples ($p < 0.0001$), demonstrating clathrin-mediated endocytosis to be the primary mechanism of internalization. **44K** of the same concentration as **44K-5** is not inhibited as significantly (31 ± 4 vs. 11 ± 1) and is inhibited less than **44K-**1 when tested at the same scaffold concentration (250 nM) (34 ± 3 vs. 48 ± 2, data not shown) suggesting that PAA endocytosis is not as dependent on a clathrin-mediated mechanism. Interestingly, ODN 1668AT shows an increase in endocytosis above 100 μM MDC (statistically significant at 400 μM MDC ($p < 0.0001$). This data suggests clathrin-mediated endocytosis to be common among ODN, scaffold and conjugates but exclusive to only to the conjugate **44K-5**.

3.3.7 ODN-PAA conjugates preferentially and rapidly colocalize with late endosomes

We employed immunocytochemistry and confocal microscopy to determine if observed differences in endocytosis mechanism correlated with alteration of intracellular trafficking. Subsequent to endocytosis, CpG ODN traffic through early endosomes into late endosomes where TLR9 activation takes place.(210) Early endosomal antigen 1 (EEA-1) is a widely used marker for early endosomes and the lysosomal associated membrane protein 1 (LAMP-1) is a similarly used protein marker for late endosomes or endolysosomal compartments.(210, 224, 225) We examined the number of colocalization events for ODN 1668AT (black), **44K** (grey) and **44K-2** (blue) with EEA-1 or LAMP-1 staining endosomes over two hours

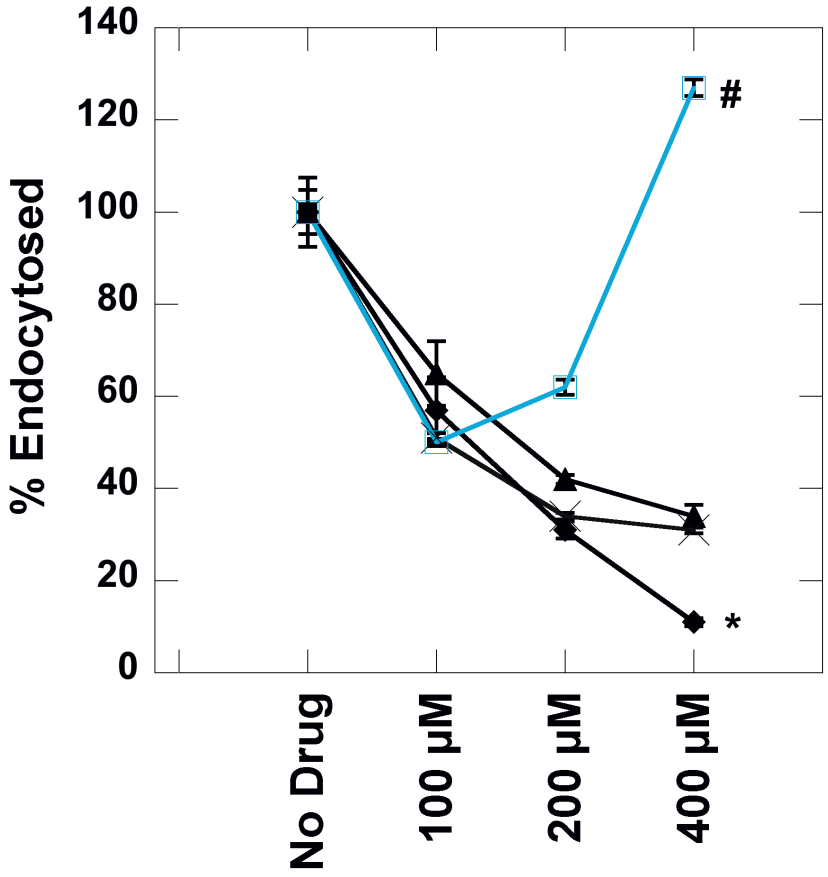

Figure 3.10 Inhibition of endocytosis for AF647 labeled ODN 1668 (250 nM) (blue square), **44K** (47 nM) (black cross) and conjugates **44K-1** (250 nM) (triangles) and **44K-5** (250 nM ODN) (diamond) by monodansylcadaverine. Inhibition was indicated by a reduction in mean fluorescent intensity from untreated samples by flow cytometry. Significant difference were observed ($p < 0.0001$ (*)) between **44K** and **44K-1** at this drug concentration (or $p < 0.0001$ (#) from all other samples). Error bars represent the standard deviation of the average of three independent samples.

and report the results in Figs. 3.11 (EEA-1) and 3.12 (LAMP-1) Consistent with the low endocytosis observed (Fig. 3.3), ODN 1668AT demonstrates much lower

colocalization at 15 and 120 minutes for both EEA-1 (47 ± 23 and 11 ± 6) and LAMP-1 (69 ± 12 and 33 ±7) despite a 4-fold higher application concentration (4μM and 1 μM ODN for 1668AT and **44K-2** respectively). These values are also significantly lower than those observed for **44K-2** at 15 and 120 minutes for EEA-1 (249 ±86 and 1496 ± 211, p = 0.021) and LAMP-1 (950 ± 272 and 2027 ± 500, p = 0.002). There are also differences in colocalization between **44K-2** and the scaffold **44K. 44K** presents significantly enhanced colocalization with EEA-1 at 15 (848 ± 156) and 120 minutes (2346 ± 411) ($p < 0.004$). This does not translate to LAMP-1 colocalization where **44K** where low colocalization is observed at both 15 (130 ± 43) and 120 minute (911 ± 230). Critically, whereas ODN 1668AT colocalization reduces with time, **44K-2** shows an increase over the time assayed. These data demonstrate much greater endocytosis of ODN-PAA than ODN, as shown in Fig. 3.3. The enhancement in endocytosis is concomitant with favorable delivery of ODN-PAA to TLR9-signaling late endosomes; delivery to late endosomes is not observed with the PAA scaffold.

3.3.8 Agonistic ODN-PAA conjugates demonstrate strong endo- and exonuclease resistance

We explored the impact of ODN PAA conjugation on their nuclease degradation profiles, on account of the fact that the ODN used in this work are phosphodiester-based, and susceptible to nuclease degradation. **44K-1** was chosen to represent all conjugates since degradation of the single ODN would be the most apparent. ODN-

PAA conjugate **44K-1** (triangles) and ODN 1668AT (circles) were assayed in vitro for nuclease degradation by Exonuclease T (open black) (ssDNA 3'exonuclease) and

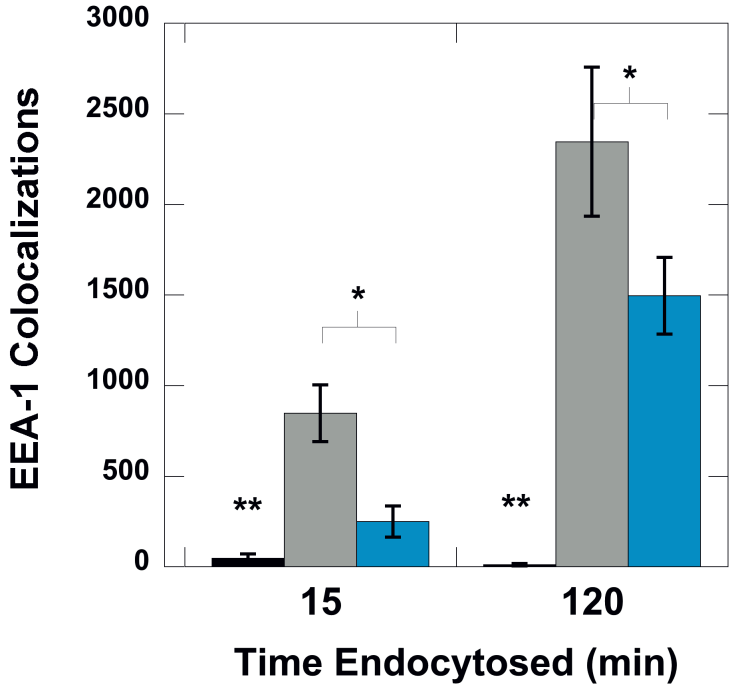

Figure 3.11 Colocalization of fluorescent ODN, polymer **44K**, or conjugate **44K-2** with the early endosomal protein early endosomal antigen 1 (EEA-1) measured by confocal microscopy and image analysis. RAW264.7 cells were exposed to AF594 labeled ODN 1668 (black) (4 μM), **44K** (grey) (0.5 μM) and conjugate **44K-2** (blue) (1 μM ODN, 0.5 μM scaffold), processed for immunocytochemistry, imaged by confocal microscopy, and analyzed for number of colocalization events with EEA-1 staining vesicles. Significant difference $p < 0.004$ (*) or $p = 0.021$ (**). Error bars represent standard deviation of four separate Z-stacks. Data are representative of the average of over three independent experiments.

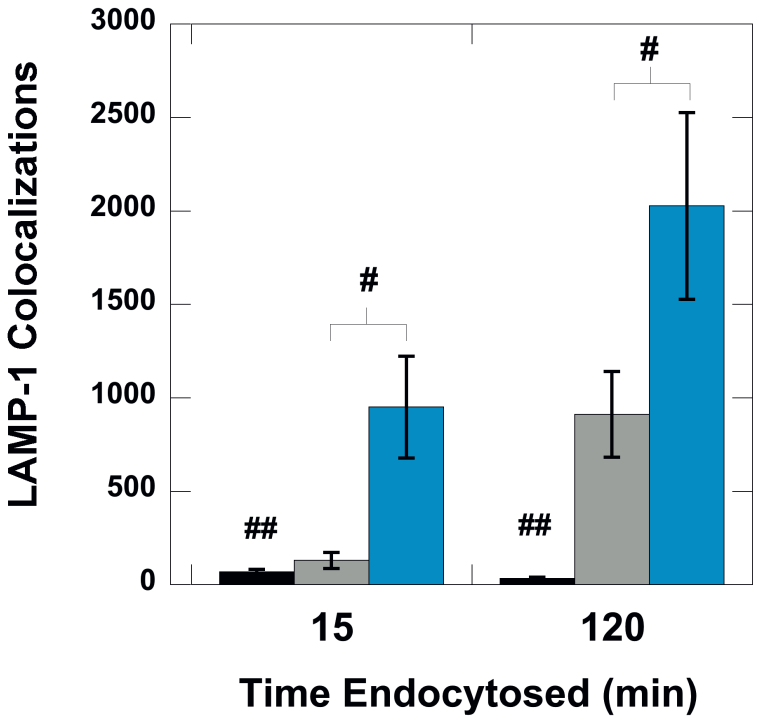

Figure 3.12 Colocalization of fluorescent ODN, polymer **44K**, or conjugate **44K-2** with the late endosomal protein lysosomal associated membrane protein 1 (LAMP-1) measured by confocal microscopy and image analysis. RAW264.7 cells were exposed to AF594 labeled ODN 1668 (black) (4 μM), **44K** (grey) (0.5 μM) and conjugate **44K-2** (blue) (0.5 μM scaffold), processed for immunocytochemistry, imaged by confocal microscopy, and analyzed for number of colocalization events with LAMP-1 staining vesicles. Significant difference $p \leq 0.002$ (#) or $p = 0.002$ (##). Error bars represent standard deviation of the average of four separate Z-stacks. Data shown are representative of over three independent experiments

Exonuclease V (blue) (ssDNA 5'-exo and endonuclease). The data shown in Fig. 3.13 illustrate the percent degradation. We exposed ODN 1668 and **44K-1**, normalized to be equimolar in ODN, to either nuclease for the specified time, stopped the reaction, purified the reaction by agarose gel electrophoresis, and measured the SYBR II

fluorescence from ssDNA in the gel band. As shown in the figure, the ODN 1668AT shows Exonuclease T and V half-lives of approximately 30 minutes, with complete Exonuclease T digestion and 83 ± 1.5% Exonuclease V digestion at 8 hours. This is in contrast to **44K-1**, which exhibits no significant digestion for Exonuclease T or V over 8 hours. These data suggest some of the enhanced activation observed in Figs. 3.4 and 3.6 could be from the significantly longer lifetime of PAA conjugated ODN.

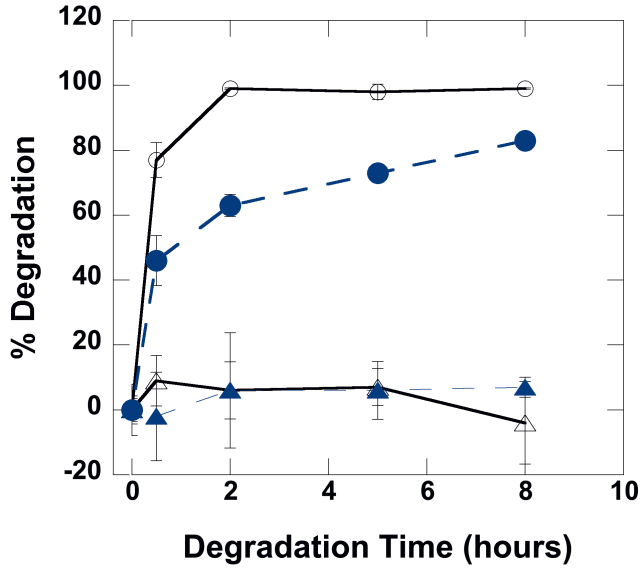

Figure 3.13 The Exonuclease T (open black) and Exonuclease V (blue) degradation profiles for ODN 1668AT (circle) and conjugate 44K-1 (triangle). ODN or conjugate were digested, purified by agarose gel electrophoresis, and the high MW products, detected by fluorescence intensity (SYBR II) on a Typhoon Imager and quantified by Image J analysis. Error bars are the standard deviation of the average of three independent samples.

3.4 Discussion

3.4.1 Design of ODN-PAA conjugates

ODN-PAA conjugates previously demonstrated that multivalent display on a PAA scaffold causes a 50 to over 100-fold increase in TNF-α and IL-6 expression by RAW264.7 macrophages.(216) It was not clear how the observed cytokine expression related to intracellular concentration with respect to multivalent construct or delivered ODN concentration. We questioned whether enhancements were from the multivalent presentation or differences in endocytosis and/or delivery to endolysosomal compartments where TLR-9 activation and signaling occur.(54, 225) This type of analysis was not possible given the non-quantitative biotin-streptavidin labeling previously employed. PAA was chosen as the presentation scaffold to have the highest conformational flexibility for engagement of the pendent ODN with TLR9 dimers. The high negative charge helps to prevent unspecific interaction with the negatively charged cellular membrane(197, 199) and also prevent molecular aggregation with the similarly charged ODN. ODN are covalently linked through the 3' end, a requirement to maintain their activity.(204) Conjugate detection is achieved via labeling the PAA scaffold with AF647, which permitted more accurate determination of valency as well as quantitative comparisons of endocytosis among all conjugates. Changes in cytokine expression can thus be correlated with intracellular delivery to more accurately determine the source of observed enhancements in cytokine expression.

3.4.2 Competent TLR9 multivalent activation requires a critical valency

At ODN concentrations employed in this work, we observe no significant expression of cytokines assayed for ODN 1668AT or the monovalent **44K-**1. Significant TLR9 activation was only apparent for higher valency ODN-PAA conjugates. IL-6 expression for ODN 1668 and **44K-1** are low relative to higher valency constructs, despite application at the same ODN concentration. For higher valency **44K-2**, **44K-3** and **44K-4** there are quantitative differences between these constructs and the next higher valency **44K-5**. Most importantly is the significant increase in IL-6 expression observed for **44K-5** (Fig.3.2). There are, however, other quantifiable differences in the expression kinetics of IL-10 and TNF-α in Figs. 3.4 and 3.6. IL-10 expression is similar or lower in concentration at 6 and 12-hour time points for **44K-1** through **44K-4**. In contrast, **44K-5** IL-10 expression, however, increases 2-fold between 6 and 12-hour time point, demonstrating more potent TLR9 activation. This trend in increasing rate and magnitude of IL-10 expression continues for **44K-7** and **44K-12**. Similarly, the TNF-α expression increases are similar in magnitude until the more than 2-fold increase between 12 and 24-hour time points for **44K-5**. The increase in expression of these two cytokines is observed although the intracellular scaffold concentrations is similar for **44K-4** and **44K-5** (Fig. 3.3), and suggests the increase in valency and enforced local concentration difference is the source of the higher activation. The observed difference could be from the higher ODN concentration of **44K-5 (**Fig. 3.3), but stimulating RAW264.7 macrophages at ODN concentrations of 250 nM and 500 nM (more than 4-fold higher than 150 nM shown

here) also demonstrate this critical activation valency (data not shown). **44K-12** was used to stimulate RAW264.7 macrophages silenced by a TLR9 siRNA to examine whether there was some additional immunostimulatory component not mediated by TLR9. Fig. S3.4 demonstrates greater than 90% reduction in activation for **44K-12** but not the LPS positive control, confirming TLR9 as the source of cytokine expression observed.

Roberts et al. demonstrated length dependence in murine macrophage activation by CPG ODN, with a critical length of 44 bp required for responses similar to bacterial DNA, and twice that of most therapeutic ODN under investigation.(89) A more recent report described the mannose receptor 1 (MRC1) as required for CpG ODN endocytosis and trafficking.(54) The role of MRC1 came to light through a CpG hyporesponsive wild-derived mouse strain fully competent in bacterial DNA recognition. The ability to fully recognize bacterial DNA, but not CpG ODN, suggests the two are not equivalent. There are noted discrepancies in CpG ODN activities between humans and studies using common laboratory mouse strains, often attributed to TLR9 expression, but perhaps other factors are additionally at play.(226) The data presented here advances the hypothesis that a critical valency promotes TLR9 activation through favorable multivalent engagement or arrangement of the TLR9 receptor complex, and perhaps, improved mimicry of bacterial DNA.

3.4.3 ODN density controls TLR9-mediated cytokine expression

When examining the IL-10 and TNF-α expression from **44K**-based scaffolds in Figs. 3.4 and 3.6, there is an increase in expression which could originate from the increase in valency or alternatively, more efficient delivery of ODN (Fig. 3.3). The **124K**-based scaffolds also show a similar increase in IL-10 expression with increasing valency, however, isovalent **44K**-based conjugates showed significantly greater expression. Critically, as displayed in Figs. 3.8 and 3.9, **44K-5** and **124K-5** have no discernable difference in intracellular scaffold or ODN concentration, or kinetics of endocytosis, identifying the difference in spatial presentation as the source of differences in cytokine expression. When the IL-10 expression data was compared to the ODN density in Fig. 3.5, a linear correlation was highly evident. This linear correlation is present over the entire 24 hours that IL-10 expression was monitored for both **44K** and **124K**-based scaffolds, suggesting TLR9 activation complexes can recognize changes in the local concentration of CpG motifs with increasing concentration regulating IL-10 expression.

IL-10 expression induced by CpG ODN was recently shown to limit infarct size and improve cardiac performance in a model of ischemia/ reperfusion cardiac injury.(227) Pre-treatment was necessary for the effect along with the use of long-lived phosphorothioate ODN and $_{D}$-GalactosamineN to further increase circulating lifetime. This suggests the maintenance of high ODN concentrations was at least partly responsible for the high IL-10 concentrations observed. Interestingly, another recent report described the tolerance-inducing effect of high concentration ODN via a

non-canonical signaling pathway employing the adapter protein TRIF (TIR-domain-containing adapter-inducing interferon-β).(226) This tolerogenic response has significant implications in the use of CpG ODN for allergic immune therapy, in addition to their known immune stimulating properties. They examined this effect largely in plasmacytoid dendritic cells, which demonstrated stable IL-10 expression in vitro; however, they remarked on the high IL-10 expression observed in vivo from administration of high concentrations of ODN. Perhaps the most relevant is work reporting high doses of CpG ODN triggering conventional dendritic cells to express high IL-10.(228) The high valency conjugates examined here are potent inducers of IL-10 expression and a clear relationship exists between the presentation density, or local concentration, and IL-10 expression. Establishing the mechanism of this observation and other potential accessory proteins in TLR9 activation complex recognition of high and low density will require further study.

We further noticed the inverse relationship between IL-10 and TNF-α expression, which was only apparent for the higher molecular weight **124K**-based conjugates (Figs. 3.4 and 3.6). To further analyze the source of this enhanced TNF- α expression, we exposed RAW264.7 macrophages to **124K-**5, **124K-12** and **124K-30**, normalized to scaffold concentration, based upon the scaffold concentration of **124K-30** employed in Fig. 3.6 (5 nM). **124K-5** employed at a 6-fold lower scaffold concentration, still elicits a high TNF-α expression, similar to **124K-30,** which delivers 6-fold higher intracellular ODN (data not shown). IL-10 is an anti-inflammatory cytokine known to regulate the expression of other inflammatory cytokines such as TNF-α and IL-6.(229) The data thus suggest that **124K-5** may have

sufficient valency to trigger a robust inflammatory response, but low enough density to limit IL-10 expression. If this general principle holds for humans in vivo, it would be a powerful principle for modifying ODN activity.

3.4.4 ODN-PAA conjugates are rapidly endocytosed by clathrin-coated pits, efficiently delivered and highly stable

Monodansylcadaverine (MDC) specifically inhibits clustering and internalization of receptors via clathrin-dependent endocytosis and has been shown by some studies to inhibit CpG ODN endocytosis.(222, 230) Several of the putative extracellular ODN receptors, including CD14(51), the receptor for advanced glycation end products (RAGE)(67) and the mannose receptor(54) are known to cluster and respond to multivalent ligands and would be endocytosed by this mechanism. Endocytosis of the conjugate **44K-5** was shown to be dependent upon clathrin-mediated endocytosis while similar concentrations of the scaffold were only partially dependent. ODN 1668AT was inhibited at the two lower concentrations of drug employed but showed an increase in endocytosis above 100 μM. This data suggests that CpG ODN can utilize at least two mechanisms of endocytosis, but ODN-PAA conjugates are only internalized through receptor-mediated endocytosis in clathrin-coated pits.

We also examined endocytosis through colocalization with EEA-1 or LAMP-1 through confocal microscopy analysis. Conjugate **44K-2** endocytosis kinetics are much more rapid, and significantly higher colocalization with LAMP-1, than either ODN 1668AT or the scaffold **44K** (Fig. 3.12). LAMP-1 is a marker of late

endosomes, where TLR9 activation takes place,(210) and demonstrates a striking increase in delivery efficiency. ODN-1668AT showed significantly higher colocalization values for both protein markers at the 15-minute time point than the 2-hour time point, unlike scaffold or conjugate values. This may be from the significantly lower resistance to nucleases (Fig. 3.13) and a sign of ODN degradation over the course of the confocal analysis.

We hypothesized that exonuclease digestion would be blocked as a result of the 3' conjugation due to steric blocking by the PAA which is larger than the ODN (hydrodynamic radius ~36-43 nm for 124 kDa PAA and ~15-18 nm for 44 kDa PAA(231) while ODN ~ 2 nm(205)). To examine this, we employed Exonuclease T (ssDNA 3' exonuclease) and Exonuclease V (ssDNA 5'-exo and endonuclease), to assess the *in vitro* nuclease degradation characteristics of ODN 1668AT and **44K-1** (Fig. 3.13). We show ODN PAA conjugation significantly protects the ODN sequence from both endo- and exo- nuclease degradation. The significant resistance to nucleases and likely enhanced intracellular lifetime may be a contributing factor in the higher activity observed for **44K-1** and all conjugates examined here.

3.5 Conclusion

We designed and synthesized the ODN-PAA conjugates described here to probe if multivalent presentation altered cellular responses initiated by TLR9 activation. We show significant changes in cytokine expression for conjugate **44K-5**, that these changes did not result from significant differences in endocytosis for

equivalent conjugates, and that they were dependent upon TLR9. Further, a direct relationship between ODN presentation density and IL-10 expression was shown for all conjugates assayed (both **44K** and **124K** scaffolds). This relationship was also true for TNF-α for the smaller **44K** scaffold but not the **124K** scaffold, where an inverse relationship between density and TNF-α expression was demonstrated. This suggests ODN-PAA conjugates with high enough valency for competent activation of TLR9 but low density overall (e.g. **124K-5**) are ideal for inducing strong inflammatory responses while higher density presentation (e.g. on the **4K** scaffolds) lowers inflammatory response and favors IL-10 expression. These principles could prove to be critical in further development of CpG ODN carriers and therapies.

3.6 Acknowledgements

This work was supported in part by the Center for Neutron Science at UD under award (U.S. Department of Commerce) #70NANB7H6178, as well as by the National Institutes of Health (1-RO1-EB006006). Its contents are solely the responsibility of the authors and do not necessarily represent the official views NIH or the Department of Commerce. Special thanks is given to Dr. Jeffery Caplan and Michael Moore for expert technical assistance with the confocal microscopy.

3.7 Supplementary Information

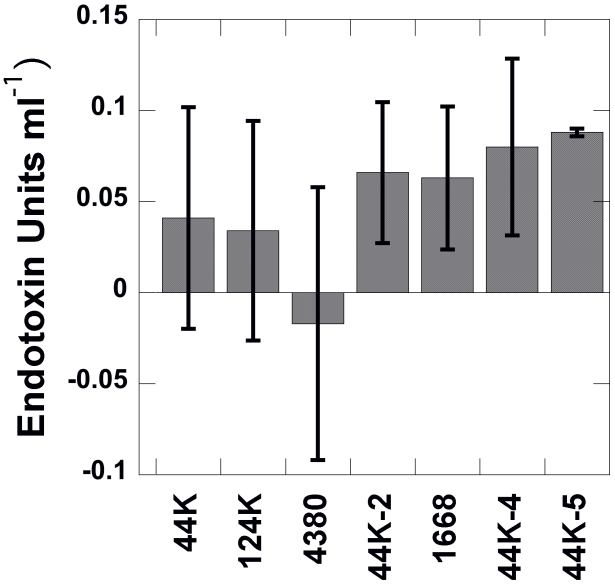

Figure 3.14 Fluorogenic limulus amoebocyte assay results for listed polymers, ODN and conjugates expressed as endotoxin units (EU) per ml. All values are below 0.1 EU ml^{-1} or 10 ng ml^{-1}. Error bars are the standard deviation of the average of three independent samples.

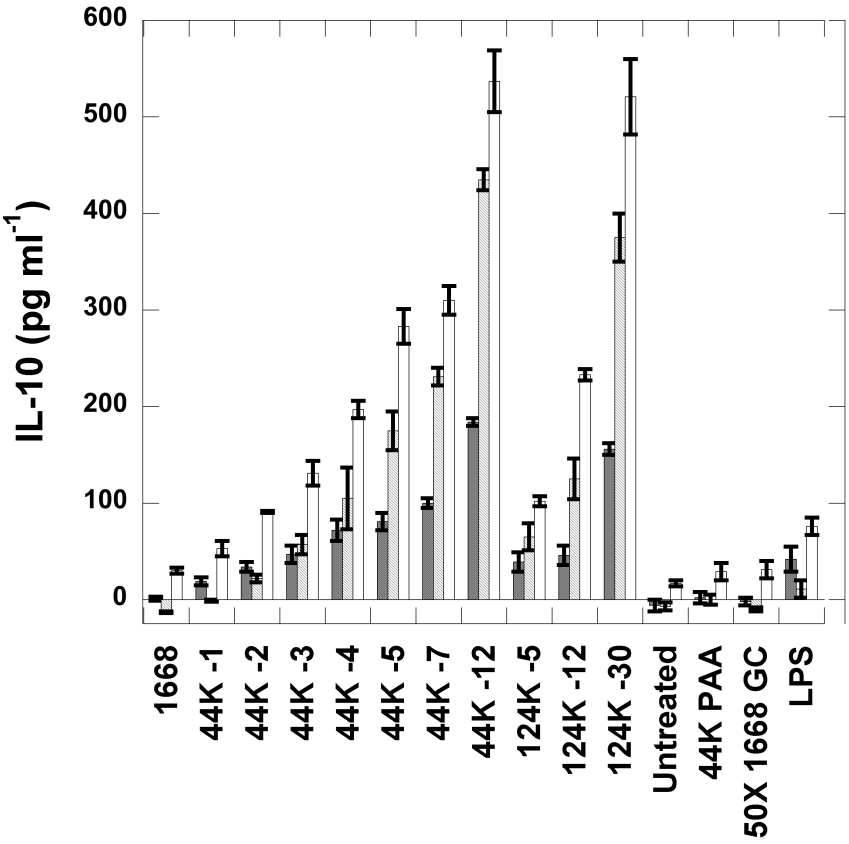

Figure 3.15 The full set of values from the experiment represented in Fig. 3.4, including the negative control (untreated), polymer **44K**, a 50X concentration of negative control ODN 1668 GC, and positive control LPS (10 ng ml^{-1}). Error bars are the standard deviation of the average of four independent samples.

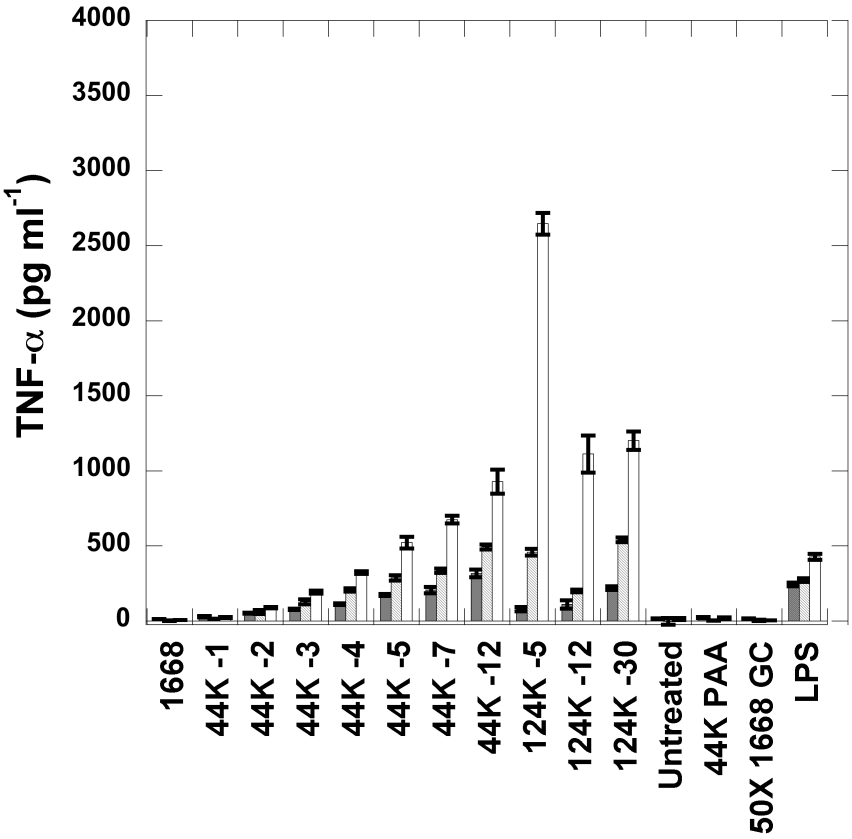

Figure 3.16 The full set of values from the experiment represented in Fig. 3.6, including the negative control (untreated), polymer **44K**, a 50X concentration of negative control ODN 1668 GC, and positive control LPS (10 ng ml^{-1}). Error bars are the standard deviation of the average of four independent samples.

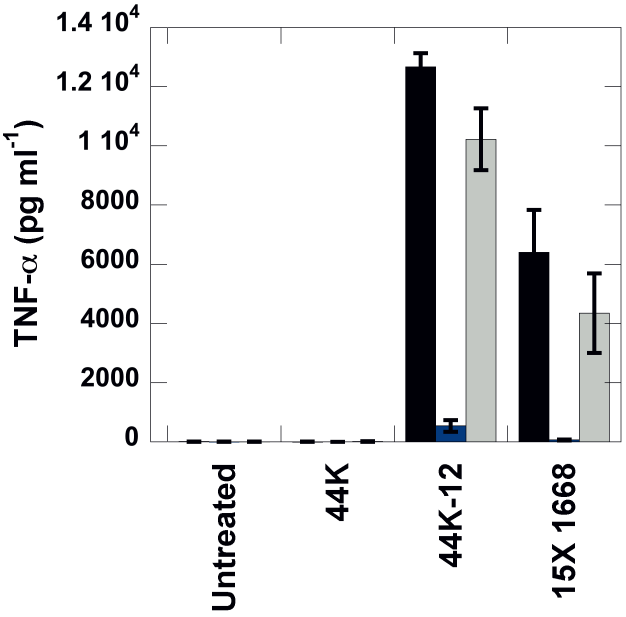

Figure 3.17 The siRNA-mediated knock down of TLR-9. The stimulation of untreated (black), TLR-9 siRNA tranfected (blue), or mock transfected (light grey) with **44K**, **44K-12**, or 15X ODN 1668AT, or no stimulation. Values are the TNF-α concentration of supernatants collected for each condition, determined by ELISA. Error bars are the standard deviation of the average of three independent samples.

Chapter 4

ENHANCED ANTAGONISM OF TOLL-LIKE RECEPTOR THROUGH MULTIVALENT DNA-POLYMER CONJUGATES

4.1 Introduction

Autoimmune diseases are a broad range of disorders affecting an estimated 7.6-9.4 % of the population;(232) these diseases have increasingly been correlated with innate immune system dysfunction.(2) Innate immune system receptors recognize molecular patterns characteristic of bacteria, fungi, and viruses, as well as endogenous damage-associated molecular patterns (DAMPs).(3) Initial recognition promotes fast immune response and proper priming of the adaptive immune system, however inappropriate or chronic activation can lead to pathological inflammation and autoimmune disease. Pattern Recognition Receptors (PRR), key receptors in these processes, comprise four families, and of these, the 10 Toll-like receptors (TLR) are the best characterized.(106) Toll-like receptors 7, 8, and 9, which are all regulated by cathepsin processing for receptor activation and endosomal localization(7), can improperly recognize self-nucleic acids and exacerbate disease symptoms of rheumatoid arthritis, lupus, psoriasis, and multiple sclerosis.(126) To manage disease progression, antagonists of these receptors are being developed, including

imidazoquinoline derivatives(4, 233), positively charged polymers(234-236), and antagonistic single-stranded (oligo) ribo- or deoxynucleotides.(4, 126, 237)

Toll-like Receptor 9 (TLR9), expressed primarily in B cells, plasmacytoid dendritic cells, and neutrophils (humans), initiates inflammatory cytokine or type I interferon production in response to unmethylated CpG dinucleotide-containing single-stranded oligodeoxynucleotides (ODN). TLR9 activation has many requirements including proteolytic processing(39), sub-cellular trafficking(40, 238), compartment specific signaling(44), and a host of accessory molecules.(38) .

To block TLR9-mediated inflammation, several classes of antagonist ODN have been developed based upon poly(guanosine), telomeric repeats, or a defined set of sequences.(97, 98) ODN antagonists, currently in clinical trials, rely upon conversion of the phosphodiester backbone to phosphorothioate (PS)(4), which alone converts poly(2-deoxyribose) to a TLR9 antagonist.(97) Phosphorothioate modification increases antagonism (≤100-fold)(98) and confers resistance to ubiquitous serum and cellular nucleases, which significantly impact the utility of ODN-based therapeutics.(211)

Despite the advantageous biological properties conferred by PS modification, significant pathophysiology has been observed in animal models. Administration of PS-ODN induces activation of the complement cascade(239), inhibition of clotting time, and basophil accumulation with mild kidney and liver dysfunction.(240) These adverse effects can be attributed to unintended immune activation and significant nonspecific binding of proteins to PS-ODN.(241)

Here, we describe strongly enhanced antagonism by phosphodiester (PO) ODN- poly(acrylic acid) (PAA) conjugates, demonstrating activity comparable to PS-based ODN. Interestingly, unlike previous results demonstrating multivalent enhancements of agonism of >100-fold, antagonistic enhancements are roughly 15-fold, suggesting different modes of action for agonistic and antagonistic ODN as noted previously.(98) ODN-PAA conjugates are rapidly endocytosed and accumulate at much higher intracellular concentrations than unconjugated ODN. Increased antagonism of multivalent conjugates is directly correlated to higher cellular endocytosis achieved only with an optimal valency range of 2-5. We also demonstrate, via chemically defined in vitro degradation assays, that 3' conjugation of PAA to ODN provides significant endo- and exonuclease degradation protection. Finally, we report the novel finding of potent antagonism of TLR9 by unmodified poly(acrylic acid). As supported by the data presented here, we propose PAA-conjugated antagonistic ODN may offer a new strategy to allow development of (PO) ODN-based autoimmune therapies.

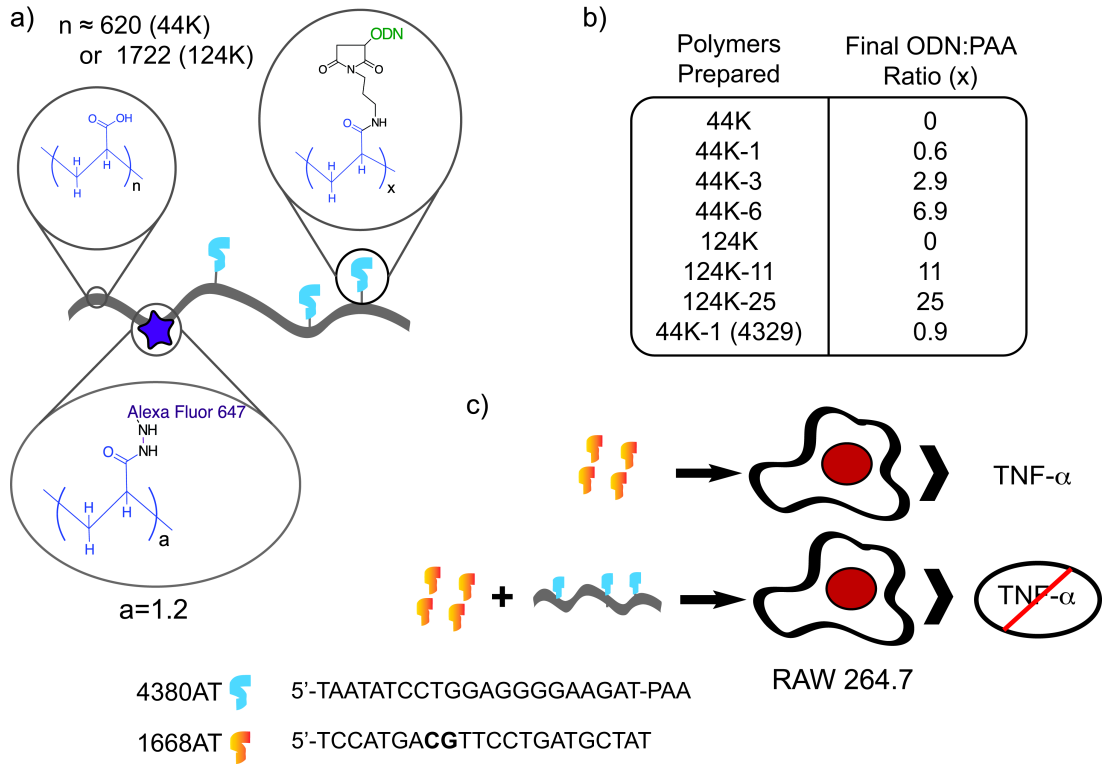

Figure 4.1 The chemical and molecular composition of PAA-ODN conjugates described in this work and a graphical representation of their antagonistic properties. A schematic representation of the conjugates synthesized, a), showing the chemical structure and number of the monomer units (n), fluorescent label (a), and ODN (x). The value of (x) for each conjugate is shown in b) with the final conjugate functionality. A graphical representation of PAA-ODN conjugates and the primary ODN sequences used in this work with their properties is shown in c.

4.2 Experimental

4.2.1 Materials

Poly(acrylic acid) of 44 kDa and 124 kDa molecular weight (MW), with poly dispersity indices (PDI) of 1.08 and 1.24 respectively, was purchased from Polymer Source (Dorval, Quebec) and purified via precipitation in 0.1 M HCl, dissolution in H_2O , filtration through a 0.22 μm PES membrane, lyophilization, and then precipitation in ether from an acetone/isopropanol 50/50 solution. Centrifugal filtration units (30 kDa molecular weight cutoff) were purchased from Millipore (Billerica, MA) and washed with sterile-filtered 30% ethanol before use. Fetal bovine serum was purchased from MP Biomedical (Santa Ana, CA) and heat inactivated. All other reagents were used without further modification. The following were purchased from Sigma Aldrich (St. Louis, MO): Ultra TMB HRP substrate, molecular grade sodium chloride, anhydrous sodium phosphate, N-(2-aminoethyl)maleimide trifluoroacetate salt (NEAM) (>95%), 1-hydroxybenzotriazole hydrate (HOBT) (97%), triethylamine (TEA) (≥99%), dimethyl sulfoxide (≥99%), and N-(3-dimethylaminopropyl)-N'-ethylcarbodiimide hydrochloride (EDC) (>99%). From Fisher Scientific (Pittsburgh, PA): 2-(N-morpholino)ethanesulfonic acid sodium salt (MES) (>99%), high melting temperature agarose, and NUNC maxisorp 96-well ELISA plates. O-(benzotriazol-1-yl)-N,N,N',N'-tetramethyluronium hexafluoro phosphate (≥99%) (HBTU) was purchased from Chem-Impex (Wood Dale, IL). All oligodeoxynucleotides (ODN) were purchased from Integrated DNA Technologies

(Coralville, IA) including oligos with the following main sequences: 1668AT CG (5'-TCCATGACGTTCCTGATGCTAT), negative control sequence ODN 1668AT GC (5'-TCCATGAGCTTCCTGATGCTAT), and antagonist sequences 4380AT (5'-TAATATCCTGGAGGGGAAGAT) and 4329AT (5'- CCTGGAGGGGAAGTAT). Additional oligos are listed in Table 4.1. SYBR II and Alexa Fluor 647 hydrazide were purchased from Invitrogen (Grand Island, NY).

4.2.2 Proton nuclear magnetic resonance spectroscopy

All spectra were collected on a Bruker AVIII-600 spectrometer with a 5mm Bruker SMART probe. NMR was performed at room temperature on samples dissolved in deuterium oxide (D_2O) purchased from Cambridge Isotopes. For all polymer samples, 128 or 256 scans were used, with a D1 of 10 s and a 90° pulse program.

4.2.3 Synthesis of Alexa Fluor 647-functionalized PAA

Precipitated and lyophilized PAA (above) was dissolved at 10 mg ml^{-1} in DMSO. To this solution, with constant stirring, both Alexa Fluor 647 hydrazide and HBTU, dissolved at 10 mg ml^{-1}, were added to the PAA solution to yield a final molar ratio of 1:12 (Alexa Fluor 647: HBTU). Triethylamine was added at a 75:1 molar ratio over Alexa Fluor 647. Alexa Fluor 647 to PAA molar ratios were 1.5:1 or 2:1 for the conjugates described. After 24 hours, the reaction mixture was purified/transferred by

centrifugal filtration in the following conditions (#washes (solvent)): 3X or until abs 650 nm stable (H_2O), 3X (250 mM NaCl and 50 mM phosphate pH 8), and 3X (75 mM MES pH 6.05 and 500 mM NaCl) and then a final time (twice) against H_2O. All solutions were prepared with molecular grade water, filter sterilized, and employed at a 1:50 volume ratio each spin. The number of Alexa Fluor 647 per polymer (functionality) was determined by proton nuclear magnetic resonance (^{1}H NMR) spectroscopy (Fig. 4.8 and 4.9); the exact structure of Alexa Fluor 647 is unknown, however 6 unambiguous downfield protons can be identified and correlated with patent application structures.(217-219) To determine functionality, the fraction (area of 6 Alexa Fluor protons/ area of PAA backbone protons) was multiplied by the 1720 (average) acrylic acid monomers per polymer. ^{1}H NMR analysis was validated by UV-VIS spectroscopy (example Figure 4.10) using ε=247000 $cm^{-1}mol^{-1}$ to determine the concentration of Alexa Fluor 647. Functionality is defined as the number of moles Alexa Fluor 647 (UV-VIS)/ moles PAA (determined gravimetrically); both methods were in agreement. ^{1}H NMR (D_2O): δ= 7.8 (m, 4H, Alexa Fluor), δ=7.3 (m, 2H, Alexa Fluor), δ=1.7-2.25 (bp, C-C**H**-C, PAA), δ=1.1-1.7 (bp, C-C**H2**-C, PAA).

4.2.4 Synthesis of maleimide-functionalized PAA

All glassware, plastic, and reagents were treated to maintain sterility to limit product contamination by LPS. Maleimide-functional polymer was synthesized as described previously.(221) Briefly, Alexa Fluor 647-labeled poly(acrylic acid), EDC, HOBT, and NEAM were all transferred/dissolved in a 75 mM MES solution buffered

at pH 6.05. EDC, HOBT, and NEAM were dissolved at a concentration of 10 mg ml^{-1} in the MES buffer. All solutions were filter sterilized. The EDC, HOBT, and NEAM were added immediately at a ratio of 1:3:4 respectively. The molar percentage of EDC (as a percent of total acid groups of the polymer) employed was: 8% for **124K-25** and **124K-11**, and 6.5% for **44K-6**, **44K-3** and **44K-1**.The reaction was conducted under nitrogen, and purified/ transferred via centrifugal filtration into the DNA reaction buffer (50 mM sodium phosphate, 11 mM citrate, 5 mM EDTA at pH 6.6 (degassed)). This maleimide-functional polymer was used immediately for conjugation of ODN (see next section).

4.2.5 Synthesis of ODN-functionalized PAA

ODN-PAA synthesis was conducted as described previously.(221) All apparatus and materials were treated as stated above. Briefly, 3' thiol-modified ODN and DTT were dissolved in 125 mM phosphate buffer at pH 7.5 to yield an excess of DTT to ODN at a molar ratio of 10:1 (25:10:1 phosphate:DTT:ODN); the ODN and DTT were incubated for one hour. After incubation, this solution was gravity filtered, via size exclusion chromatography, using sterilized G 15 resin (10X resin volume). The eluate was fractionated and fractions tested for the presence of DNA by UV absorbance (NanoDrop 2000 Wilmington, DE). DNA-positive fractions were combined with maleimide-functionalized polymer from dialysis at ratios (initial ODN:PAA) of 40:1, 15:1, 14:1, 5:1 and 0.8:1 for **124K-25**, **124K-11**, **44K-6**, **44K-3** and **44K-1 respectively**. This reaction mixture was placed in a ported bell jar, vacuum

purged 3 times with nitrogen with constant stirring, and incubated under nitrogen for 5 days. The polymer control samples (PAA) were collected as a fraction of the total synthesis, before ODN reaction, diluted 2X into 200 mM pH 8 phosphate buffer and reacted for 24 hours to ring open or react any maleimide groups. This ODN-free control polymer (**44K**) was purified/transferred by centrifugal filtration to the ODN storage buffer of 10mM Tris and 1 mM EDTA at pH 7.5.

4.2.6 UV characterization of ODN-PAA conjugates

Reaction mixtures (from above) were diluted with 50 mM phosphate pH 8 buffer made with molecular grade water (Mediatech, Manassas, VA). This solution was filter-sterilized and passed through a centrifugal filter. After filtration, the volume was brought back to 4 ml with molecular grade water and again passed through a centrifugal filter. This process was repeated until absorbance at 260 nm was stable. The high molecular weight fraction was analyzed by UV-Vis spectroscopy on a NanoDrop 2000 (Wilmington, DE). The 260 nm absorbance values allow determination of DNA concentration by the calculated extinction coefficient (201,800$cm^{-1}mol^{-1}$ and 200,400$cm^{-1}mol^{-1}$ for the CG and GC sequences respectively (193, 194)); for each synthesis, the DNA functionality of the polymer was calculated from the DNA concentration of the HMW fraction (UV-Vis) divided by the polymer concentration (gravimetric). The polymer concentration (UV-Vis) was determined as the Alexa Fluor 647 concentration (Alexa Fluor 647 ε=247000 $cm^{-1}mol^{-1}$) divided by the NMR functionality, as described above. The DNA concentration in the low-MW

fractions was also monitored; the total amount of DNA across all fractions corresponded to the total ODN employed during the reaction. Experimentally determined conjugate functionalities are given in Fig. 1b (Final ODN:PAA ratios).

4.2.7 Cell culture

RAW264.7 cells (ATCC, Manassas, VA) were cultured on tissue culture polystyrene plates (Cell Treat; Shirley, MA) in DMEM supplemented with 10 mM HEPES, 55 μM β-mercaptoethanol, antibiotic/antimycotic, sodium pyruvate (Invitrogen, Grand Island, NY)), and 10% fetal bovine serum (Mediatech, Manassas, VA). Cells were not cultured past passage 8 and were maintained at between 20 and 90% confluence. Passage was accomplished by scraping the cells after a wash with calcium- and magnesium-free PBS.

4.2.8 Nuclease degradation assay

Kinetic nuclease degradation was measured for both monomeric and conjugated ODN via Exonuclease T (3' exonuclease) and Exonuclease V (5' exonuclease and endonuclease) (New England Biolabs, Ipswich, MA). Reactions were assembled to include 9.9E-11 moles of ODN (oligo and conjugate) and the supplied reaction buffers (New England Biolabs) to a final volume of 10 μL. Enzyme used was diluted 1:24 in the supplied reaction buffer (#4) and 2 μL of the dilution was used to provide 0.41 and 0.83 activity units per reaction for Exonuclease T and V,

respectively. Immediately after dissolution, reactions were conducted at room temperature (Exonuclease T) or 37°C (Exonuclease V) and at the indicated time, quenched by addition of 2 µL stop buffer (275 mM EDTA, 1.5 wt% SDS pH 7) and boiled for 10 minutes. From this inactivated reaction, 2 µL was removed and combined with 6X loading buffer and 0.5 µL SYBR II stain (Invitrogen, Grand Island, NY), and brought to 12 µL final volume with PCR-grade water (BioExpress, Kaysville, UT). This solution was loaded on an 0.8% agarose gel and run for 45 minutes at 60 mV. Gels were immediately imaged for fluorescence on a Typhoon 9410 (GE Healthcare Biosciences, Pittsburg, PA), with excitation at 457 mn (laser) and emission monitored at 520 nm. Images were saved as *.tiff files, look-up tables (LUT) reversed, and bands measured using Image J64 (area kept static). Time 0 is the 0% degradation value. The data given at each time point (0, 0.5, 2, 8 hours) represents 3 independent replicates.

4.2.9 Flow cytometric analysis

Flow cytometry was used for analysis of ODN and conjugate endocytosis in addition to endocytosis at a fixed time for analysis of relative intracellular concentration. RAW264.7 cells were cultured as described above. The day of the experiment, cells were washed with phosphate-buffered saline (no calcium or magnesium), with a second wash for 5 minutes followed by cell scraping. Live cells were counted using trypan blue, and bulk cells were treated with ethidium homodimer (Invitrogen; Grand Island, NY) for 5 minutes to mark dead cells (<2%) for exclusion

from analysis; cells were washed three times with 37°C PBS to remove dead stain. Treated cells were aliquoted to a concentration of 500,000 cells per tube (Falcon 352054). These cells were centrifuged (300*g* for 5 minutes at room temperature) and resuspended in 500 μL 37°C DMEM containing 250 nM conjugate (normalized by ODN) or fluorescently labeled ODN and polymer **44K,** both used at a concentration of 250 nM. To ensure fluorescence values represent only endocytosed conjugate, three replicates were centrifuged at 4°C, resuspended in 4°C sample-containing DMEM, and maintained at 4°C for 90 minutes to differentiate surface interactions from endocytosed label.(216) The remaining samples were incubated at 37°C for 90 minutes, followed by three centrifugation/ wash cycles at 4°C, resuspension in 300 μL 4°C flow buffer (phosphate-buffered saline, 1% BSA, and 2.5 mM EDTA pH 7), and incubation on wet ice until measurement. The intracellular fraction was calculated as the difference in the mean fluorescence values at 37°C and 4°C; this difference is the mean fluorescence intensity value reported. Studies to determine the kinetics of endocytosis were accomplished by incubation for the time indicated and then treated as described above. Samples used for subtraction were all subjected to a 4°C two hour incubation. All centrifugation steps were conducted at 300*g*. Cell detection was conducted on a BD LSR II cell analyzer (BD Biosciences, San Jose, CA); a total of 10,000 events were collected within a gate set using untreated cells (Forward Scatter (FSC)/Side Scatter (SSC)) and treated cells to exclude those positive for ethidium homodimer. Each sample (replicates of three) was analyzed (FlowJo software, Tree Star; Ashland, OR) to determine the geometric mean fluorescence intensity.

4.2.10 Determination of IC_{50} for ODN and ODN-PAA conjugates

A dose-response curve was constructed for each of the ODN and ODN-PAA conjugates synthesized. RAW264.7 cells were seeded the night before the experiment, at 75,000 cells per wellin a 96-well tissue culture plate. ODN and conjugates were heated to 95°C to remove secondary structure and flash cooled to 4°C before addition to media.(220) Samples were then diluted into DMEM to achieve the highest concentration assayed and were then diluted 1:1 serially with DMEM. DMEM employed for sample dilution contained 2.5 μM of the agonist sequence1668AT. 200 μL of these diluted samples were added per well. The supernatant was removed and frozen after 24 hours. The TNF-α concentration of supernatants was assayed by ELISA (below). Dose-response curves were constructed by normalizing the TNF-α values to a 0 to 100 % inhibition scale (Origin; Northampton, MA) and plotting against log(concentration of ODN). IC_{50} values were calculated using the raw TNF-α values and the log(concentration) using the Origin dose-response function $y=A^1 + \frac{A_2-A_1}{1+10^{(LOGx0-x)p-1}}$, as a nonlinear fit where x is the logarithmic dose and LOGx0 is the center of the curve. ODN and conjugate concentrations were determined from averaging the concentrations determined for three separate stock dilutions and at least two different dilution values.

4.2.11 Enzyme-linked immunosorbent assay (ELISA)

ELISA was performed by analysis of the supernatants collected from the experiments described above, after dilution of the supernatants with 10% FBS in PBS (1:3). The TNF-α concentrations of supernatants were assayed by a monoclonal antibody set (BD Biosciences, San Jose, CA), with adherence to the provided protocol. Independent values are from two independent measurements at two different concentrations within the linear range of the standard curve. ELISA measurements were measured using a Perkin Elmer VICTOR3V multilabel counter (Perkin Elmer, Waltham, MA).

4.2.12 Limulus amoebocyte assay

The fluorogenic limulus amoebocyte assay (Lonza, Allendale, NJ) was conducted on all materials in accordance with the manufacturer-provided protocol. Conjugates, as well as purified polymer and ODN, were tested for endotoxin and found to have endotoxin concentrations < 10 pg ml^{-1}.

4.2.13 Data analysis and statistics

Statistical analysis was calculated on Kaleidagraph (Synergy Software, Reading, PA); statistical significance (p) was calculated via one-way ANOVA with post hoc Tukey's analysis at the 99% confidence level. A minimum of three

independent samples were used for analysis, and all experiments were repeated a minimum of three times for validation. Origin (Northampton, MA) was used to calculate IC_{50} values (dose-response non-linear fit) and to graph dose-response curves.

4.3 Results

4.3.1 Design and Synthesis of PAA-ODN antagonistic conjugates

We have previously shown that conjugation of PAA to agonist TLR ODN enhances the stimulatory properties of the ODN;the synthetic strategies for the conjugation have been described in detail in recently published work.(216) PAA was chosen as the polymer scaffold for these conjugates to limit intramolecular interactions and aggregation, as well as to prevent nonspecific interactions with negatively charged cellular membranes. The intended activity of these conjugates was interaction with TLR9 or associated proteins on the plasma membrane or in endolysosomal compartments.(51, 65, 67, 242) The optimized chemical conjugation conditions(221) easily accommodated modifications that permitted conjugation of a dye to the polymer for expanded options for polymer detection.

Relative intracellular concentrations of ODN and ODN-PAA conjugates were quantified by direct labeling of PAA with Alexa Fluor 647, as shown in Fig. 4.1a. Direct labeling of the PAA, and ^{1}H NMR spectroscopic analysis of Alexa Fluor 647 conjugation allowed direct comparison of mean fluorescence intensity values determined by flow cytometry, regardless of the identity or valency of the scaffold.

Alexa Fluor 647 labeling of PAA was accomplished through the procedure detailed in section 4.2.3; the resulting chemical linkage and Alexa Fluor 647 functionality are delineated in Fig. 4.1a. Labeled polymer was purified by centrifugal separation through a series of buffer conditions to remove all unconjugated fluorophore. The high molecular weight fraction was monitored by UV-Vis until the absorbance value at 650 nm was stable. ^{1}H NMR analysis of peak areas for syntheses of polymers **44K** and **124K** allowed determination of the number of Alexa Fluor 647 dye molecules conjugated to each polymer (functionality); conjugation was indirectly indicated by the broadening of the fluorophore peaks in the NMR analysis (Figs. 4.8 and 4.9). The conjugates were also analyzed by UV-Vis spectroscopy; the calculated ODN functionality agreed with the value determined via NMR (< 2% difference) (Fig. 4.10 **44K**).

Alexa Fluor-labeled PAA was used as the scaffold for the synthesis of the ODN-PAA conjugates detailed in section 4.2.4 and 4.2.5, with the final product schematically portrayed in Fig. 4.1a. The full list of constructs synthesized with experimentally determined ODN functionalities are provided in Fig. 4.1b. The final functionality of reported constructs was a fraction of the initial stoichiometry used in the reaction. The primary antagonist sequence used in this work (4380AT) (Fig. 4.1c and Table 4.1) is a slight modification of a previously published sequence (4380); in that work, 4380-PS possesses 5 times the activity relative to the 4380-PO(98) Under our experimental conditions, 4380AT-PS has approximately 9 times the activity of the PO sequence (4380AT) used for conjugation. The choice of this ODN introduced a greater contrast between the potency of PS and PO ODN forms to help differentiate if

PAA conjugation significantly improves PO-ODN inhibitory potential equivalent to an optimized PS-ODN. An adenine-thymine dinucleotide linker was added to the 3' end of the ODN to help reduce any steric hindrance the conjugated PAA might introduce; this linker does not significantly impact secondary structure or homodimer formation (data not shown). These fluorescently labeled ODN-PAA conjugates allow assessment of the central hypothesis via direct comparison of endocytosed ODN and conjugate concentrations obtained by flow cytometry.

Table 4.1. Oligonucleotides

ODN	Sequence (5'-3')
1668AT	TCCATGACGTTCCTGATGCTAT
4380AT	TAATATCCTGGAGGGGAAGAT
4380AT-HD	TAATATCCTGGAGGGGAAGAT -HD
4380AT-A647	TAATATCCTGGAGGGGAAGAT –A647
4380AT-PS	TAATATCCTGGAGGGGAAGAT
4380AT-PS-A647	TAATATCCTGGAGGGGAAGAT – A647
4380AT-SH	TAATATCCTGGAGGGGAAGAT - SH
4329AT	CCTGGAGGGGAAGTAT
4329AT-SH	CCTGGAGGGGAAGTAT - SH

HD (hexanediol), A647 (Alexa 647), SH (thiol), PS (Phosphorothioate)

4.3.2 PAA conjugation enhances antagonistic ODN inhibitory potential

We hypothesized that conjugation of TLR9 antagonistic sequences to PAA would improve inhibition of TLR9, based upon our previous results that demonstrated conjugation of agonistic sequences to PAA provided strong enhancements in cytokine release.(221) To test the possibility of similar enhancements in antagonism, dose

response data was obtained by titrating the antagonist against a constant concentration of agonist. Various concentrations of ODN 4380AT, phosphorothioate derivative 4380AT-PS and conjugate **44K-**1 were incubated with the agonist 1668AT (2.5 mM) and samples were applied to RAW647.7 cells in vitro (schematically shown in Fig. 4.1c). The supernatants were collected 24 hours later, and the TNF-α concentrations were analyzed by ELISA.

Dose response curves (Fig. 4.2) were assembled by converting the calculated TNF-α concentrations to reflect the percentage reduction from concentrations achieved by 2.5 mM ODN 1668AT, and then plotting this percent inhibition against the log of the concentration of antagonist. 4380AT-PS and 4380AT demonstrate IC_{50} values 18.6 ± 1.6 nM and 161.8 ± 10.2 nM respectively ($p < 0.0001$) and as expected, the 4380AT-PS (blue wedge) is > 8-fold more potent than the PO 4380AT (red circle). Surprisingly, the **44K-1** conjugate (light blue diamonds) also showed significant enhancements, comparable to those observed for 4380AT-PS, demonstrating an IC_{50} of 24.1 ± 2.4 nM for a 6.7-fold improvement over the monovalent ODN ($p = .0089$). Modification of the 3' end of ODN is known to protect against 3' exonuclease degradation.(243, 244) To examine whether 3' modification of the ODN could explain the observed antagonist enhancements, a hexanediol modification was made to the 3' end (4380AT-HD); the dose response curve for these experiments is also shown in Fig. 4.2. 4380AT-HD yielded an IC_{50} of 200.5 ± 8 nM ($p = 0.0008$ from 4380AT (161.8 ± 10.2 nM)), an unexpected reduction of the inhibitory potential of the 4380AT sequence. This contrasts with results reported for PO TLR9 agonists, as these show potency enhancements with 3' end modification with small molecules.(244)

Of note, unmodified PAA demonstrated TLR9 antagonism. **44K** and **124K** employed at equimolar concentration to that of 4380AT and **44K-1** in Fig. 4.2, exhibited 3.8 ±0.4-fold and 2.5 ±0.4-fold higher IC_{50} values than 4380AT (Fig. 4.11). These values are significantly different ($p = 0.013$) and show a molecular weight dependence on inhibition.

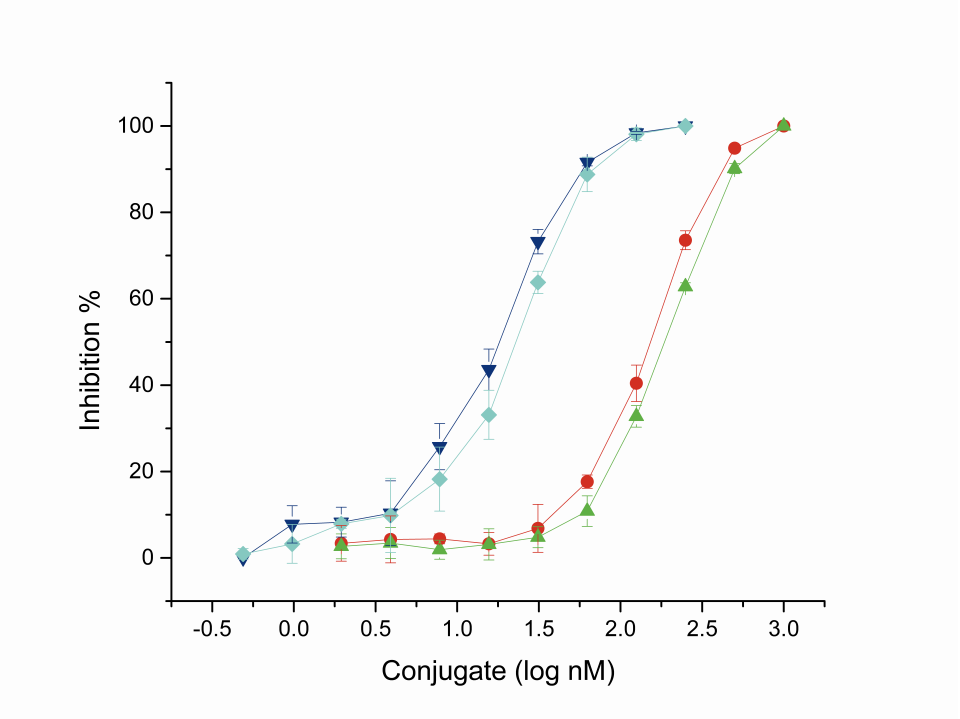

Figure 4.2 Dose response curves for ODN 4380AT (red circles), 4380AT-HD (green triangles), 4380AT-PS (light blue diamonds), and conjugate **44K**-1 (dark blue wedges), plotted as percent inhibition against the log of the concentration of ODN (nM). RAW264.7 cells were exposed for 24 hours to 2.5 μM ODN 1668AT and a serial dilution of the indicated antagonist (normalized to [ODN]). Data shown are [TNF-α] of RAW264.7 supernatants, converted to a 0 to 100 scale (Origin) and then to percent inhibition. Error bars indicate the standard deviation from the average of four independent samples.

Overall, our data suggest that PAA conjugation enhances PO-ODN antagonism to activities comparable to the activities observed for PS-ODN, and these enhancements are not simply from the modification of the ODN 3' end.

4.3.3 Valency alters antagonism of ODN-PAA conjugates

Based upon previous work(221), we hypothesized that multivalent presentation of ODN would more effectively engage TLR9, or accessory proteins, to further inhibit TLR9 activation, presumptively through better engagement of organized protein complexes.(51, 75, 79) Conjugates **44K-1**, **44K-3**, **44K-6**, **124K-11** and **124K-25** were synthesized as described in section 4.2.5; IC_{50} values, from dose response data and represented as fold decrease (improvement) in IC_{50} over ODN 4380, are shown in Fig. 4.3. All data is normalized to ODN concentration, not scaffold concentration, in order to illustrate the effectiveness, on an ODN basis, of the various conjugates. Conjugate **44K-1** showed an improvement of 6.8 ± .6 fold over ODN 4380AT, as previously displayed (Fig. 4.2), and shown here for comparison to the multivalent constructs. Remarkably, **44K-3** exhibits an IC_{50} fold-improvement of 13.4 ± 1.7 over 4380AT, the most potent IC_{50} recorded (IC_{50} = 11.7 ± 1.3, which is 1.6-fold more potent than 4380PS). This optimal peak in TLR9 inhibition was over 2-fold greater than that observed for the monovalent **44K-1** or for the 6-functional **44K-6** ($p \leq$

0.0002). The trend of decreasing potency with increasing functionality continued through the significantly higher valency **124K-11** and **124K-25,** which were constructed with a higher molecular weight PAA scaffold (124kDa) to permit higher valencies. The **124K-**11 and **124K-**25 scaffolds show decreasing potency with increasing functionality (>3) from 5 ± 0.1 to 2.4 ±0.5 respectively ($p < 0.05$).

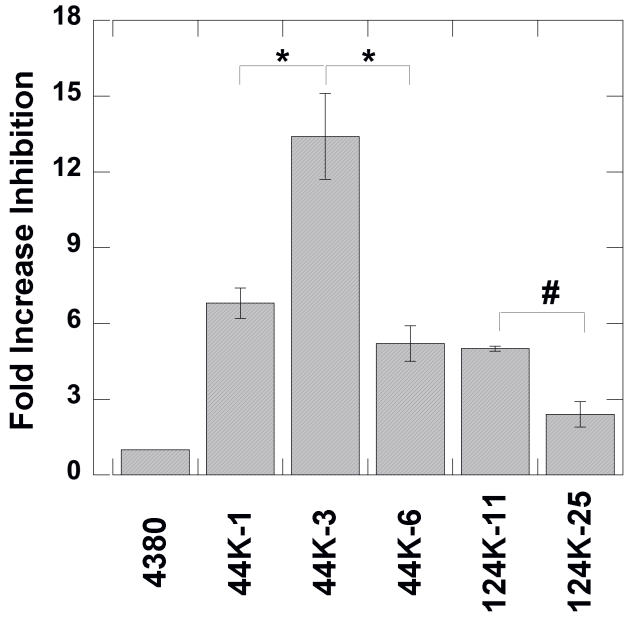

Figure 4.3 Potency of multivalent PAA-ODN conjugates, shown as the fold-increase in inhibition over that observed for ODN 4380AT. Values shown are IC_{50} values determined from dose response experiments, normalized to the IC_{50} value of 4380AT. Experimentally applied antagonist concentrations are normalized to the concentration ODN. Error bars represent the standard deviation of the average of three or four independent samples. Symbols indicate statistically significant differences; * indicates $p \leq 0.0002$ and # indicates $p < 0.005$.

Multivalency enhances the inhibitory potential of ODN when presented as ODN-PAA conjugates; however, this increase is suggested to be limited to a critical functionality.

4.3.4 Optimal valency corresponds with enhanced endocytosis

Conjugate **44K-3** displayed significant enhancement in TLR9 inhibition over all other ODN and constructs, with higher functionality conjugates having progressively decreased potency. As normalizing sample concentrations by ODN concentration yielded decreasing scaffold concentrations with increasing functionality, we hypothesized that differences in intracellular concentration could explain the observed potencies of conjugates and ODN tested. Relative intracellular concentration was determined via flow cytometric analysis of RAW264.7 cells exposed to Alexa Fluor 647-labeled 4380AT 4380AT-A647, **44K-1**, **44K-3**, **44K-6** and 4380AT-PS-A647 (Fig. 4.4). The concentrations of the ODN and conjugates employed in these studies were normalized to ODN. Polymer **44K** is also shown, assayed at the same concentration as **44K-1** while **124K**-based scaffolds were not assayed because of their lower IC_{50} values. Cells were incubated at both 37°C and 4°C to mark active endocytosis/ surface labeling and surface labeling respectively. The 4°C values were subtracted from those at 37°C to represent only intracellular species. Fig. 4.4 shows that ODN 4380AT-PS-A647 displays a significantly greater relative value (6828 ± 33) than all other samples ($p < 0.0001$), consistent with previous reports that PS-ODN demonstrate significantly enhanced endocytosis over PO-ODN.(245) All conjugates,

the parent polymer **44K**, and 4380AT-PS-A647 all have significantly higher intracellular concentrations than 4380AT-A647 (486 ± 2, $p < 0.0001$). **44K-3** has the highest value of the conjugates (2770±30, $p < 0.0001$)), compared to **44K-1** (2150 ± 10) and **44K-6** (2030 ±20). Critically, the intracellular concentration trend of the conjugates is the same as that of inhibition improvement observed in Fig. 4.3,

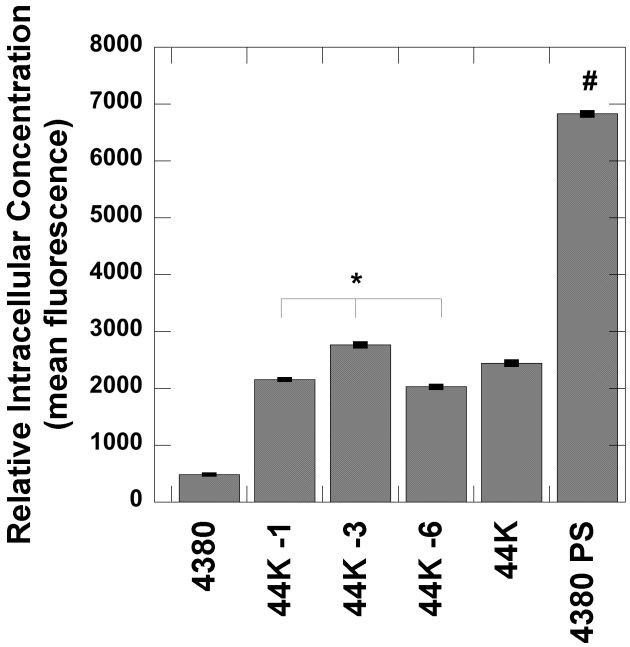

Figure 4.4 The relative intracellular scaffold concentrations of 4380AT, 44K-1, 44K-3, 44K-6, polymer 44K and 4380AT-PS. Values are the difference between 37°C and 4°C flow cytometric mean fluorescence intensity values for RAW264.7 cells exposed (90 min) to Alexa Fluor 647-labeled ODN and conjugates. Error bars are the standard deviation of the average of three independent samples. Symbols indicate statistically significant differences; * indicates $p < 0.0001$ and # indicates $p < 0.0001$ against all other samples.

connecting increased intracellular scaffold concentration with enhanced inhibition. These data collectively demonstrate that while increasing multivalency enhances intracellular delivery of ODN (Fig. 4.12), antagonism of TLR9 is not similarly enhanced. Optimal antagonism only occurs within a very defined range of valency.

4.3.5 Optimal functionality promotes rapid endocytosis

Data from Figs. 4.3 and 4.4 establish that the enhanced antagonism observed for **44K-3** arises from enhanced endocytosis and greater intracellular concentration. To further support this correlation, we examined the endocytosis kinetics of 4380AT-A647, **44K-1**, **44K-3**, **44K-6** and 4380AT-PS-A647, again normalized to ODN concentration, and polymer **44K** ([**44K**] = [**44K-1**]) (Fig. 4.5). Observing whether **44K-3** is more rapidly endocytosed at early time points or has altered kinetics with respect to **44K-1** and **44K-6**, could suggest a possible mechanism of enhancement. **44K-3** again demonstrates significantly higher intracellular concentration than **44K-1** and **44K-6** ($p < 0.0001$ for all time points). It is also clear **44K-3** endocytosis is much more rapid with the relative intracellular concentration 7-fold higher than those of **44K-1** and **44K-6** at 20 minutes despite **44K-1** having a three-fold higher initial scaffold concentration in the media. Despite **44K-1** and **44K** having identical media concentrations, **44K** shows rapid early endocytosis followed by similar internalization kinetics to **44K-1**. This suggests similar, but different, endocytic mechanisms for PAA and ODN-PAA, which is supported by recent monodansylcadaverine inhibition studies (manuscript in preparation). 4380AT-PS-A647 shows both higher initial values

and increased endocytosis rate two-fold higher than **44K-3** at 120 minutes ($p < 0.0001$). These results again agree with previous reports of rapid intracellular delivery, predominantly from high unspecific protein binding.(240) The functionality of **44K-3** preferentially promotes rapid endocytosis much greater than **44K-1** or **44K-6** as well as the ODN 4380AT-PS. This data again suggests enhanced endocytosis as the source of the **44K-3**'s activity.

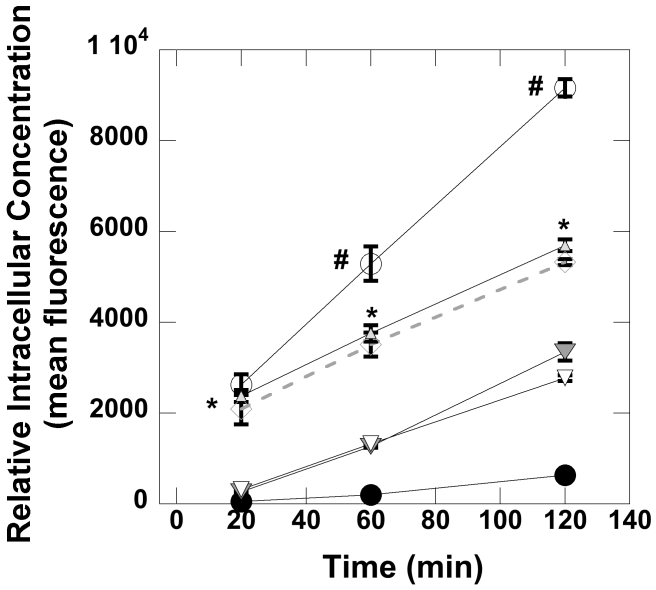

Figure 4.5 The kinetic profiles of scaffold endocytosis from 20 minutes to 2 hours for 4380AT (solid circle), 4380AT-PS (open circle), polymer **44K** (open diamond/dashed line), and conjugates (blue lines) **44K-1** (closed wedge), **44K-3** (triangle), and **44K-6** (open wedge). Values are the difference in flow cytometric mean fluorescence intensity values for RAW264.7 cells exposed to Alexa Fluor 647 labeled ODN and conjugates at 37°C and 4°C for each time point. Error bars are the standard deviation of the averages of three independent samples. Statistically significant differences; * is $p < 0.0001$ and # is $p < 0.0001$ against all other samples at 60 and 120 minutes.

4.3.6 PAA conjugation imparts nuclease resistance to PO-ODN

PS-ODN manifest significantly greater antagonism over PO-ODN counterparts and this enhancement is attributed to their higher intracellular delivery, greater avidity for TLR9, and significantly greater resistance to nucleases.(240) We hypothesized 3' ODN conjugation would also block 3' exonucleases and the greater size of the PAA (hydrodynamic radii of ~36-43 nm for 124 kDa PAA and ~15-18 nm for 44 kDa PAA) and ODN (~2 nm) (39, 221)) would provide a steric block against endonucleases. In vitro assessments of 3'-exo (Fig. 4.6 (a)) and endonuclease (Fig. 4.6 (b)) degradation of 4380AT and **44K-1** were performed to quantify the possible contribution of exo- and endonuclease resistance to the observed enhancements in antagonism. ODN 4380AT (circle), **44K-1** (triangle) and the 3'-end blocked 4380AT-HD (diamond) were treated with Exonuclease T (ssDNA 3' exonuclease) and Exonuclease V (ssDNA 5'-exo and endonuclease) as detailed in section 4.2.8. As expected, both **44K-1** and 4380AT-HD show no significant degradation from 3'exonuclease activity (Fig. 4.6 (a)). This is in contrast to what was observed for 4380AT, which showed 84 ± 4.4 % degradation under the conditions assayed. **44K-1** also showed significant resistance against the 5' exo and endonuclease activities of Exonuclease V with only 29 ±11.4 % degradation at 8 hours, while both 4380AT and 4380AT-HD showed 96 ± 1.6 and 94 ±2.1 % degradation respectively (Fig. 4.6 (b)). Collectively, the data show that conjugation of ODN to PAA confers significant resistance to degradation by exo- and endonucleases and another possible mechanism explaining the enhancement in antagonism observed.

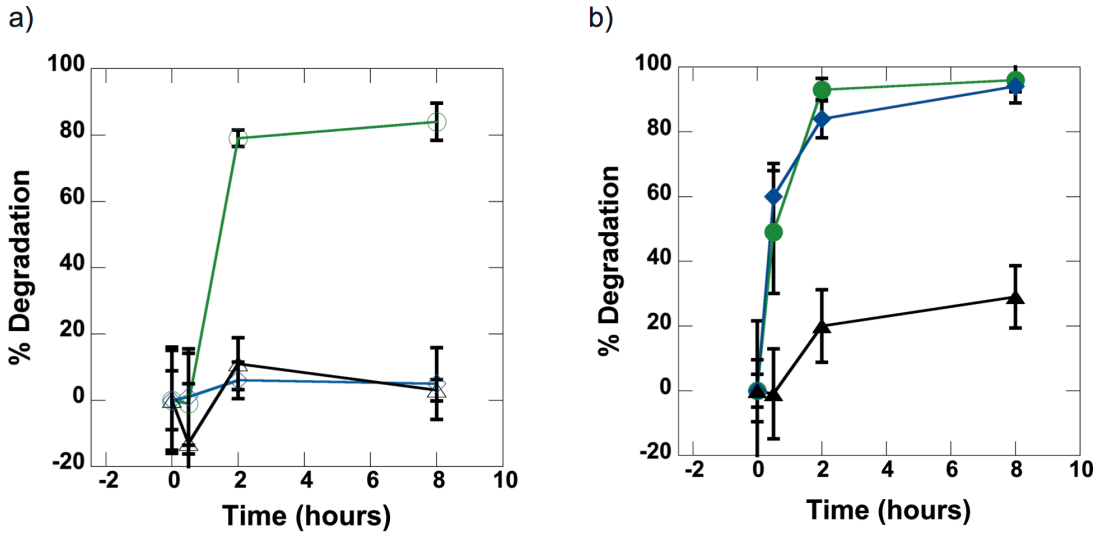

Figure 4.6 The Exonuclease T (a) and Exonuclease V (b) degradation profiles for 4380AT (circle), 4380AT-HD (diamond), and conjugate 44K-1 (triangle). ODN or conjugate were digested, purified by agarose gel electrophoresis, and the high MW products, detected by fluorescence intensity (SYBR II) on a Typhoon Imager and quantified by Image J analysis. Error bars are the standard deviation of the averages of three independent samples.

4.3.7 PAA-ODN antagonistic enhancement is broadly applicable

To determine if polymer conjugation could improve the antagonism of any ODN sequence, we synthesized another 1:1 conjugate, **44K-1 (4329)** using the previously described sequence 4329 (Table 4.1)(98), modified with a 3' AT linker. The results for these experiments are shown in Fig. 4.8. Under the conditions employed here, IC_{50} values for 4380AT and 4329AT were 161.8 ± 10.2 nM and 11.7 ± 0.6 nM (Fig. 4.7) respectively ($p < 0.0001$); indicating that the 4329AT is 13.8-fold more potent. **44K-1 (4329)** (circles) and 4329AT demonstrate IC_{50} values of 7.9 ± 0.1

nM and 11.7 ± 0.6 nM respectively (p = 0.0007) (Fig. 4.7). The dose response data shown in Fig. 4.7 illustrates that **44K-1 (4329)** (circles), like **44K-1**, is more potent than the unmodified ODN 4329AT (squares). These data suggest ODN-PAA conjugation is a broadly applicable strategy for the enhancement of TLR9 antagonism.

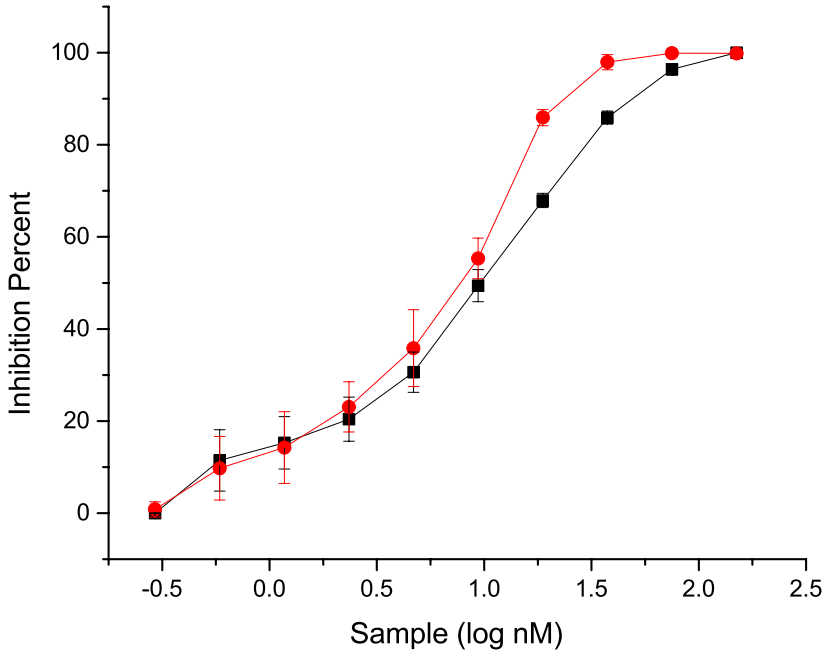

Figure 4.7 Dose response curves for ODN 4329AT (squares) and conjugate **44K-1 (4329)** (circles) plotted as percent inhibition against the log of the concentration ODN (nM). RAW264.7 cells were exposed for 24 hours to 2.5 μM ODN 1668AT and a serial dilution of the indicated antagonist (normalized to concentration ODN). Data shown are TNF-α concentrations of RAW264.7 supernatants, converted to a 0 to 100 scale (origin) and then to percent inhibition. Error bars are standard deviation of the average of four independent samples.

4.4. Discussion

4.4.1 PAA conjugation enhances ODN lifetime and cellular delivery

The dose response data in Fig. 4.2 clearly illustrate that the ODN-PAA conjugate **44K-1** shows antagonistic properties similar to the activity of 4380AT-PS. This enhanced activity is observed even though 4380AT-PS displays much more rapid and greater overall endocytosis (Figs. 4.5 and 4.4 respectively). We additionally show enhancement in antagonism by PAA conjugation of the optimized PO sequence 4329 ((98)).This PO backbone ODN demonstrates > 500% increase in activity over the PS-ODN as a result of a 5' truncation and allows determination if an optimized PO-ODN can have further enhancements in activity through PAA conjugation. Further sequence optimization in the context of PAA conjugation, could potentially lead to even significantly higher potency for either of the sequences employed here.

PS ODN are thought to gain their improved antagonism through higher intracellular delivery(245), nuclease resistance(246), and better binding to TLR9(97). Here we show simple PAA conjugation to the ODN 3' end drastically improves PO-ODN intracellular delivery (Fig. 4.3). Intracellular delivery is not as great as that observed for PS-ODN; however the greater nonspecific binding and endocytosis of PS-ODN correlate with pathology observed with their administration(246). With similar antagonistic properties and lower intracellular concentration, ODN-PAA conjugates have greater antagonistic efficiency.

PAA conjugation also provides complete 3' exonuclease protection and significant 5' exo- and endonuclease protection (Fig. 4.6). Under conditions used in this work, we observe 4380AT half-lives of 1 hour for degradation by 3' exonuclease activity, and 0.5 hours for degradation by 5' exo- and endonuclease activity. **44K-1** demonstrates 3' exonuclease and 5' exo- and endonuclease half-lives greater than 8 hours; well within the range of enhancement observed for PS-ODN. 3' Exonuclease and endonuclease activity are the major extracellular and intracellular nucleic acid degradative mechanisms, respectively.(243, 246) Our data from Fig 4.6 suggests 3' exonuclease resistance is not the mechanism of antagonistic improvement for the conjugates described here. Interestingly, 3' conjugation was recently reported to promote TLR9 agonism(244); however, we observed simple 3' hexanediol protection (4380AT-HD) to reduce antagonism; another indication these two types of ODN have different cellular targets. This reduction however, was overcome by PAA conjugation, perhaps through increased intracellular delivery or endonuclease resistance demonstrated in Figs. 4.4 and 4.6.

4.4.2 Valency enhancements occur within an optimal range

ODN valency further improves antagonism beyond the enhancement demonstrated through PAA conjugation by **44K-1. 44K-3** exhibits an ODN normalized IC_{50} value of 11.7 ± 1.3, a 1.5-fold improvement over that of **44K-1** (Fig. 4.3)**.** The highest antagonistic activities displayed by **44K-3** correlated with enhanced

early kinetics and greater overall intracellular delivery than both **44K-1** and **44K-6**. We hypothesize this is the main mechanism of antagonistic enhancement for **44K-3**.

Ashman et al. have shown TLR9 antagonism does not correlate with TLR9 binding and have hypothesized the target of antagonistic ODN is an accessory protein and not TLR9.(98) Here, **44K-3** displayed significantly greater endocytosis than other conjugates; this is not the case for agonistic ODN where endocytosis is correlated only to the concentration of polymer in media (manuscript in preparation). This suggests the enhancement in endocytosis of **44K-3** may arise from favorable interaction with a TLR9 accessory protein responsible for CpG delivery to endosomal TLR9. Many accessory proteins have been reported for TLR9 including granulin(47), HMGB1(65), LL37(247), defensins(248), CD14(51) and the mannose receptor(54). Among this group, both CD14 and the mannose receptor are known to oligomerize. CD14 is a glycosylphosphatidylinositol (GPI)-anchored protein.(51) GPI-anchored proteins are associated with lipid rafts and their cellular sorting is partly controlled by ligand or protein induced clustering.(249) The mannose receptor was recently shown to be required for endocytosis and trafficking of CpG ODN to endolysosomal compartments for TLR9 activation in murine macrophages.(54) The mannose receptor is known to homodimerize.(250) It is tempting to speculate the optimal valency of **44K-3** is preferential interaction with oligomerized accessory proteins of TLR9. Regardless, additional studies will be required to determine relevancy to human CpG recognition..

4.4.3 PAA is a novel inhibitor of TLR9 activation

We unexpectedly, but not surprisingly, identified PAA as a potent inhibitor of TLR9 activation. As described above, we choose PAA as the scaffold for several reasons including the inherent negative charge to discourage aggregation and promote the greatest ligand accessibility. We previously observed PAA to be a weak agonist (data not shown) but show potent TLR9 inhibition at the concentrations assayed in Fig. 4.11. It is important to note **44K** enhancement over 4380AT (3.8 ±0.4) is not as potent as **44K-1** (6.8 ±0.6), despite **44K** having significantly enhanced intracellular concentration 7.8-fold and 2.8-fold higher than **44K-1** at 20 and 60 minutes respectively (Fig. 4.5). The superior inhibition of the conjugates is even more apparent for **44K-3** with 3.5-fold greater inhibition at a three fold lower applied concentration than **44K.** Additionally, the improvement of **44K-1** over **44K** was 1.8-fold, while the improvement of **44K-1 (4329)** over **44K** is 5.5-fold, supporting the above assertion that PAA is an effective carrier, however, the antagonistic activities displayed by ODN-PAA are regulated by the independent activities of the ODN.

TLR9 ODN binding has been shown to be dependent upon the 2-deoxyribose-phosphate backbone, not base specificity or sequence.(94) Interestingly, many putative accessory molecules including LL37(68), HMGB1(67), scavenger receptors(251), CD14(51, 252), and even TLR9 itself(25, 253), may rely more upon charge interaction than any base or sequence requirements for ODN interaction. This perhaps explains the discrepancy in our observations that PAA is a weak agonist of TLR9, but at lower concentrations, is potentially scavenging one or more positively charged TLR9

accessory proteins. This is analogous to recent reports describing positively charged polymers as scavengers for extracellular nucleic acids to prevent inflammation.(234-236) Two molecular weights of PAA were used in this work with the lower molecular weight demonstrating greater inhibition of TLR9. This novel finding suggests a possible application of inexpensive and easily synthesized PAA as an inhibitor of TLR9 and possibly other nucleic acid receptors.

4.5 Conclusion

Here, we report PAA conjugation enhances antagonistic PO-ODN activities to those similar or better than equivalent PS-ODN. This enhancement can be attributed to significantly higher cellular internalization and resistance to both exo- and endonuclease activities. **44K-1 and 4380AT-PS have** equivalent activities, but the lower intracellular delivery of **44K-1** with respect to 4380AT-PS suggests higher efficiency of activation. Furthermore, multivalency augments antagonism but only for a limited range of valency. The conjugate demonstrating greatest antagonism, **44K-3,** exhibits more rapid and overall higher cellular internalization, resulting in the lowest IC_{50} values observed . Outside of this optimal range, antagonism decreases with increasing valency and decreasing intracellular delivery. Polymer conjugation presents a strategy for nucleic acid-based therapies to enhance activity, delivery and stability of natural PO-ODN.

4.6 Acknowledgments

This work was supported in part by the Center for Neutron Science at UD under award (U.S. Department of Commerce) #70NANB7H6178, as well as by the National Institutes of Health (1-RO1-EB006006). Its contents are solely the responsibility of the authors and do not necessarily represent the official views of NIH or the Department of Commerce.

4.7 Supplementary Information

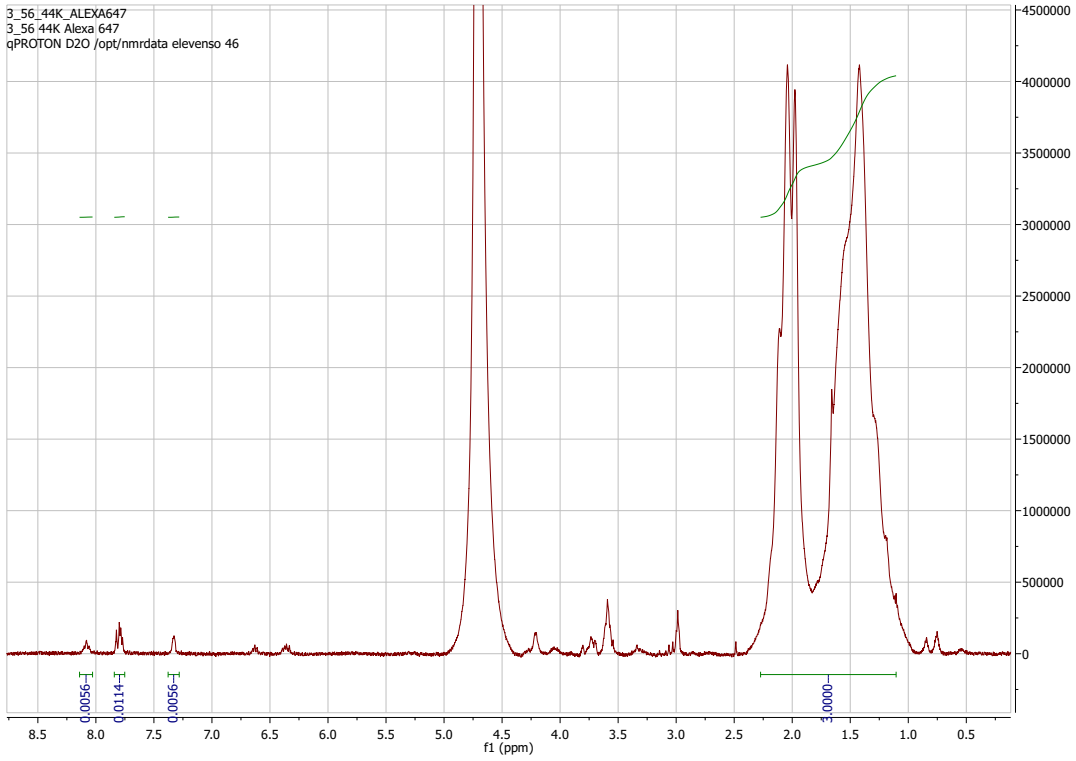

Figure 4.8 ^{1}H NMR spectra of Alexa Fluor 647 modified polymer **44K**. Calculated Alexa Fluor 647 functionality of 1.74.

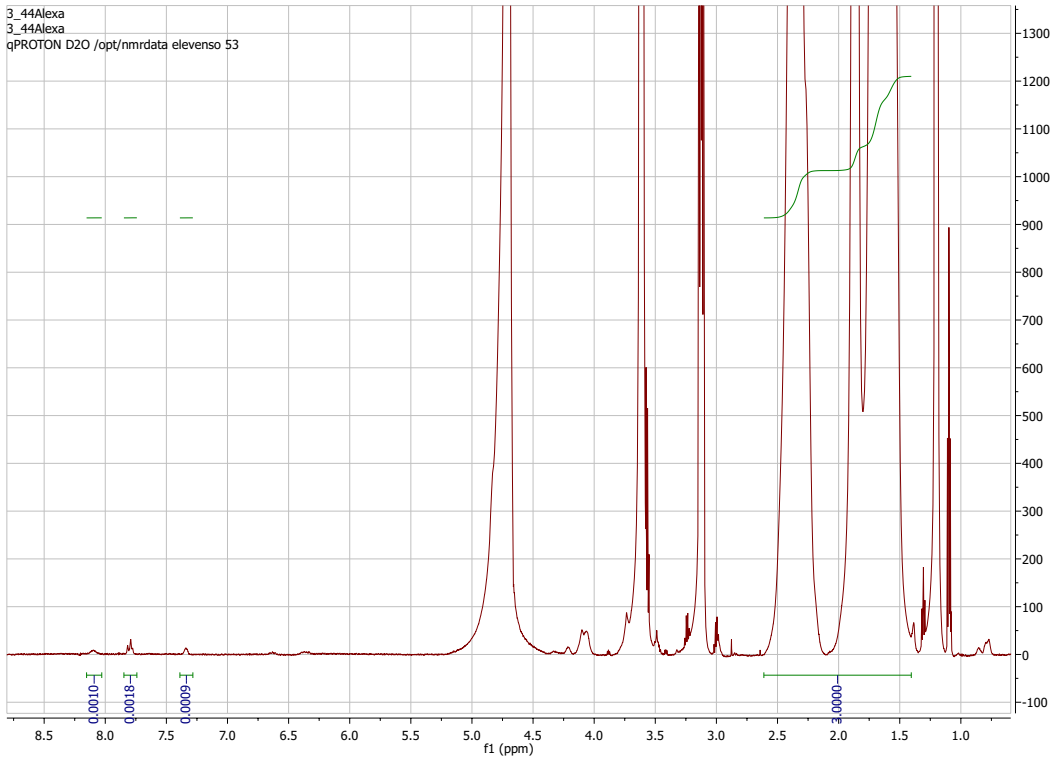

Figure 4.9 ^{1}H NMR spectra of Alexa Fluor 647 modified polymer **124K** used in the study and determined to have an Alexa Fluor 647 functionality of 0.7.

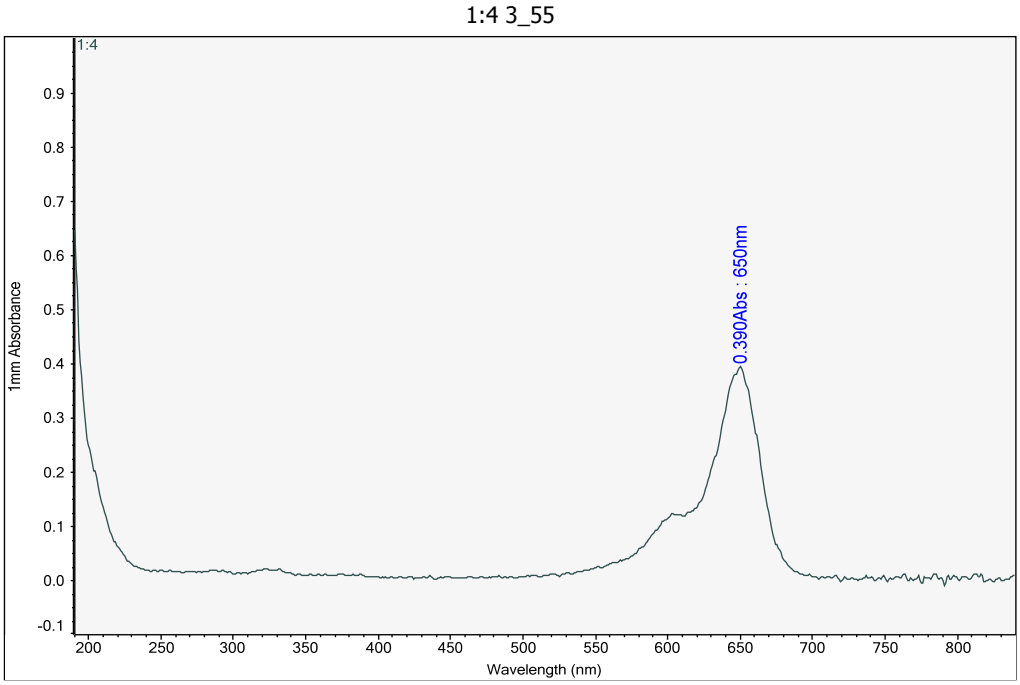

Figure 4.10 UV-VIS spectroscopy of Alexa Fluor 647 modified polymer **44K**. UV-VIS chromatogram of Alexa Fluor 647 modified polymer **44K** (ε=247000 $cm^{-1}mol^{-}1$) demonstrates 141.1 nmoles of Alexa 647. Using ^{1}H NMR determined functionality of 1.74 (above), leads to calculation of 81.1 nmoles **44K**, in agreement with synthesis scale of 82.5 nmoles (error <2%).

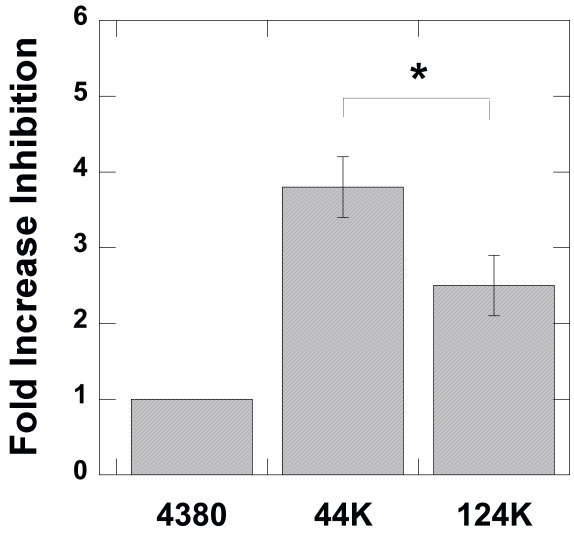

Figure 4.11 PAA is an inhibitor of TLR9. PAA at MW of 44K and 124K PAA were analyzed by dose response curves against the TLR9 agonist 1668. Data shown as IC_{50} fold-reduction, normalized to ODN 4380AT. Values represent three independent samples. Error bars are the standard deviation of the average. Statistically significant differences; * is p=0.013.

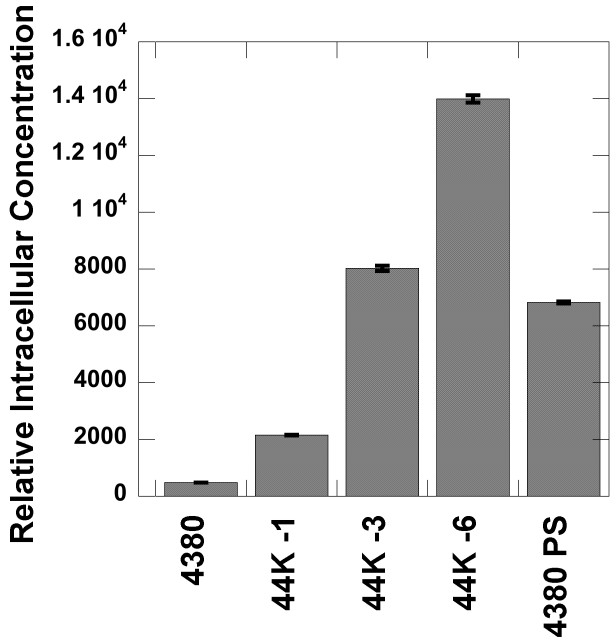

Figure 4.12 The relative intracellular ODN concentrations of 4380AT, **44K-1**, **44K-3**, **44K-6** and 4380AT-PS from figure 4.4, normalized to ODN concentration. Values are the difference in 37°C and 4°C flow cytometric mean fluorescence intensity values for RAW264.7 cells exposed to Alexa Fluor 647 labeled ODN and conjugates multiplied by the ODN functionality. Error bars are the standard deviation of the average of three independent samples.

Chapter 5

CONCLUSION

5.1 Work completed

The work in this dissertation demonstrates the use of a novel synthetic probe to elucidate the role of spatial presentation in Toll-like receptor 9 recognition of CpG oligonucleotides. These probes are comprised of a poly acrylic acid scaffold, chosen for its conformation of flexibility, high negative charge and carboxylic acid functionality for facile covalent modification, and single-stranded oligonucleotides with agonistic or antagonistic activities for Toll-like receptor 9. These novel ODN-PAA conjugates required the development of a synthetic scheme which allowed precise control over functionality, small-scale of synthesis, high efficiency and maintenance of an environment free from lipopolysaccharide. Poly(acrylic acid) was covalently modified via amide bond formation with addition of N-(2-aminoethyl)maleimide. This modified polymer was purified by centrifugal filtration and modified with thiol-modified oligonucleotides. Achieving high functionality required extensive optimization with specific requirements for oligonucleotide reduction, pH, salinity and buffer compositions. Ultimately, a synthetic scheme

incorporating all necessary elements for precise control of the resulting oligonucleotide functionality was achieved and reported in Chapter 2.

We characterized these novel constructs with proton nuclear magnetic resonance, size exclusion chromatography and UV-Vis-based spectrophotometry. These methods confirmed the covalent attachment of ODN to the polymer scaffold. Conjugate solution diameter was determined by dynamic light scattering; the resulting value was in agreement with theoretical calculations. The scaffold size is not modified by the addition of significantly smaller ODN.

These constructs were also examined for cell cytotoxicity using a measure of cellular metabolism. Over the time periods of administration in this study, no deficits in cellular metabolism were observed, and in fact, increases in cellular metabolism due to cellular activation were observed for the highest functionality ODN-PAA conjugate.

Flow cytometry, confocal microscopy, and transmission electron microscopy were used to monitor endocytosis of biotin-labeled ODN-PAA conjugates via biotin-streptavidin-mediated labeling with quantum dots. Endocytosis was shown to be an active process. Through confocal microscopy, we also demonstrated that intracellular constructs originated from the plasma membrane and showed punctate labeling in structures approximately 300 to 500 nm, indicating vesicular localization. Transmission electron microscopy confirmed the localization of ODN-PAA within membrane-bound compartments.

Significant enhancements in cytokine expression were demonstrated for all

conjugates synthesized with much greater expression for multivalent constructs, which increased with increasing valency. The most striking alteration of cytokine expression was for IL-6.

In chapter 3 we extended this investigation to determine whether a critical valency was required for Toll-like receptor 9 activation and if the molecular weight of the scaffold could impact observed activation through alteration of construct size and the number of possible receptors engaged. We modified the detection strategy from that employed in Chapter 2 to allow quantitative analysis of intracellular concentration. The use of biotin-streptavidin hybridization for labeling, although adventitious in amplifying fluorescent signal, was not sufficiently quantitative to discern differences in relative scaffold and resulting oligonucleotide concentrations. Alexa Fluor 647 was incorporated by covalent modification of the PAA scaffold and quantitative determination of labeling by NMR. This new fluorescently labeled scaffold now provided an internal standard to more accurately define conjugate functionality as well as allow direct relative comparisons to other conjugates and labeled ODN in flow cytometry and confocal microscopy studies.

We synthesized a library of ODN-PAA conjugates of increasing valency with values increasing by one up to a functionality of 7 on a 44 kDa PAA scaffold. We also synthesized a maximally functional conjugate (sterically hindered above this functionality) with a valency of 12 on this scaffold. To compliment this, three conjugates were synthesized conjugates using a larger 124 kDa PAA scaffold with

functionalities of 5, 12, and 30. This allowed direct comparison of the impact of functionality with conjugates of equal valency, but larger dimensions. These conjugates were used to stimulate the same RAW264.7 macrophages employed in Chapter 2 and the cell supernatants assayed for the cytokines IL-6, TNF-α and IL-10.

We demonstrated, through investigation of the **44K**-based series of conjugates, that there is a critical functionality for competent activation. This functionality represented by **44K-5** showed a significant increase in IL-6 expression, as well as significant changes in the kinetics of expression for TNF-α and IL-6. Through flow cytometry analysis of intracellular concentration, we demonstrate that there was no difference in intracellular scaffold concentration between **44K-5** and the next lowest functionality conjugate **44K-4**. This suggests that increased functionality and not subtle changes in intracellular concentration were the source of these observations.

An impact of presented ODN density was also shown to have biological implications. A linear increase in expression of TNF-α and IL-10 concomitant with increasing valency was observed for **44K**-based conjugates. This also applied for **124K**-based conjugates, but there were striking differences in expression comparing the isovalent constructs. ODN density (the ODN functionality divided by the M.W. of the scaffold) was shown to have a linear correlation to the concentration of IL-10 observed over 24 hours. This surprising result was only true for the earliest time point for TNF-α expression. TNF-α displayed a striking inverse relationship between

density and expression, but only for the higher M.W. **124K**-based scaffold. **124K-5** promoted significantly higher TNF-α expression than other conjugates. These drastic changes in expression between **44K**-based and **124K**-based isovalent constructs could not be attributed to differences in endocytosis. **44K-5** and **124K-5** had indistinguishable intracellular scaffold and ODN concentrations.

We further examined endocytosis through inhibition with the drug monodansylcadaverine, which inhibits clathrin-mediated endocytosis. This mechanism of endocytosis is used for receptor-mediated endocytosis and was a likely candidate for endocytosis of these multivalent conjugates. Literature reports also stated inhibition of ODN endocytosis by monodansylcadaverine. We determined that endocytosis of only the multivalent conjugate assayed was clathrin dependent. Both scaffold and ODN were inhibited by the drug, but to a lesser extent than the conjugate **44K-5**, which was inhibited up to ~90%. Additionally, ODN 1668AT demonstrated increased endocytosis at higher MDC concentrations, suggesting there are at least two mechanisms of endocytosis for ODN.

Confocal microscopy was employed to explore colocalization of conjugates with early and late endosomal markers EEA-1 and LAMP-1. TLR9 ligands are endocytosed and transit through EEA-1 endosomes. Ligand is then intracellularly transported to LAMP-1 endosomes where TLR9 activation and signaling take place. Conjugate **44K-2** showed much more significant colocalization with both markers than ODN, corroborating the flow cytometry data that showed much lower values for

the ODN 1668AT. Furthermore, colocalization with LAMP-1 increased with time and was significantly different from that of the bare scaffold, which preferentially accumulated in EEA-1 compartments. This data demonstrates preferential delivery of ODN-PAA conjugates to TLR9 providing significantly increased efficiency of delivery.

We hypothesized that TLR9 antagonists would also show enhancements from multivalent presentation. We utilized the same synthesis scheme and Alex Fluor 647 labeling of Chapter 3. RAW264.7 macrophages were employed in dose response experiments of antagonistic conjugates of the ODN 4380 (against the agonist ODN 1668) to determine IC_{50} values of modified and unmodified ODN. We demonstrated **44K-1** (antagonistic) has similar potency to a phosphorothioate version of the same ODN sequence. Increasing valency did decrease the observed IC_{50} value, but only for a conjugate with a functionality of three. Increasing valency past this resulted in a steady decrease in potency. This result was shown to correlate with increased endocytosis and intracellular scaffold concentration. This suggests that multivalency does promote endocytosis, but only for a limited range. Further increases in valency, due to the normalization based upon ODN concentration, decreased the extracellular scaffold concentration and resulting intracellular concentration. Additionally, this suggests antagonistic sequences do not benefit from multivalent display, only from enhanced intracellular delivery. This delivery was shown to be less than that of a corresponding phosphorothioate sequence, but demonstrates ODN-PAA antagonistic

conjugates more efficient than PS ODN for TLR9 antagonism.

Further optimization of the antagonistic sequence could likely lead to antagonistic conjugates of very high potency. The utility of this strategy was tested using a phosphodiester ODN sequence optimized for activity. This ODN, despite its unfavorable shorter length, yielded a conjugate with an IC_{50} value approaching 1 nM under our assay conditions. Surprisingly, we also found PAA to be a potent inhibitor of TLR9 activation. The potency was not as great as ODN-PAA conjugates, but the low cost and ease of synthesis of PAA could yield a simple an inexpensive therapy to limit TLR9, and perhaps other innate nucleic acid receptors. Phosphorothioate ODN have demonstrated adverse side effects such as organ damage and inhibition of the clotting cascade. Beyond the enhanced potency observed for ODN-PAA conjugates, the use of natural phosphodiester sequences may provide safer long-term therapies for TLR7, 8 and 9 antagonism.

5.2 Significance

Here, we employed the synthesis of rationally designed multivalent conjugates of ODN and poly(acrylic acid) to probe TLR9 ligand specificities for agonistic and antagonistic sequences. This strategy proved to be highly successful at demonstrating some key discoveries in the role of multivalency and ODN modification on TLR9 biological properties such as activation, inhibition, endocytosis, and subcellular localization.

Perhaps of greatest significance is the discovery that multivalent display regulates TLR9 activation through changes in valency and density of presentation. Activation was shown to correlate with increasing valency; however potent activation had a minimal functionality threshold. This could potentially be reporting specificities of receptor organization, suggested previously in the literature, and discussed in detail in Chapter 1.

Surprisingly, another specificity of TLR9 activation came to light examining the relationship of ODN presentation density and cytokine expression. A linear correlation was observed between density and IL-10 expression. For the higher molecular weight **124K**-based scaffolds, where valency was above the critical threshold, but lower in density, anomalous TNF-α expression was detected. This could be predicted from the anti-inflammatory properties of IL-10, which decrease the expression of inflammatory cytokines like TNF-α. The data for conjugate **124K-5** suggest that low-density presentation, but above a critical activation threshold, yields a potent inducer of inflammation. Likewise, the lower molecular weight but high valency **44K-12** is a potent inducer of IL-10 and represents a potential strategy for IL-10-based therapy and induction of antigen tolerance. The rationally designed ODN-PAA conjugates studied may have favorable conformational flexibility and therefore receptor engagement that has not been recapitulated in other particle-based delivery systems. These conjugates have not only led to insight in TLR9 biology, but may lead to new avenues for ODN-based therapeutics.

The examination of multivalent effects in TLR9 antagonism led to three significant findings. Perhaps the most important is the discovery that multivalency does not impact TLR9 antagonism but does enhance endocytosis at a critical valency. This corroborates the hypothesis that TLR9 antagonists interact with an unidentified accessory protein, not TLR9 directly, and antagonistic ODN sequence specificities are not representative of TLR9.(98) The specific range of valency, which enhanced antagonistic sequences, demonstrated in **Figs. 4.3** and **4.5**, was not evident for agonistic sequences **Fig. 3.3**. The dichotomous endocytosis preferences of agonistic and antagonistic sequences suggest the two do not share the same endocytosis mechanism. The enhancement in delivery reduced the IC_{50} value through increasing intracellular scaffold concentration, but not [ODN]. Higher functionality conjugates delivered higher intracellular ODN, but failed to be as potent in TLR9 antagonism. These data suggest a critical valency favorably targets an unknown protein and adds another mechanism of enhancing TLR9 antagonism.

Two other significant findings were described. The first is the inhibition of TLR9 activation by PAA. This could be significant through providing a low cost inhibitor of innate nucleic acid receptors, analogous to the work of the Sullenger lab.(236) Also, we reported decreased antagonism by a 3' modified ODN; modification with a simple Hexanediol significantly reduced the ODN potency. This is at odds with a report that 3' modification enhances TLR agonistic sequences and

further supports the above hypothesis that TLR9 antagonistic sequences function through a protein other than TLR9.

Taken together this data demonstrates the power and utility of rationally designed polymer-based probes for determining the molecular specificities of biological systems. With respect to the work presented here, this strategy could be applied to other TLR ligands to determine if multivalent presentation could be a generally applicable method of increasing activity and help elucidate how innate receptors respond to more biologically relevant spatial displays.

5.3 Future Work

The work presented in this thesis has opened many opportunities for future work. These possible directions include determining whether the principles shown here hold true in humans, whether multivalent recognition is generally applicable to all TLRs, and the use of these novel TLR ligand-polymer probes to discern the nature and specificities of the TLR signaling complex.

As detailed in section **1.1.4**, human expression of TLR9 is limited to B cells, pDC and neutrophils. TLR9 *in vitro* studies have predominantly been done in the RAW264.7 cell line since mice additionally express TLR9 in macrophages. This cell line is much easier to propagate and modify with siRNA or knock outs. Initial future work could be done with mouse isolated primary B cells or pDC, however, given the significant differences in murine and human immune response, human primary cells

would be the most appropriate. Human B cells and pDC must be continually isolated from patient samples such as blood. B cells could be assayed for changes in the cell surface markers CD80 and CD86. They could also functionally be assayed for changes in plasma cell development or antigen presentation. pDC responses could be monitored by proinflammatory cytokine expression of markers like TNF-α or IL-6. Changes in IFN expression could also be assayed; however, a recent report suggests the conjugates described in this thesis would not promote IFN expression.(86) Only ODN condensed through positively charged carriers promote IFN expression.

The TLR2 ligand muramyl dipeptide might also be used as a possible ligand for conjugation but was not explored further with concerns of possible aggregation through this ligands C_{12} to C_{16} fatty acid alkyl chains . As detailed throughout the thesis and particularly sections **1.1.3** and **1.1.4**, significant evidence suggests the TLRs respond to the context of presentation as well as the chemical structures of their ligands. Conjugates of other TLR ligands could be synthesized and examined in analogous methods to those presented within the thesis. The most similar ligand would be single stranded RNA, which can be synthesized with defined chemical functionalities. TLR7 and TLR8 have broader expression in humans, including dendritic cell types, and perhaps a greater impact on innate immune response.

Finally, additional studies to demonstrate the role of any signaling adapters or accessory proteins would be of great interest. Section **1.1.3** gives a detailed analysis of the current literature of signaling adapter, accessory or regulatory proteins of TLR9,

which could be responsible for the observed multivalent response in RAW264.7 cells. Many of these proteins have multiple roles or activities, requiring careful experimental design and analysis.

REFERENCES

1. Iwasaki A, Medzhitov R (2010) Regulation of adaptive immunity by the innate immune system. *Science* 327:291–295.

2. Takeuchi O, Akira S (2010) Pattern recognition receptors and inflammation. *Cell* 140:805–820.

3. Schenten D, Medzhitov R (2011) The control of adaptive immune responses by the innate immune system. *Adv Immunol* 109:87–124.

4. Connolly DJ, O'Neill LA (2012) New developments in Toll-like receptor targeted therapeutics. *Curr Opin Pharmacol* 12:510–518.

5. Gürtler C, Bowie AG (2013) Innate immune detection of microbial nucleic acids. *Trends Microbiol* 21:413–420.

6. Desmet CJ, Ishii KJ (2012) Nucleic acid sensing at the interface between innate and adaptive immunity in vaccination. *Nature Publishing Group* 12:479–491.

7. Fukui R, Miyake K (2012) Controlling systems of nucleic acid sensing-TLRs restrict homeostatic inflammation. *Experimental Cell Research* 318:1461–1466.

8. Trinchieri G, Sher A (2007) Cooperation of Toll-like receptor signals in innate immune defence. *Nature Reviews Immunology* 7:179–190.

9. Pålsson-McDermott EM, O'Neill LAJ (2007) Building an immune system from nine domains. *Biochem Soc Trans* 35:1437–1444.

10. Broz P, Monack DM (2013) Newly described pattern recognition receptors team up against intracellular pathogens. *Nature Publishing Group*.

11. Civril F et al. (2013) Structural mechanism of cytosolic DNA sensing by cGAS. *Nature*.

12. Sun L, Wu J, Du F, Chen X, Chen ZJ (2013) Cyclic GMP-AMP synthase is a cytosolic DNA sensor that activates the type I interferon pathway. *Science* 339:786–791.

13. Truhlar SME, Komives EA (2008) LRR domain folding: just put a cap on it! *Structure* 16:655–657.

14. Ng ACY et al. (2011) Human leucine-rich repeat proteins: a genome-wide bioinformatic categorization and functional analysis in innate immunity. *Proc Natl Acad Sci USA* 108 Suppl 1:4631–4638.

15. Barbalat R, Ewald SE, Mouchess ML, Barton GM (2011) Nucleic Acid Recognition by the Innate Immune System. *Annu Rev Immunol* 29:185–214.

16. Hemmi H et al. (2000) A Toll-like receptor recognizes bacterial DNA. *Nature* 408:740–745.

17. Krieg AM et al. (1995) CpG motifs in bacterial DNA trigger direct B-cell activation. *Nature* 374:546–549.

18. Ewald SE et al. (2008) The ectodomain of Toll-like receptor 9 is cleaved to generate a functional receptor. *Nature* 456:658–662.

19. Park B et al. (2008) Proteolytic cleavage in an endolysosomal compartment is required for activation of Toll-like receptor 9. *Nat Immunol* 9:1407–1414.

20. Qi R, Singh D, Kao CC (2012) Proteolytic Processing Regulates Toll-like Receptor 3 Stability and Endosomal Localization. *J Biol Chem* 287:32617–32629.

21. Ewald SE, Barton GM (2011) Nucleic acid sensing Toll-like receptors in autoimmunity. *Curr Opin Immunol* 23:3–9.

22. Tanji H, Ohto U, Shibata T, Miyake K, Shimizu T (2013) Structural reorganization of the Toll-like receptor 8 dimer induced by agonistic ligands. *Science* 339:1426–1429.

23. Choe J, Kelker MS, Wilson IA (2005) Crystal structure of human toll-like receptor 3 (TLR3) ectodomain. *Science* 309:581–585.

24. Bell JK et al. (2005) The molecular structure of the Toll-like receptor 3 ligand-binding domain. *Proc Natl Acad Sci USA* 102:10976–10980.

25. Onji M et al. (2013) An essential role for the N-terminal fragment of Toll-like receptor 9 in DNA sensing. *Nature Communications* 4:1949.

26. Hartmann G, Krieg AM (1999) CpG DNA and LPS induce distinct patterns of activation in human monocytes. *Gene Ther* 6:893–903.

27. Maurer T et al. (2002) CpG-DNA aided cross-presentation of soluble antigens by dendritic cells. *Eur J Immunol* 32:2356–2364.

28. Tighe H et al. (2000) Conjugation of protein to immunostimulatory DNA results in a rapid, long-lasting and potent induction of cell-mediated and humoral immunity. *Eur J Immunol* 30:1939–1947.

29. Tighe H et al. (2000) Conjugation of immunostimulatory DNA to the short ragweed allergen amb a 1 enhances its immunogenicity and reduces its allergenicity. *J Allergy Clin Immunol* 106:124–134.

30. Horner AA et al. (2001) Immunostimulatory DNA-based vaccines elicit multifaceted immune responses against HIV at systemic and mucosal sites. *J Immunol* 167:1584–1591.

31. Shirota H et al. (2001) Novel roles of CpG oligodeoxynucleotides as a leader for the sampling and presentation of CpG-tagged antigen by dendritic cells. *J Immunol* 167:66–74.

32. Shirota H, Sano K, Kikuchi T, Tamura G, Shirato K (2000) Regulation of murine airway eosinophilia and Th2 cells by antigen-conjugated CpG oligodeoxynucleotides as a novel antigen-specific immunomodulator. *J Immunol* 164:5575–5582.

33. Cho HJ et al. (2000) Immunostimulatory DNA-based vaccines induce cytotoxic lymphocyte activity by a T-helper cell-independent mechanism. *Nat Biotechnol* 18:509–514.

34. Ishii KJ, Akira S (2007) Toll or toll-free adjuvant path toward the optimal vaccine development. *J Clin Immunol* 27:363–371.

35. Heit A et al. (2003) Cutting edge: Toll-like receptor 9 expression is not required for CpG DNA-aided cross-presentation of DNA-conjugated antigens

but essential for cross-priming of CD8 T cells. *J Immunol* 170:2802–2805.

36. Miyake K (2006) Roles for accessory molecules in microbial recognition by Toll-like receptors. *J Endotoxin Res* 12:195–204.

37. Saitoh S-I, Miyake K (2009) Regulatory molecules required for nucleotide-sensing Toll-like receptors. *Immunol Rev* 227:32–43.

38. Lee CC, Avalos AM, Ploegh HL (2012) Accessory molecules for Toll-like receptors and their function. *Nature Publishing Group* 12:168–179.

39. Ewald SE et al. (2011) Nucleic acid recognition by Toll-like receptors is coupled to stepwise processing by cathepsins and asparagine endopeptidase. *Journal of Experimental Medicine* 208:643–651.

40. Brooks JC, Sun W, Chiosis G, Leifer CA (2012) Heat shock protein gp96 regulates Toll-like receptor 9 proteolytic processing and conformational stability. *Biochemical and Biophysical Research Communications* 421:780–784.

41. Liu B et al. (2010) Folding of Toll-like receptors by the HSP90 paralogue gp96 requires a substrate-specific cochaperone. *Nature Communications* 1:1–10.

42. Okuya K et al. (2010) Spatiotemporal Regulation of Heat Shock Protein 90-Chaperoned Self-DNA and CpG-Oligodeoxynucleotide for Type I IFN Induction via Targeting to Static Early Endosome. *The Journal of Immunology* 184:7092–7099.

43. Fukui R et al. (2009) Unc93B1 biases Toll-like receptor responses to nucleic acid in dendritic cells toward DNA- but against RNA-sensing. *J Exp Med* 206:1339–1350.

44. Sasai M, Linehan MM, Iwasaki A (2010) Bifurcation of Toll-like receptor 9 signaling by adaptor protein 3. *Science* 329:1530–1534.

45. Gursel M, Gursel I, Mostowski HS, Klinman DM (2006) CXCL16 influences the nature and specificity of CpG-induced immune activation. *J Immunol* 177:1575–1580.

46. Ruan BH et al. (2010) Complement C3a, CpG Oligos, and DNA/C3a Complex Stimulate IFN- Production in a Receptor for Advanced Glycation End Product-Dependent Manner. *The Journal of Immunology* 185:4213–4222.

47. Park B et al. (2011) Granulin is a soluble cofactor for toll-like receptor 9 signaling. *Immunity* 34:505–513.

48. Chockalingam A, Brooks JC, Cameron JL, Blum LK, Leifer CA (2009) TLR9 traffics through the Golgi complex to localize to endolysosomes and respond to CpG DNA. *Immunol Cell Biol* 87:209–217.

49. Takeda K, Akira S (2005) Toll-like receptors in innate immunity. *International Immunology* 17:1–14.

50. Lee H-K, Dunzendorfer S, Soldau K, Tobias PS (2006) Double-stranded RNA-mediated TLR3 activation is enhanced by CD14. *Immunity* 24:153–163.

51. Baumann CL et al. (2010) CD14 is a coreceptor of Toll-like receptors 7 and 9. *Journal of Experimental Medicine* 207:2689–2701.

52. Watanabe A et al. (2011) Raftlin is involved in the nucleocapture complex to induce poly(I:C)-mediated TLR3 activation. *J Biol Chem* 286:10702–10711.

53. Ranjith-Kumar CT et al. (2008) Single-stranded oligonucleotides can inhibit cytokine production induced by human toll-like receptor 3. *Mol Cell Biol* 28:4507–4519.

54. Moseman AP et al. (2013) Mannose Receptor 1 Mediates Cellular Uptake and Endosomal Delivery of CpG-Motif Containing Oligodeoxynucleotides. *The Journal of Immunology* 191:5615–5624.

55. Saitoh T et al. (2011) Antiviral Protein Viperin Promotes Toll-like Receptor 7- and Toll-like Receptor 9-Mediated Type I Interferon Production in Plasmacytoid Dendritic Cells. *Immunity* 34:352–363.

56. Liu X et al. (2011) Intracellular MHC class II molecules promote TLR-triggered innate immune responses by maintaining activation of the kinase Btk. *Nat Immunol* 12:416–424.

57. Russo C et al. (2011) Small molecule Toll-like receptor 7 agonists localize to the MHC class II loading compartment of human plasmacytoid dendritic cells. *Blood* 117:5683–5691.

58. Strong BSI, Unanue ER (2011) Presentation of Type B Peptide-MHC Complexes from Hen Egg White Lysozyme by TLR Ligands and Type I IFNs Independent of H2-DM Regulation. *The Journal of Immunology* 187:2193–2201.

59. Blander JM, Medzhitov R (2006) Toll-dependent selection of microbial antigens for presentation by dendritic cells. *Nature* 440:808–812.

60. Mantegazza AR et al. (2012) Adaptor Protein-3 in Dendritic Cells Facilitates Phagosomal Toll-like Receptor Signaling and Antigen Presentation to CD4(+) T Cells. *Immunity* 36:782–794.

61. Kenny EF et al. (2013) Bruton's Tyrosine Kinase Mediates the Synergistic Signalling between TLR9 and the B Cell Receptor by Regulating Calcium and Calmodulin. *PLoS ONE* 8:e74103.

62. (null) et al. (2011) Human serum amyloid P functions as a negative regulator of the innate and adaptive immune responses to DNA vaccines. *J Immunol* 186:2860–2870.

63. Nakamura N et al. (2009) Characterization of the interaction between serum mannan-binding protein and nucleic acid ligands. *Journal of Leukocyte Biology* 86:737–748.

64. Chen G-Y, Tang J, Zheng P, Liu Y (2009) CD24 and Siglec-10 selectively repress tissue damage-induced immune responses. *Science* 323:1722–1725.

65. Ivanov S et al. (2007) A novel role for HMGB1 in TLR9-mediated inflammatory responses to CpG-DNA. *Blood* 110:1970–1981.

66. Herold K et al. (2007) Receptor for advanced glycation end products (RAGE) in a dash to the rescue: inflammatory signals gone awry in the primal response to stress. *Journal of Leukocyte Biology* 82:204–212.

67. Tian J et al. (2007) Toll-like receptor 9-dependent activation by DNA-containing immune complexes is mediated by HMGB1 and RAGE. *Nat Immunol* 8:487–496.

68. Lande R et al. (2007) Plasmacytoid dendritic cells sense self-DNA coupled with antimicrobial peptide. *Nature* 449:564–569.

69. Gürsel M, Verthelyi D, Gürsel I, Ishii KJ, Klinman DM (2002) Differential and competitive activation of human immune cells by distinct classes of CpG oligodeoxynucleotide. *Journal of Leukocyte Biology* 71:813–820.

70. Hayashi F, Means TK, Luster AD (2003) Toll-like receptors stimulate human neutrophil function. *Blood* 102:2660–2669.

71. Bell JK et al. (2003) Leucine-rich repeats and pathogen recognition in Toll-like receptors. *Trends Immunol* 24:528–533.

72. Latz E et al. (2007) Ligand-induced conformational changes allosterically activate Toll-like receptor 9. *Nat Immunol* 8:772–779.

73. O'Neill LAJ, Bowie AG (2007) The family of five: TIR-domain-containing adaptors in Toll-like receptor signalling. *Nature Reviews Immunology* 7:353–364.

74. Pauls E et al. (2013) Two Phases of Inflammatory Mediator Production Defined by the Study of IRAK2 and IRAK1 Knock-in Mice. *The Journal of Immunology* 191:2717–2730.

75. Gay NJ, Gangloff M, O'Neill LAJ (2011) What the Myddosome structure tells us about the initiation of innate immunity. *Trends Immunol* 32:104–109.

76. Pirher N, Ivicak K, Pohar J, Bencina M, Jerala R (2008) A second binding site for double-stranded RNA in TLR3 and consequences for interferon activation. *Nat Struct Mol Biol* 15:761–763.

77. Gay NJ, Gangloff M (2007) Structure and function of Toll receptors and their ligands. *Annu Rev Biochem* 76:141–165.

78. Hipp MM et al. (2013) Processing of Human Toll-like Receptor 7by Furin-like Proprotein Convertases Is Required for Its Accumulation and Activity in Endosomes. *Immunity* 39:711–721.

79. Motshwene PG et al. (2009) An oligomeric signaling platform formed by the Toll-like receptor signal transducers MyD88 and IRAK-4. *J Biol Chem* 284:25404–25411.

80. Dan JM, Wang JP, Lee CK, Levitz SM (2008) Cooperative stimulation of dendritic cells by Cryptococcus neoformans mannoproteins and CpG oligodeoxynucleotides. *PLoS ONE* 3:e2046.

81. Bafica A et al. (2005) TLR9 regulates Th1 responses and cooperates with TLR2 in mediating optimal resistance to Mycobacterium tuberculosis. *J Exp Med* 202:1715–1724.

82. Sato A, Linehan MM, Iwasaki A (2006) Dual recognition of herpes simplex viruses by TLR2 and TLR9 in dendritic cells. *Proc Natl Acad Sci USA* 103:17343–17348.

83. Hanagata N (2012) Structure-dependent immunostimulatory effect of CpG oligodeoxynucleotides and their delivery system. *IJN* 7:2181–2195.

84. Hanagata N et al. (2012) Effect of molecular weight of polyethyleneimine on loading of CpG oligodeoxynucleotides onto flake-shell silica nanoparticles for enhanced TLR9-mediated induction of interferon-&alpha. *IJN*:3625.

85. Kerkmann M et al. (2005) Spontaneous formation of nucleic acid-based nanoparticles is responsible for high interferon-alpha induction by CpG-A in plasmacytoid dendritic cells. *J Biol Chem* 280:8086–8093.

86. Chinnathambi S, Chen S, Ganesan S, Hanagata N (2012) Binding mode of CpG oligodeoxynucleotides to nanoparticles regulates bifurcated cytokine induction via Toll-like receptor 9. *Sci Rep* 2:534.

87. Kerkmann M et al. (2006) Immunostimulatory properties of CpG-oligonucleotides are enhanced by the use of protamine nanoparticles. *Oligonucleotides* 16:313–322.

88. Shimada N et al. (2007) A polysaccharide carrier to effectively deliver native phosphodiester CpG DNA to antigen-presenting cells. *Bioconjug Chem* 18:1280–1286.

89. Roberts TL et al. (2005) Differences in macrophage activation by bacterial DNA and CpG-containing oligonucleotides. *J Immunol* 175:3569–3576.

90. Suwarti S, Yamazaki T, Svetlana C, Hanagata N (2013) Recognition of CpG oligodeoxynucleotides by human Toll-like receptor 9 and subsequent cytokine induction. *Biochemical and Biophysical Research Communications* 430:1234–1239.

91. Wang Y, Krieg AM (2003) Synergy between CpG- or non-CpG DNA and specific antigen for B cell activation. *International Immunology* 15:223–231.

92. Yasuda K et al. (2006) CpG motif-independent activation of TLR9 upon endosomal translocation of “natural” phosphodiester DNA. *Eur J Immunol* 36:431–436.

93. Yasuda K et al. (2009) Requirement for DNA CpG content in TLR9-dependent dendritic cell activation induced by DNA-containing immune complexes. *J Immunol* 183:3109–3117.

94. Haas T et al. (2008) The DNA sugar backbone 2' deoxyribose determines toll-like receptor 9 activation. *Immunity* 28:315–323.

95. Liu Y, Luo X, Yang C, Yu S, Xu H (2011) Three CpG oligodeoxynucleotide classes differentially enhance antigen-specific humoral and cellular immune responses in mice. *Vaccine* 29:5778–5784.

96. Marshall JD et al. (2003) Novel chimeric immunomodulatory compounds containing short CpG oligodeoxyribonucleotides have differential activities in human cells. *Nucleic acids research* 31:5122–5133.

97. Lenert PS (2010) Classification, Mechanisms of Action, and Therapeutic Applications of Inhibitory Oligonucleotides for Toll-Like Receptors (TLR) 7 and 9. *Mediators of Inflammation* 2010:1–10.

98. Ashman RF, Goeken JA, Latz E, Lenert P (2011) Optimal oligonucleotide sequences for TLR9 inhibitory activity in human cells: lack of correlation with TLR9 binding. *International Immunology* 23:203–214.

99. Honda K et al. (2005) Spatiotemporal regulation of MyD88-IRF-7 signalling for robust type-I interferon induction. *Nature* 434:1035–1040.

100. Guiducci C et al. (2006) Properties regulating the nature of the plasmacytoid dendritic cell response to Toll-like receptor 9 activation. *J Exp Med* 203:1999–2008.

101. Vollmer J, Krieg AM (2009) Immunotherapeutic applications of CpG oligodeoxynucleotide TLR9 agonists. *Advanced Drug Delivery Reviews* 61:195–204.

102. Gupta K, Cooper C (2008) A review of the role of CpG oligodeoxynucleotides as toll-like receptor 9 agonists in prophylactic and therapeutic vaccine development in infectious diseases. *Drugs R D* 9:137–145.

103. Coffman RL, Sher A, Seder RA (2010) Vaccine adjuvants: putting innate immunity to work. *Immunity* 33:492–503.

104. Lande R, Gilliet M (2010) Plasmacytoid dendritic cells: key players in the initiation and regulation of immune responses. *Ann N Y Acad Sci* 1183:89–103.

105. Lee J et al. (2012) Activation of innate immunity is required for efficient nuclear reprogramming. *Cell* 151:547–558.

106. Kawai T, Akira S (2010) The role of pattern-recognition receptors in innate immunity: update on Toll-like receptors. *Nat Immunol* 11:373–384.

107. Marshak-Rothstein A (2006) Toll-like receptors in systemic autoimmune disease. *Nature Reviews Immunology* 6:823–835.

108. Gomez CR, Nomellini V, Faunce DE, Kovacs EJ (2008) Innate immunity and aging. *Experimental Gerontology* 43:718–728.

109. Van Duin D, Shaw AC (2007) Toll-like receptors in older adults. *Journal of the American Geriatrics Society* 55:1438–1444.

110. Lafyatis R, Marshak-Rothstein A (2007) Toll-like receptors and innate immune responses in systemic lupus erythematosus. *Arthritis Res Ther* 9:222.

111. Gilliet M, Cao W, Liu Y-J (2008) Plasmacytoid dendritic cells: sensing nucleic acids in viral infection and autoimmune diseases. *Nature Publishing Group* 8:594–606.

112. Allam R, Anders H-J (2008) The role of innate immunity in autoimmune tissue injury. *Curr Opin Rheumatol* 20:538–544.

113. Marchant DJ et al. (2012) Inflammation in myocardial diseases. *Circ Res* 110:126–144.

114. López J et al. (2012) Viral and bacterial patterns induce TLR-mediated sustained inflammation and calcification in aortic valve interstitial cells. *Int J Cardiol* 158:18–25.

115. Lenert P (2010) Nucleic acid sensing receptors in systemic lupus erythematosus: development of novel DNA- and/or RNA-like analogues for treating lupus. *Clin Exp Immunol* 161:208–222.

116. Kawasaki T, Kawai T, Akira S (2011) Recognition of nucleic acids by pattern-recognition receptors and its relevance in autoimmunity. *Immunol Rev* 243:61–73.

117. Grubeck-Loebenstein B et al. (2009) Immunosenescence and vaccine failure in the elderly. *Aging Clin Exp Res* 21:201–209.

118. Pérez-Cabezas B et al. (2007) Reduced numbers of plasmacytoid dendritic cells in aged blood donors. *Experimental Gerontology* 42:1033–1038.

119. Csiszar A, Wang M, Lakatta EG, Ungvari Z (2008) Inflammation and endothelial dysfunction during aging: role of NF-kappaB. *J Appl Physiol* 105:1333–1341.

120. Lambeth JD (2007) Nox enzymes, ROS, and chronic disease: an example of antagonistic pleiotropy. *Free Radic Biol Med* 43:332–347.

121. Stout-Delgado HW, Yang X, Walker WE, Tesar BM, Goldstein DR (2008) Aging impairs IFN regulatory factor 7 up-regulation in plasmacytoid dendritic cells during TLR9 activation. *J Immunol* 181:6747–6756.

122. Agrawal A, Agrawal S, Tay J, Gupta S (2008) Biology of dendritic cells in aging. *J Clin Immunol* 28:14–20.

123. Sharma S, Dominguez AL, Hoelzinger DB, Lustgarten J (2008) CpG-ODN but not other TLR-ligands restore the antitumor responses in old mice: the implications for vaccinations in the aged. *Cancer Immunol Immunother* 57:549–561.

124. Green NM, Moody K-S, Debatis M, Marshak-Rothstein A (2012) Activation of Autoreactive B Cells by Endogenous TLR7 and TLR3 RNA Ligands. *J Biol Chem* 287:39789–39799.

125. Green NM, Marshak-Rothstein A (2011) Toll-like receptor driven B cell activation in the induction of systemic autoimmunity. *Semin Immunol* 23:106–112.

126. Kandimalla ER et al. (2013) Design, synthesis and biological evaluation of novel antagonist compounds of Toll-like receptors 7, 8 and 9. *Nucleic acids research* 41:3947–3961.

127. Bournazos S, Hart SP, Chamberlain LH, Glennie MJ, Dransfield I (2009) Association of FcgammaRIIa (CD32a) with lipid rafts regulates ligand binding activity. *J Immunol* 182:8026–8036.

128. Zhu X et al. (2010) Macrophage ABCA1 reduces MyD88-dependent Toll-like receptor trafficking to lipid rafts by reduction of lipid raft cholesterol. *The Journal of Lipid Research* 51:3196–3206.

129. Dil N, Marshall AJ (2009) Role of phosphoinositide 3-kinase p110 delta in TLR4- and TLR9-mediated B cell cytokine production and differentiation. *Mol Immunol* 46:1970–1978.

130. Schlessinger J (1988) The epidermal growth factor receptor as a multifunctional allosteric protein. *Biochemistry* 27:3119–3123.

131. Holm CK et al. (2012) Virus-cell fusion as a trigger of innate immunity dependent on the adaptor STING. *Nat Immunol* 13:737–743.

132. Mariathasan S, Monack DM (2007) Inflammasome adaptors and sensors: intracellular regulators of infection and inflammation. *Nature Reviews Immunology* 7:31–40.

133. Chikh G et al. (2009) Synthetic methylated CpG ODNs are potent in vivo adjuvants when delivered in liposomal nanoparticles. *International Immunology* 21:757–767.

134. Rutz M et al. (2004) Toll-like receptor 9 binds single-stranded CpG-DNA in a sequence- and pH-dependent manner. *Eur J Immunol* 34:2541–2550.

135. Baddeley D et al. (2011) 4D super-resolution microscopy with conventional fluorophores and single wavelength excitation in optically thick cells and tissues. *PLoS ONE* 6:e20645.

136. Leung BO, Chou KC (2011) Review of super-resolution fluorescence microscopy for biology. *Appl Spectrosc* 65:967–980.

137. Shu D, Zhang H, Jin J, Guo P (2007) Counting of six pRNAs of phi29 DNA-packaging motor with customized single-molecule dual-view system. *The EMBO Journal* 26:527–537.

138. Luo J et al. (2012) Lateral clustering of TLR3:dsRNA signaling units revealed by TLR3ecd:3Fabs quaternary structure. *Journal of Molecular Biology* 421:112–124.

139. Lillemeier BF et al. (2009) TCR and Lat are expressed on separate protein islands on T cell membranes and concatenate during activation. *Nat Immunol* 11:90–96.

140. Abulrob A et al. (2010) Nanoscale imaging of epidermal growth factor receptor clustering: effects of inhibitors. *J Biol Chem* 285:3145–3156.

141. Greenfield D et al. (2009) Self-organization of the Escherichia coli chemotaxis network imaged with super-resolution light microscopy. *PLoS Biol* 7:e1000137.

142. Baddeley D et al. (2009) Optical single-channel resolution imaging of the ryanodine receptor distribution in rat cardiac myocytes. *Proc Natl Acad Sci USA* 106:22275–22280.

143. Aaron JS, Carson BD, Timlin JA (2012) Characterization of Differential Toll-like Receptor Responses below the Optical Diffraction Limit. *Small* 8:3041–3049.

144. Barbalat R, Lau L, Locksley RM, Barton GM (2009) Toll-like receptor 2 on inflammatory monocytes induces type I interferon in response to viral but not bacterial ligands. *Nat Immunol* 10:1200–1207.

145. Mukherjee S et al. (2013) Monovalent and Multivalent Ligation of the B Cell Receptor Exhibit Differential Dependence upon Syk and Src Family Kinases. *Science Signaling* 6:ra1.

146. Natkanski E et al. (2013) B cells use mechanical energy to discriminate antigen affinities. *Science* 340:1587–1590.

147. Tong GJ, Hsiao SC, Carrico ZM, Francis MB (2009) Viral capsid DNA aptamer conjugates as multivalent cell-targeting vehicles. *J Am Chem Soc* 131:11174–11178.

148. Rinker S, Ke Y, Liu Y, Chhabra R, Yan H (2008) Self-assembled DNA nanostructures for distance-dependent multivalent ligand-protein binding. *Nat Nanotechnol* 3:418–422.

149. O'Reilly MK et al. (2008) Bifunctional CD22 ligands use multimeric immunoglobulins as protein scaffolds in assembly of immune complexes on B cells. *J Am Chem Soc* 130:7736–7745.

150. Nangreave J, Han D, Liu Y, Yan H (2010) DNA origami: a history and current perspective. *Curr Opin Chem Biol* 14:608–615.

151. Wei B, Dai M, Yin P (2012) Complex shapes self-assembled from single-stranded DNA tiles. *Nature* 485:623–626.

152. Li J et al. (2011) Self-Assembled Multivalent DNA Nanostructures for Noninvasive Intracellular Delivery of Immunostimulatory CpG Oligonucleotides. *ACS Nano* 5:8783–8789.

153. Schüller VJ et al. (2011) Cellular Immunostimulation by CpG-Sequence-Coated DNA Origami Structures. *ACS Nano* 5:9696–9702.

154. Kim Y, Cao Z, Tan W (2008) Molecular assembly for high-performance bivalent nucleic acid inhibitor. *Proc Natl Acad Sci USA* 105:5664–5669.

155. Nishikawa M, Matono M, Rattanakiat S, Matsuoka N, Takakura Y (2008) Enhanced immunostimulatory activity of oligodeoxynucleotides by Y-shape formation. *Immunology* 124:247–255.

156. Mohri K et al. (2012) Increased immunostimulatory activity of polypod-like structured DNA by ligation of the terminal loop structures. *J Control Release* 163:285–292.

157. Rattanakiat S, Nishikawa M, Funabashi H, Luo D, Takakura Y (2009) The assembly of a short linear natural cytosine-phosphate-guanine DNA into dendritic structures and its effect on immunostimulatory activity. *Biomaterials* 30:5701–5706.

158. Boniface JJ et al. (1998) Initiation of signal transduction through the T cell receptor requires the multivalent engagement of peptide/MHC ligands [corrected]. *Immunity* 9:459–466.

159. Liu AP, Aguet F, Danuser G, Schmid SL (2010) Local clustering of transferrin receptors promotes clathrin-coated pit initiation. *The Journal of Cell Biology* 191:1381–1393.

160. Gong X, Dubois DH, Miller DJ, Shur BD (1995) Activation of a G protein complex by aggregation of beta-1,4-galactosyltransferase on the surface of sperm. *Science* 269:1718–1721.

161. Cremesti A et al. (2001) Ceramide enables fas to cap and kill. *J Biol Chem* 276:23954–23961.

162. Li Q et al. (2010) Chemically Self-Assembled Antibody Nanorings (CSANs): Design and Characterization of an Anti-CD3 IgM Biomimetic. *J Am Chem Soc*.

163. Dintzis HM, Dintzis RZ, Vogelstein B (1976) Molecular determinants of immunogenicity: the immunon model of immune response. *Proc Natl Acad Sci USA* 73:3671–3675.

164. Dintzis RZ, Vogelstein B, Dintzis HM (1982) Specific cellular stimulation in the primary immune response: experimental test of a quantized model. *Proc Natl Acad Sci USA* 79:884–888.

165. Dintzis RZ, Middleton MH, Dintzis HM (1983) Studies on the immunogenicity and tolerogenicity of T-independent antigens. *J Immunol* 131:2196–2203.

166. Dintzis RZ, Okajima M, Middleton MH, Greene G, Dintzis HM (1989) The immunogenicity of soluble haptenated polymers is determined by molecular mass and hapten valence. *J Immunol* 143:1239–1244.

167. Lee Y, Sampson NS (2009) Polymeric ADAM protein mimics interrogate mammalian sperm-egg binding. *ChemBioChem* 10:929–937.

168. Jacobson KA (2010) GPCR ligand-dendrimer (GLiDe) conjugates: future smart drugs? *Trends in Pharmacological Sciences* 31:575–579.

169. Keene AM, Balasubramanian R, Lloyd J, Shainberg A, Jacobson KA (2010) Multivalent dendrimeric and monomeric adenosine agonists attenuate cell death in HL-1 mouse cardiomyocytes expressing the A3 receptor. *Biochemical Pharmacology* 80:188–196.

170. Gestwicki JE, Strong LE, Kiessling LL (2000) Tuning chemotactic responses with synthetic multivalent ligands. *Chemistry & Biology* 7:583–591.

171. Puffer EB, Pontrello JK, Hollenbeck JJ, Kink JA, Kiessling LL (2007) Activating B cell signaling with defined multivalent ligands. *ACS Chem Biol* 2:252–262.

172. Smith EA, Thomas WD, Kiessling LL, Corn RM (2003) Surface plasmon resonance imaging studies of protein-carbohydrate interactions. *J Am Chem Soc* 125:6140–6148.

173. Kiessling LL, Grim JC (2013) Glycopolymer probes of signal transduction. *Chem Soc Rev* 42:4476–4491.

174. Duckworth BP et al. (2007) A universal method for the preparation of covalent protein-DNA conjugates for use in creating protein nanostructures. *Angew Chem Int Ed Engl* 46:8819–8822.

175. Milani S, Bombelli FB, Berti D, Baglioni P (2007) Nucleolipoplexes: a new paradigm for phospholipid bilayer-nucleic acid interactions. *J Am Chem Soc* 129:11664–11665.

176. Ono A (2006) DNA‐Synthetic Polymer Conjugates. *Macromolecular Chemistry and Physics* 207:1629–1632.

177. de Lambert B et al. (2005) Polymer-oligonucleotide conjugate synthesis from an amphiphilic block copolymer. Applications to DNA detection on microarray. *Bioconjug Chem* 16:265–274.

178. de Lambert B et al. (2008) Block copolymer-oligonucleotide conjugates for genotyping on microarrays. *Anal Biochem* 373:229–238.

179. Kawai T, Akira S (2009) The roles of TLRs, RLRs and NLRs in pathogen recognition. *International Immunology* 21:317–337.

180. Krieg AM (2012) CpG still rocks! Update on an accidental drug. *Nucleic Acid Ther* 22:77–89.

181. de Jong SD et al. (2010) The Immunostimulatory Activity of Unmethylated and Methylated CpG Oligodeoxynucleotide Is Dependent on Their Ability To Colocalize with TLR9 in Late Endosomes. *The Journal of Immunology* 184:6092–6102.

182. Chen HC, Sun B, Tran KK, Shen H (2011) Effects of particle size on toll-like receptor 9-mediated cytokine profiles. *Biomaterials* 32:1731–1737.

183. Wei M et al. (2011) Polyvalent Immunostimulatory Nanoagents with Self-Assembled CpG Oligonucleotide-Conjugated Gold Nanoparticles. *Angew Chem Int Ed* 51:1202–1206.

184. Zhao D et al. (2011) Carbon Nanotubes Enhance CpG Uptake and Potentiate Antiglioma Immunity. *Clinical Cancer Research* 17:771–782.

185. Matsuoka N, Nishikawa M, Mohri K, Rattanakiat S, Takakura Y (2010) Structural and immunostimulatory properties of Y-shaped DNA consisting of phosphodiester and phosphorothioate oligodeoxynucleotides. *J Control Release* 148:311–316.

186. Minari J et al. (2011) Enhanced Cytokine Secretion from Primary Macrophages due to Dectin-1 Mediated Uptake of CpG DNA/β-1,3-Glucan Complex. *Bioconjug Chem* 22:9–15.

187. Obata M et al. (2011) Synthesis, characterization and cellular internalization of poly (2-hydroxyethyl methacrylate) bearing α-D-mannopyranose. *Polym Chem* 2:651–658.

188. Geng J et al. (2007) Site-directed conjugation of "clicked" glycopolymers to form glycoprotein mimics: binding to mammalian lectin and induction of immunological function. *J Am Chem Soc* 129:15156–15163.

189. Bonora GM, Ivanova E, Zarytova V, Burcovich B, Veronese FM (1997) Synthesis and characterization of high-molecular mass polyethylene glycol-conjugated oligonucleotides. *Bioconjug Chem* 8:793–797.

190. Lifland AW, Zurla C, Santangelo PJ (2010) Single Molecule Sensitive Multivalent Polyethylene Glycol Probes for RNA Imaging. *Bioconjug Chem* 21:483–488.

191. Rapozzi V et al. (2002) Antigene Effect in K562 Cells of a PEG-Conjugated Triplex-Forming Oligonucleotide Targeted to the bcr/ ablOncogene †. *Biochemistry* 41:502–510.

192. Meyer M et al. (2009) Synthesis and Biological Evaluation of a Bioresponsive and Endosomolytic siRNA−Polymer Conjugate. *Mol Pharm* 6:752–762.

193. Cantor CR, Warshaw MM, Shapiro H (1970) Oligonucleotide interactions. 3. Circular dichroism studies of the conformation of deoxyoligonucleotides. *Biopolymers* 9:1059–1077.

194. Cavaluzzi MJ (2004) Revised UV extinction coefficients for nucleoside-5'-monophosphates and unpaired DNA and RNA. *Nucleic acids research* 32:13e–13.

195. Lacey DC et al. (2012) Defining GM-CSF- and macrophage-CSF-dependent macrophage responses by in vitro models. *The Journal of Immunology* 188:5752–5765.

196. Wang G, Petzke MM, Iyer R, Wu H, Schwartz I (2008) Pattern of proinflammatory cytokine induction in RAW264.7 mouse macrophages is identical for virulent and attenuated Borrelia burgdorferi. *J Immunol* 180:8306–8315.

197. Gust TC, Diebold SS, Cotten M, Zenke M (2004) RNA-containing adenovirus/polyethylenimine transfer complexes effectively transduce dendritic cells and induce antigen-specific T cell responses. *J Gene Med* 6:464–470.

198. Liu Y, Reineke TM (2007) Poly(glycoamidoamine)s for gene delivery. structural effects on cellular internalization, buffering capacity, and gene expression. *Bioconjug Chem* 18:19–30.

199. Hartmann L, Häfele S, Peschka-Süss R, Antonietti M, Börner HG (2008) Tailor-made poly(amidoamine)s for controlled complexation and condensation of DNA. *Chemistry* 14:2025–2033.

200. Delude RL et al. (1995) CD14 enhances cellular responses to endotoxin without imparting ligand-specific recognition. *Proc Natl Acad Sci USA* 92:9288–9292.

201. Lien E et al. (2000) Toll-like receptor 4 imparts ligand-specific recognition of bacterial lipopolysaccharide. *J Clin Invest* 105:497–504.

202. Forget AL, Kowalczykowski SC (2012) Single-molecule imaging of DNA pairing by RecA reveals a three-dimensional homology search. *Nature* 482:423–427.

203. Yellepeddi VK, Kumar A, Palakurthi S (2009) Biotinylated poly(amido)amine (PAMAM) dendrimers as carriers for drug delivery to ovarian cancer cells in vitro. *Anticancer Res* 29:2933–2943.

204. Putta MR et al. (2010) Peptide conjugation at the 5'-end of oligodeoxynucleotides abrogates toll-like receptor 9-mediated immune stimulatory activity. *Bioconjug Chem* 21:39–45.

205. Murphy MC, Rasnik I, Cheng W, Lohman TM, Ha T (2004) Probing single-stranded DNA conformational flexibility using fluorescence spectroscopy. *Biophys J* 86:2530–2537.

206. Barysch SV, Aggarwal S, Jahn R, Rizzoli SO (2009) Sorting in early endosomes reveals connections to docking- and fusion-associated factors. *Proc Natl Acad Sci USA* 106:9697–9702.

207. Bakker AC, Webster P, Jacob WA, Andrews NW (1997) Homotypic fusion between aggregated lysosomes triggered by elevated [Ca2+]i in fibroblasts. *Journal of Cell Science* 110 (Pt 18):2227–2238.

208. Bauer S et al. (2001) Human TLR9 confers responsiveness to bacterial DNA via species-specific CpG motif recognition. *Proc Natl Acad Sci USA* 98:9237–9242.

209. Sparwasser T et al. (1998) Bacterial DNA and immunostimulatory CpG oligonucleotides trigger maturation and activation of murine dendritic cells. *Eur J Immunol* 28:2045–2054.

210. Ahmad-Nejad P et al. (2002) Bacterial CpG-DNA and lipopolysaccharides activate Toll-like receptors at distinct cellular compartments. *Eur J Immunol* 32:1958–1968.

211. Agrawal S, Zhao Q (1998) Antisense therapeutics. *Curr Opin Chem Biol* 2:519–528.

212. Verthelyi D, Zeuner RA (2003) Differential signaling by CpG DNA in DCs and B cells: not just TLR9. *Trends Immunol* 24:519–522.

213. Mammen M, Choi S-K, Whitesides GM (1998) Polyvalent interactions in biological systems: implications for design and use of multivalent ligands and inhibitors. *Angew Chem Int Ed Engl* 37:2754–2794.

214. Kiessling LL, Gestwicki JE, Strong LE (2006) Synthetic multivalent ligands as probes of signal transduction. *Angew Chem Int Ed Engl* 45:2348–2368.

215. Borrok MJ, Kolonko EM, Kiessling LL (2008) Chemical probes of bacterial signal transduction reveal that repellents stabilize and attractants destabilize the chemoreceptor array. *ACS Chem Biol* 3:101–109.

216. Levenson EA, Kiick KL (2014) DNA-polymer conjugates for immune stimulation through Toll-like receptor 9 mediated pathways. *Acta Biomater* 10:1134–1145.

217. Terpetschnig EA, Patsenkar LD, Oswald B (2000) Luminescent compounds.

218. Terpetschnig EA, Patsenkar LD, Tatarets A (2003) Luminescent compounds.

219. Chiuman W, Li Y (2007) Efficient signaling platforms built from a small catalytic DNA and doubly labeled fluorogenic substrates. *Nucleic acids research* 35:401–405.

220. Ashman RF, Goeken JA, Lenert PS (2011) Aggregation and secondary loop structure of oligonucleotides do not determine their ability to inhibit TLR9. *International Immunopharmacology* 11:1032–1037.

221. Levenson EA, Kiick KL (2014) DNA-polymer conjugates for immune stimulation through Toll-like receptor 9 mediated pathways. *Acta Biomater* 10:1134–1145.

222. Rikihisa Y, Zhang Y, Park J (1994) Inhibition of infection of macrophages with Ehrlichia risticii by cytochalasins, monodansylcadaverine, and taxol. *Infection and Immunity* 62:5126–5132.

223. Davies PJ et al. (1980) Transglutaminase is essential in receptor-mediated endocytosis of alpha 2-macroglobulin and polypeptide hormones. *Nature* 283:162–167.

224. Chaturvedi A, Pierce SK (2009) How location governs toll-like receptor signaling. *Traffic* 10:621–628.

225. Hazeki K, Uehara M, Nigorikawa K, Hazeki O (2013) PIKfyve Regulates the Endosomal Localization of CpG Oligodeoxynucleotides to Elicit TLR9-Dependent Cellular Responses. *PLoS ONE* 8:e73894.

226. Volpi C et al. (2013) High doses of CpG oligodeoxynucleotides stimulate a tolerogenic TLR9-TRIF pathway. *Nature Communications* 4:1852.

227. Markowski P et al. (2013) Pre-conditioning with synthetic CpG-oligonucleotides attenuates myocardial ischemia/reperfusion injury via IL-10 up-regulation. *Basic Res Cardiol* 108:376.

228. Waibler Z et al. (2008) Excessive CpG 1668 stimulation triggers IL-10 production by cDC that inhibits IFN-alpha responses by pDC. *Eur J Immunol* 38:3127–3137.

229. Murray PJ (2005) The primary mechanism of the IL-10-regulated antiinflammatory response is to selectively inhibit transcription. *Proc Natl Acad Sci USA* 102:8686–8691.

230. Khan S et al. (2007) Distinct uptake mechanisms but similar intracellular processing of two different toll-like receptor ligand-peptide conjugates in dendritic cells. *J Biol Chem* 282:21145–21159.

231. Adamczyk Z, Bratek A, Jachimska B, Jasinski T, Warszynski P (2006) Structure of poly(acrylic acid) in electrolyte solutions determined from simulations and viscosity measurements. *J Phys Chem B* 110:22426–22435.

232. Cooper GS, Bynum MLK, Somers EC (2009) Recent insights in the epidemiology of autoimmune diseases: improved prevalence estimates and understanding of clustering of diseases. *Journal of Autoimmunity* 33:197–207.

233. Kuznik A et al. (2011) Mechanism of Endosomal TLR Inhibition by Antimalarial Drugs and Imidazoquinolines. *The Journal of Immunology* 186:4794–4804.

234. Lee J et al. (2011) Nucleic acid-binding polymers as anti-inflammatory agents. *Proc Natl Acad Sci USA* 108:14055–14060.

235. Stearns NA, Lee J, Leong KW, Sullenger BA, Pisetsky DS (2012) The Inhibition of Anti-DNA Binding to DNA by Nucleic Acid Binding Polymers. *PLoS ONE* 7:e40862.

236. Holl EK, Shumansky KL, Pitoc G, Ramsburg E, Sullenger BA (2013) Nucleic acid scavenging polymers inhibit extracellular DNA-mediated innate immune activation without inhibiting anti-viral responses. *PLoS ONE* 8:e69413.

237. Kandimalla ER, Agrawal S (2012) Modulation of endosomal Toll-like receptor-mediated immune responses by synthetic oligonucleotides. 61–93.

238. Kim J et al. (2013) Acidic Amino Acid Residues in the Juxtamembrane Region of the Nucleotide-Sensing TLRs Are Important for UNC93B1 Binding and Signaling. *The Journal of Immunology* 190:5287–5295.

239. Henry SP et al. (2002) Complement activation is responsible for acute toxicities in rhesus monkeys treated with a phosphorothioate oligodeoxynucleotide. *International Immunopharmacology* 2:1657–1666.

240. Levin AA (1999) A review of the issues in the pharmacokinetics and toxicology of phosphorothioate antisense oligonucleotides. *Biochim Biophys Acta* 1489:69–84.

241. Brown DA et al. (1994) Effect of phosphorothioate modification of oligodeoxynucleotides on specific protein binding. *J Biol Chem* 269:26801–26805.

242. Bauer S (2013) Toll-like receptor 9 processing: the key event in Toll-like receptor 9 activation? *Immunol Lett* 149:85–87.

243. Sands H et al. (1995) Biodistribution and metabolism of internally 3H-labeled oligonucleotides. II. 3“,5-”blocked oligonucleotides. *Mol Pharmacol* 47:636–646.

244. Meng W, Yamazaki T, Nishida Y, Hanagata N (2011) Nuclease-resistant immunostimulatory phosphodiester CpG oligodeoxynucleotides as human Toll-like receptor 9 agonists. *BMC Biotechnology* 11:88.

245. Stein CA, Subasinghe C, Shinozuka K, Cohen JS (1988) Physicochemical properties of phosphorothioate oligodeoxynucleotides. *Nucleic acids research* 16:3209–3221.

246. Gilar M, Belenky A, Smisek DL, Bourque A, Cohen AS (1997) Kinetics of phosphorothioate oligonucleotide metabolism in biological fluids. *Nucleic acids research* 25:3615–3620.

247. Hurtado P, Peh CA (2010) LL-37 promotes rapid sensing of CpG oligodeoxynucleotides by B lymphocytes and plasmacytoid dendritic cells. *J Immunol* 184:1425–1435.

248. Tewary P et al. (2013) β-Defensin 2 and 3 Promote the Uptake of Self or CpG DNA, Enhance IFN-α Production by Human Plasmacytoid Dendritic Cells, and Promote Inflammation. *The Journal of Immunology* 191:865–874.

249. Fivaz M et al. (2002) Differential sorting and fate of endocytosed GPI-anchored proteins. *The EMBO Journal* 21:3989–4000.

250. Ghosh P, Dahms NM, Kornfeld S (2003) Mannose 6-phosphate receptors: new twists in the tale. *Nat Rev Mol Cell Biol* 4:202–212.

251. Canton J, Neculai D, Grinstein S (2013) Scavenger receptors in homeostasis and immunity. *Nature Publishing Group* 13:621–634.

252. Kelley SL, Lukk T, Nair SK, Tapping RI (2013) The Crystal Structure of Human Soluble CD14 Reveals a Bent Solenoid with a Hydrophobic Amino-Terminal Pocket. *The Journal of Immunology* 190:1304–1311.

253. Pan X et al. (2012) Leucine-rich Repeat 11 of Toll-like Receptor 9 Can Tightly Bind to CpG-containing Oligodeoxynucleotides, and the Positively Charged Residues Are Critical for the High Affinity. *J Biol Chem* 287:30596–30609.

APPENDIX

LICENSES FOR COPYRIGHTED MATERIAL

ELSEVIER LICENSE TERMS AND CONDITIONS

Nov 01, 2013

This is a License Agreement between Nemours ("You") and Elsevier ("Elsevier") provided by Copyright Clearance Center ("CCC"). The license consists of your order details, the terms and conditions provided by Elsevier, and the payment terms and conditions.

All payments must be made in full to CCC. For payment instructions, please see information listed at the bottom of this form.

Supplier Elsevier Limited
The Boulevard,Langford Lane
Kidlington,Oxford,OX5 1GB,UK

Registered Company

Number 1982084

Customer name University of Delaware

Customer address Newark, DE 19716

License number 3260350333048

License date Nov 01, 2013

Licensed content publisher Elsevier

Licensed content publication Trends in Microbiology

Licensed content title Innate immune detection of microbial nucleic acids

Licensed content author Claudia Gürtler,Andrew G. Bowie

Licensed content date August 2013

Licensed content volume 21 number

Licensed content issue 8 number

Number of pages 8

Start Page 413

End Page 420

Type of Use reuse in a thesis/dissertation

Portion figures/tables/illustrations

Number of 2 figures/tables/illustrations

Format both print and electronic

Are you the author of this Elsevier article? No

Will you be translating? No

Order reference number Eric_Ch1

Title of your thesis/dissertation Investigation of Toll-like receptor 9 ligand recognition and function via multivalent oligodeoxynucleotide-polymer conjugates

Expected completion date May 2014

Estimated size (number of pages) 180

Elsevier VAT number GB 494 6272 12

Permissions price 0.00 USD VAT/Local Sales Tax 0.0 USD / 0.0 GBP

Total 0.00 USD

Terms and Conditions

INTRODUCTION

1. The publisher for this copyrighted material is Elsevier. By clicking "accept" in connection with completing this licensing transaction, you agree that the following terms and conditions apply to this transaction (along with the Billing and Payment terms and conditions established by Copyright Clearance Center, Inc. ("CCC"), at the time that you opened your Rightslink account and that are available at any time at http://myaccount.copyright.com).

GENERAL TERMS

2. Elsevier hereby grants you permission to reproduce the aforementioned material subject to the terms and conditions indicated.

3. Acknowledgement: If any part of the material to be used (for example, figures) has appeared in our publication with credit or acknowledgement to another source, permission must also be sought from that source. If such permission is not obtained then that material may not be included in your publication/copies. Suitable acknowledgement to the source must be made, either as a footnote or in a reference list at the end of your publication, as follows:

"Reprinted from Publication title, Vol /edition number, Author(s), Title of article / title of chapter, Pages No., Copyright (Year), with permission from Elsevier [OR APPLICABLE SOCIETY COPYRIGHT OWNER]." Also Lancet special credit - "Reprinted from The Lancet, Vol. number, Author(s), Title of article, Pages No., Copyright (Year), with permission from Elsevier."

4. Reproduction of this material is confined to the purpose and/or media for which permission is hereby given.

5. Altering/Modifying Material: Not Permitted. However figures and illustrations may be altered/adapted minimally to serve your work. Any other abbreviations, additions,

deletions and/or any other alterations shall be made only with prior written authorization of Elsevier Ltd. (Please contact Elsevier at permissions@elsevier.com)

6. If the permission fee for the requested use of our material is waived in this instance, please be advised that your future requests for Elsevier materials may attract a fee.

7. Reservation of Rights: Publisher reserves all rights not specifically granted in the combination of (i) the license details provided by you and accepted in the course of this licensing transaction, (ii) these terms and conditions and (iii) CCC's Billing and Payment terms and conditions.

8. License Contingent Upon Payment: While you may exercise the rights licensed immediately upon issuance of the license at the end of the licensing process for the transaction, provided that you have disclosed complete and accurate details of your proposed use, no license is finally effective unless and until full payment is received from you (either by publisher or by CCC) as provided in CCC's Billing and Payment terms and conditions. If full payment is not received on a timely basis, then any license preliminarily granted shall be deemed automatically revoked and shall be void as if never granted. Further, in the event
that you breach any of these terms and conditions or any of CCC's Billing and Payment terms and conditions, the license is automatically revoked and shall be void as if never granted. Use of materials as described in a revoked license, as well as any use of the materials beyond the scope of an unrevoked license, may constitute

copyright infringement and publisher reserves the right to take any and all action to protect its copyright in the materials.

9. Warranties: Publisher makes no representations or warranties with respect to the licensed material.

10. Indemnity: You hereby indemnify and agree to hold harmless publisher and CCC, and their respective officers, directors, employees and agents, from and against any and all claims arising out of your use of the licensed material other than as specifically authorized pursuant to this license.

11. No Transfer of License: This license is personal to you and may not be sublicensed, assigned, or transferred by you to any other person without publisher's written permission.

12. No Amendment Except in Writing: This license may not be amended except in a writing signed by both parties (or, in the case of publisher, by CCC on publisher's behalf).

13. Objection to Contrary Terms: Publisher hereby objects to any terms contained in any purchase order, acknowledgment, check endorsement or other writing prepared by you, which terms are inconsistent with these terms and conditions or CCC's Billing and Payment terms and conditions. These terms and conditions, together with CCC's

Billing and Payment terms and conditions (which are incorporated herein), comprise the entire agreement
between you and publisher (and CCC) concerning this licensing transaction. In the event of any conflict between your obligations established by these terms and conditions and those established by CCC's Billing and Payment terms and conditions, these terms and conditions shall control.

14. Revocation: Elsevier or Copyright Clearance Center may deny the permissions described in this License at their sole discretion, for any reason or no reason, with a full refund payable to you. Notice of such denial will be made using the contact information provided by you. Failure to receive such notice will not alter or invalidate the denial. In no event will Elsevier or Copyright Clearance Center be responsible or liable for any costs, expenses or damage incurred by you as a result of a denial of your permission request, other than a refund of the amount(s) paid by you to Elsevier and/or Copyright Clearance Center for denied
permissions.

LIMITED LICENSE

The following terms and conditions apply only to specific license types:

15. Translation: This permission is granted for non-exclusive world English rights only unless your license was granted for translation rights. If you licensed translation

rights you may only translate this content into the languages you requested. A professional translator must perform all translations and reproduce the content word for word preserving the integrity of the article. If this license is to re-use 1 or 2 figures then permission is granted for non-exclusive world rights in all languages.

16. Website: The following terms and conditions apply to electronic reserve and author websites:

Electronic reserve: If licensed material is to be posted to website, the web site is to be password-protected and made available only to bona fide students registered on a relevant course if:

This license was made in connection with a course,

This permission is granted for 1 year only. You may obtain a license for future website posting,

All content posted to the web site must maintain the copyright information line on the bottom of each image,

A hyper-text must be included to the Homepage of the journal from which you are licensing at http://www.sciencedirect.com/science/journal/xxxxx or the Elsevier homepage for books at http://www.elsevier.com , and

Central Storage: This license does not include permission for a scanned version of the material to be stored in a central repository such as that provided by Heron/XanEdu.

17. Author website for journals with the following additional clauses:

All content posted to the web site must maintain the copyright information line on the bottom of each image, and the permission granted is limited to the personal version of your paper. You are not allowed to download and post the published electronic version of your article (whether PDF or HTML, proof or final version), nor may you scan the printed edition to create an electronic version. A hyper-text must be included to the Homepage of the
journal from which you are licensing at
http://www.sciencedirect.com/science/journal/xxxxx
. As part of our normal production process, you will receive an e-mail notice when your article appears on Elsevier's online service ScienceDirect (www.sciencedirect.com). That e- mail will include the article's Digital Object Identifier (DOI). This number provides the electronic link to the published article and should be included in the posting of your personal version. We ask that you wait until you receive this e-mail and have the DOI to do any posting.

Central Storage: This license does not include permission for a scanned version of the material to be stored in a central repository such as that provided by Heron/XanEdu.

18. Author website for books with the following additional clauses: Authors are permitted to place a brief summary of their work online only.
A hyper-text must be included to the Elsevier homepage at http://www.elsevier.com .
All content posted to the web site must maintain the copyright information line on the bottom of each image. You are not allowed to download and post the published

electronic version of your chapter, nor may you scan the printed edition to create an electronic version.

Central Storage: This license does not include permission for a scanned version of the material to be stored in a central repository such as that provided by Heron/XanEdu.

19. Website (regular and for author): A hyper-text must be included to the Homepage of the journal from which you are licensing at http://www.sciencedirect.com/science/journal/xxxxx. or for books to the Elsevier homepage at http://www.elsevier.com

20. Thesis/Dissertation: If your license is for use in a thesis/dissertation your thesis may be submitted to your institution in either print or electronic form. Should your thesis be published commercially, please reapply for permission. These requirements include permission for the Library and Archives of Canada to supply single copies, on demand, of the complete thesis and include permission for UMI to supply single copies, on demand, of the complete thesis. Should your thesis be published commercially, please reapply for permission.

21. Other Conditions:

v1.6

If you would like to pay for this license now, please remit this license along with your payment made payable to "COPYRIGHT CLEARANCE CENTER" otherwise you will be invoiced within 48 hours of the license date. Payment should be in the form of a check or money order referencing your account number and this invoice number RLNK501149717.
Once you receive your invoice for this order, you may pay your invoice by credit card. Please follow instructions provided at that time.

Make Payment To: Copyright Clearance Center Dept 001
P.O. Box 843006
Boston, MA 02284-3006

For suggestions or comments regarding this order, contact RightsLink Customer Support: customercare@copyright.com or +1-877-622-5543 (toll free in the US) or +1-978-646-2777.

Gratis licenses (referencing $0 in the Total field) are free. Please retain this printable license for your reference. No payment is required.

ELSEVIER LICENSE TERMS AND CONDITIONS

Dec 19, 2013

This is a License Agreement between Nemours ("You") and Elsevier ("Elsevier") provided by Copyright Clearance Center ("CCC"). The license consists of your order details, the terms and conditions provided by Elsevier, and the payment terms and conditions.

All payments must be made in full to CCC. For payment instructions, please see information listed at the bottom of this form.

Supplier Elsevier Limited
The Boulevard,Langford Lane
Kidlington,Oxford,OX5 1GB,UK

Registered Company Number 1982084
Customer name University of Delaware
Customer address Newark, DE 19716
License number 3292521096394

License date Dec 19, 2013

Licensed content publisher Elsevier

Licensed content publication Acta Biomaterialia

Licensed content title DNA–polymer conjugates for immune stimulation through Toll-like receptor 9 mediated pathways

Licensed content author Eric A. Levenson, Kristi L. Kiick

Licensed content date 6 December 2013

Licensed content volume number

Licensed content issue number

Number of pages 1

Start Page 0

End Page 0

Type of Use reuse in a thesis/dissertation

Portion full article

Format both print and electronic

Are you the author of this Elsevier article? Yes

Will you be translating? No

Title of your thesis/dissertation Investigation of Toll-like receptor 9 ligand recognition and function via multivalent oligodeoxynucleotide-polymer conjugates

Expected completion date May 2014

Estimated size (number of pages) 180

Elsevier VAT number GB 494 6272 12

Permissions price 0.00 USD

VAT/Local Sales Tax 0.00 USD / 0.00 GBP Total 0.00 USD

Terms and Conditions

INTRODUCTION

1. The publisher for this copyrighted material is Elsevier. By clicking "accept" in connection with completing this licensing transaction, you agree that the following terms and conditions apply to this transaction (along with the Billing and Payment terms and conditions established by Copyright Clearance Center, Inc. ("CCC"), at the time that you opened your Rightslink account and that are available at any time at http://myaccount.copyright.com).

GENERAL TERMS

2. Elsevier hereby grants you permission to reproduce the aforementioned material subject to the terms and conditions indicated.

3. Acknowledgement: If any part of the material to be used (for example, figures) has appeared in our publication with credit or acknowledgement to another source, permission must also be sought from that source. If such permission is not obtained then that material may not be included in your publication/copies. Suitable acknowledgement to the source must be made, either as a footnote or in a reference list at the end of your publication, as follows:

"Reprinted from Publication title, Vol /edition number, Author(s), Title of article / title of chapter, Pages No., Copyright (Year), with permission from Elsevier [OR APPLICABLE SOCIETY COPYRIGHT OWNER]." Also Lancet special credit - "Reprinted from The Lancet, Vol. number, Author(s), Title of article, Pages No., Copyright (Year), with permission from Elsevier."

4. Reproduction of this material is confined to the purpose and/or media for which permission is hereby given.

5. Altering/Modifying Material: Not Permitted. However figures and illustrations may be altered/adapted minimally to serve your work. Any other abbreviations, additions, deletions and/or any other alterations shall be made only with prior written authorization of Elsevier Ltd. (Please contact Elsevier at permissions@elsevier.com)

6. If the permission fee for the requested use of our material is waived in this instance, please be advised that your future requests for Elsevier materials may attract a fee.

7. Reservation of Rights: Publisher reserves all rights not specifically granted in the combination of (i) the license details provided by you and accepted in the course of this licensing transaction, (ii) these terms and conditions and (iii) CCC's Billing and Payment terms and conditions.

8. License Contingent Upon Payment: While you may exercise the rights licensed immediately upon issuance of the license at the end of the licensing process for the transaction, provided that you have disclosed complete and accurate details of your proposed use, no license is finally effective unless and until full payment is received from you (either by publisher or by CCC) as provided in CCC's Billing and Payment terms and conditions. If full payment is not received on a timely basis, then any license preliminarily granted shall be deemed automatically revoked and shall be void as if never granted. Further, in the event
that you breach any of these terms and conditions or any of CCC's Billing and Payment terms and conditions, the license is automatically revoked and shall be void as if never granted. Use of materials as described in a revoked license, as well as any use of the materials beyond the scope of an unrevoked license, may constitute copyright infringement and publisher reserves the right to take any and all action to protect its copyright in the materials.

9. Warranties: Publisher makes no representations or warranties with respect to the licensed material.

10. Indemnity: You hereby indemnify and agree to hold harmless publisher and CCC, and their respective officers, directors, employees and agents, from and against any and all claims arising out of your use of the licensed material other than as specifically authorized pursuant to this license.

11. No Transfer of License: This license is personal to you and may not be sublicensed, assigned, or transferred by you to any other person without publisher's written permission.

12. No Amendment Except in Writing: This license may not be amended except in a writing signed by both parties (or, in the case of publisher, by CCC on publisher's behalf).

13. Objection to Contrary Terms: Publisher hereby objects to any terms contained in any purchase order, acknowledgment, check endorsement or other writing prepared by you, which terms are inconsistent with these terms and conditions or CCC's Billing and Payment terms and conditions. These terms and conditions, together with CCC's Billing and Payment terms and conditions (which are incorporated herein), comprise the entire agreement
between you and publisher (and CCC) concerning this licensing transaction. In the event of any conflict between your obligations established by these terms and

conditions and those established by CCC's Billing and Payment terms and conditions, these terms and conditions shall control.

14. Revocation: Elsevier or Copyright Clearance Center may deny the permissions described in this License at their sole discretion, for any reason or no reason, with a full refund payable to you. Notice of such denial will be made using the contact information provided by you. Failure to receive such notice will not alter or invalidate the denial. In no event will Elsevier or Copyright Clearance Center be responsible or liable for any costs, expenses or damage incurred by you as a result of a denial of your permission request, other than a refund of the amount(s) paid by you to Elsevier and/or Copyright Clearance Center for denied
permissions.

LIMITED LICENSE

The following terms and conditions apply only to specific license types:

15. Translation: This permission is granted for non-exclusive world English rights only unless your license was granted for translation rights. If you licensed translation rights you may only translate this content into the languages you requested. A professional translator must perform all translations and reproduce the content word for word preserving the integrity of the article. If this license is to re-use 1 or 2 figures then permission is granted for non-exclusive world rights in all languages.

16. Website: The following terms and conditions apply to electronic reserve and author websites:

Electronic reserve: If licensed material is to be posted to website, the web site is to be password-protected and made available only to bona fide students registered on a relevant course if:

This license was made in connection with a course,

This permission is granted for 1 year only. You may obtain a license for future website posting,

All content posted to the web site must maintain the copyright information line on the bottom of each image,

A hyper-text must be included to the Homepage of the journal from which you are licensing at http://www.sciencedirect.com/science/journal/xxxxx or the Elsevier homepage for books at http://www.elsevier.com , and

Central Storage: This license does not include permission for a scanned version of the material to be stored in a central repository such as that provided by Heron/XanEdu.

17. Author website for journals with the following additional clauses:

All content posted to the web site must maintain the copyright information line on the bottom of each image, and the permission granted is limited to the personal version of your paper. You are not allowed to download and post the published electronic version of your article (whether PDF or HTML, proof or final version), nor may you scan the

printed edition to create an electronic version. A hyper-text must be included to the Homepage of the
journal from which you are licensing at
http://www.sciencedirect.com/science/journal/xxxxx
. As part of our normal production process, you will receive an e-mail notice when your article appears on Elsevier's online service ScienceDirect (www.sciencedirect.com). That e- mail will include the article's Digital Object Identifier (DOI). This number provides the electronic link to the published article and should be included in the posting of your personal version. We ask that you wait until you receive this e-mail and have the DOI to do any posting.

Central Storage: This license does not include permission for a scanned version of the material to be stored in a central repository such as that provided by Heron/XanEdu.

18. Author website for books with the following additional clauses: Authors are permitted to place a brief summary of their work online only.
A hyper-text must be included to the Elsevier homepage at http://www.elsevier.com . All content posted to the web site must maintain the copyright information line on the bottom of each image. You are not allowed to download and post the published electronic version of your chapter, nor may you scan the printed edition to create an electronic version.

Central Storage: This license does not include permission for a scanned version of the material to be stored in a central repository such as that provided by Heron/XanEdu.

19. Website (regular and for author): A hyper-text must be included to the Homepage of the journal from which you are licensing at http://www.sciencedirect.com/science/journal/xxxxx. or for books to the Elsevier homepage at http://www.elsevier.com

20. Thesis/Dissertation: If your license is for use in a thesis/dissertation your thesis may be submitted to your institution in either print or electronic form. Should your thesis be published commercially, please reapply for permission. These requirements include permission for the Library and Archives of Canada to supply single copies, on demand, of the complete thesis and include permission for UMI to supply single copies, on demand, of the complete thesis. Should your thesis be published commercially, please reapply for permission.

21. Other Conditions

v1.6

If you would like to pay for this license now, please remit this license along with your payment made payable to "COPYRIGHT CLEARANCE CENTER" otherwise you

will be invoiced within 48 hours of the license date. Payment should be in the form of a check or money order referencing your account number and this invoice number RLNK501186106.
Once you receive your invoice for this order, you may pay your invoice by credit card. Please follow instructions provided at that time.

Make Payment To: Copyright Clearance Center Dept 001
P.O. Box 843006
Boston, MA 02284-3006

For suggestions or comments regarding this order, contact RightsLink Customer Support: customercare@copyright.com or +1-877-622-5543 (toll free in the US) or +1-978-646-2777.

Gratis licenses (referencing $0 in the Total field) are free. Please retain this printable license for your reference. No payment is required.

THE AMERICAN ASSOCIATION FOR THE ADVANCEMENT OF SCIENCE LICENSE TERMS AND CONDITIONS

May 07, 2014

This is a License Agreement between Nemours ("You") and The American Association for the Advancement of Science ("The American Association for the Advancement of Science") provided by Copyright Clearance Center ("CCC"). The license consists of your order details, the terms and conditions provided by The American Association for the Advancement of Science, and the payment terms and conditions.

All payments must be made in full to CCC. For payment instructions, please see information listed at the bottom of this form.

License Number 3383111439272

License date May 06, 2014

Licensed content publisher	The American Association for the Advancement of Science
Licensed content publication	Science
Licensed content title	Structural Reorganization of the Toll-Like Receptor 8 Dimer Induced by Agonistic Ligands
Licensed content author	Hiromi Tanji, Umeharu Ohto, Takuma Shibata, Kensuke Miyake, Toshiyuki Shimizu
Licensed content date	Mar 22, 2013
Volume number	339
Issue number	6126
Type of Use	Thesis / Dissertation
Requestor type	Scientist/individual at a research institution
Format	Print and electronic

Portion	Figure
Number of figures/tables	1
Order reference number	None
Title of your dissertation	Investigation of Toll-like receptor 9 ligand recognition and function via multivalent oligodeoxynucleotide-polymer conjugates
Expected completion date	May 2014
Estimated size(pages)	180

Total 0.00 USD Terms and Conditions

American Association for the Advancement of Science TERMS AND CONDITIONS
Regarding your request, we are pleased to grant you non-exclusive, non-transfera permission, to republish the AAAS material identified above in your work identified above, subject to the terms and conditions herein. We must be contacted for permission for any uses other than those specifically identified in your request above.

The following credit line must be printed along with the AAAS material: "From [Full Reference Citation]. Reprinted with permission from AAAS."

All required credit lines and notices must be visible any time a user accesses any part of the
AAAS material and must appear on any printed copies and authorized user might make.

This permission does not apply to figures / photos / artwork or any other content or materials included in your work that are credited to non-AAAS sources. If the requested material is sourced to or references non-AAAS sources, you must obtain authorization from that source as well before using that material. You agree to hold harmless and indemnify AAAS against any claims arising from your use of any content in your work that is credited to non-AAAS sources.

If the AAAS material covered by this permission was published in Science during the years

1974 - 1994, you must also obtain permission from the author, who may grant or withhold permission, and who may or may not charge a fee if permission is granted. See original article for author's address. This condition does not apply to news articles.

The AAAS material may not be modified or altered except that figures and tables may be modified with permission from the author. Author permission for any such changes must be secured prior to your use.

Whenever possible, we ask that electronic uses of the AAAS material permitted herein include a hyperlink to the original work on AAAS's website (hyperlink may be embedded in the reference citation).

AAAS material reproduced in your work identified herein must not account for more than
30% of the total contents of that work.

AAAS must publish the full paper prior to use of any text.

AAAS material must not imply any endorsement by the American Association for the Advancement of Science.

This permission is not valid for the use of the AAAS and/or Science logos.

AAAS makes no representations or warranties as to the accuracy of any information contained in the AAAS material covered by this permission, including any warranties of

merchantability or fitness for a particular purpose.

If permission fees for this use are waived, please note that AAAS reserves the right to charge for reproduction of this material in the future.

Permission is not valid unless payment is received within sixty (60) days of the issuance of this permission. If payment is not received within this time period then all rights granted herein shall be revoked and this permission will be considered null and void.

In the event of breach of any of the terms and conditions herein or any of CCC's Billing and Payment terms and conditions, all rights granted herein shall be revoked and this permission will be considered null and void.

AAAS reserves the right to terminate this permission and all rights granted herein at its discretion, for any purpose, at any time. In the event that AAAS elects to terminate this permission, you will have no further right to publish, publicly perform, publicly display, distribute or otherwise use any matter in which the AAAS content had been included, and all fees paid hereunder shall be fully refunded to you. Notification of termination will be sent to the contact information as supplied by you during the request process and termination shall be immediate upon sending the notice. Neither AAAS nor CCC shall be liable for any costs,
expenses, or damages you may incur as a result of the termination of this permission, beyond the refund noted above.
This Permission may not be amended except by written document signed by both parties. The terms above are applicable to all permissions granted for the use of AAAS material.
Below you will find additional conditions that apply to your particular type of use.

FOR A THESIS OR DISSERTATION
If you are using figure(s)/table(s), permission is granted for use in print and electronic versions of your dissertation or thesis. A full text article may be used in print versions only of a dissertation or thesis.

Permission covers the distribution of your dissertation or thesis on demand by ProQuest / UMI, provided the AAAS material covered by this permission remains in situ.

If you are an Original Author on the AAAS article being reproduced, please refer to your
License to Publish for rules on reproducing your paper in a dissertation or thesis.

FOR JOURNALS:
Permission covers both print and electronic versions of your journal article, however the
AAAS material may not be used in any manner other than within the context of your article.

FOR BOOKS/TEXTBOOKS:
If this license is to reuse figures/tables, then permission is granted for non-exclusive world rights in all languages in both print and electronic formats (electronic formats are defined below).

If this license is to reuse a text excerpt or a full text article, then permission is granted for non-exclusive world rights in English only. You have the option of securing either

print or electronic rights or both, but electronic rights are not automatically granted and do garner additional fees. Permission for translations of text excerpts or full text articles into other languages must be obtained separately.

Licenses granted for use of AAAS material in electronic format books/textbooks are valid only in cases where the electronic version is equivalent to or substitutes for the print version of the book/textbook. The AAAS material reproduced as permitted herein must remain in situ and must not be exploited separately (for example, if permission covers the use of a full text article, the article may not be offered for access or for purchase as a stand-alone unit), except in the case of permitted textbook companions as noted below.

You must include the following notice in any electronic versions, either adjacent to the reprinted AAAS material or in the terms and conditions for use of your electronic products: "Readers may view, browse, and/or download material for temporary copying purposes only, provided these uses are for noncommercial personal purposes. Except as provided by law, this material may not be further reproduced, distributed, transmitted, modified, adapted,
performed, displayed, published, or sold in whole or in part, without prior written permission from the publisher."

If your book is an academic textbook, permission covers the following companions to your textbook, provided such companions are distributed only in conjunction with your textbook at no additional cost to the user:

- Password-protected website
- Instructor's image CD/DVD and/or PowerPoint resource
- Student CD/DVD

All companions must contain instructions to users that the AAAS material may be used for non-commercial, classroom purposes only. Any other uses require the prior written permission from AAAS.

If your license is for the use of AAAS Figures/Tables, then the electronic rights granted herein permit use of the Licensed Material in any Custom Databases that you distribute the electronic versions of your textbook through, so long as the Licensed Material remains within the context of a chapter of the title identified in your request and cannot be downloaded by a user as an independent image file.

Rights also extend to copies/files of your Work (as described above) that you are required to provide for use by the visually and/or print disabled in compliance with state and federal laws.

This permission only covers a single edition of your work as identified in your request.

FOR NEWSLETTERS:
Permission covers print and/or electronic versions, provided the AAAS material reproduced as permitted herein remains in situ and is not exploited separately (for example, if
permission covers the use of a full text article, the article may not be offered for access or for purchase as a stand-alone unit)

FOR ANNUAL REPORTS:
Permission covers print and electronic versions provided the AAAS material reproduced as permitted herein remains in situ and is not exploited separately (for example, if permission covers the use of a full text article, the article may not be offered for access or for purchase as a stand-alone unit)

FOR PROMOTIONAL/MARKETING USES:
Permission covers the use of AAAS material in promotional or marketing pieces such as information packets, media kits, product slide kits, brochures, or flyers limited to a single print run. The AAAS Material may not be used in any manner which implies endorsement or promotion by the American Association for the Advancement of Science (AAAS) or
Science of any product or service. AAAS does not permit the reproduction of its name, logo

or text on promotional literature.

If permission to use a full text article is permitted, The Science article covered by this permission must not be altered in any way. No additional printing may be set onto an article copy other than the copyright credit line required above. Any alterations must be approved in advance and in writing by AAAS. This includes, but is not limited to, the placement of
sponsorship identifiers, trademarks, logos, rubber stamping or self-adhesive stickers onto the article copies.

Additionally, article copies must be a freestanding part of any information package (i.e. media kit) into which they are inserted. They may not be physically attached to anything, such as an advertising insert, or have anything attached to them, such as a

sample product. Article copies must be easily removable from any kits or informational packages in which they are used. The only exception is that article copies may be inserted into three-ring binders.

FOR CORPORATE INTERNAL USE:
The AAAS material covered by this permission may not be altered in any way. No additional printing may be set onto an article copy other than the required credit line. Any alterations must be approved in advance and in writing by AAAS. This includes, but is not limited to the placement of sponsorship identifiers, trademarks, logos, rubber stamping or self-adhesive stickers onto article copies.

If you are making article copies, copies are restricted to the number indicated in your request and must be distributed only to internal employees for internal use.

If you are using AAAS Material in Presentation Slides, the required credit line must be visible on the slide where the AAAS material will be reprinted

If you are using AAAS Material on a CD, DVD, Flash Drive, or the World Wide Web, you must include the following notice in any electronic versions, either adjacent to the reprinted AAAS material or in the terms and conditions for use of your electronic products: "Readers may view, browse, and/or download material for temporary copying purposes only, provided these uses are for noncommercial personal purposes. Except as provided by law, this
material may not be further reproduced, distributed, transmitted, modified, adapted, performed, displayed, published, or sold in whole or in part, without prior written permission from the publisher." Access to any such CD, DVD, Flash Drive or Web page must be restricted to your organization's employees only.

FOR CME COURSE and SCIENTIFIC SOCIETY MEETINGS:
Permission is restricted to the particular Course, Seminar, Conference, or Meeting indicated in your request. If this license covers a text excerpt or a Full Text Article, access to the reprinted AAAS material must be restricted to attendees of your event only (if you have
been granted electronic rights for use of a full text article on your website, your website must be password protected, or access restricted so that only attendees can access the content on your site).

If you are using AAAS Material on a CD, DVD, Flash Drive, or the World Wide Web, you must include the following notice in any electronic versions, either adjacent to the reprinted AAAS material or in the terms and conditions for use of your electronic

products: "Readers may view, browse, and/or download material for temporary copying purposes only, provided

these uses are for noncommercial personal purposes. Except as provided by law, this material may not be further reproduced, distributed, transmitted, modified, adapted, performed, displayed, published, or sold in whole or in part, without prior written permission from the publisher."

FOR POLICY REPORTS:
These rights are granted only to non-profit organizations and/or government agencies. Permission covers print and electronic versions of a report, provided the required credit line appears in both versions and provided the AAAS material reproduced as permitted herein remains in situ and is not exploited separately.

FOR CLASSROOM PHOTOCOPIES:
Permission covers distribution in print copy format only. Article copies must be freestanding and not part of a course pack. They may not be physically attached to anything or have anything attached to them.

FOR COURSEPACKS OR COURSE WEBSITES:
These rights cover use of the AAAS material in one class at one institution. Permission is valid only for a single semester after which the AAAS material must be removed from the Electronic Course website, unless new permission is obtained for an additional semester. If the material is to be distributed online, access must be restricted to students and instructors enrolled in that particular course by some means of password or access control.

FOR WEBSITES:
You must include the following notice in any electronic versions, either adjacent to the reprinted AAAS material or in the terms and conditions for use of your electronic products: "Readers may view, browse, and/or download material for temporary copying purposes only, provided these uses are for noncommercial personal purposes. Except as provided by law, this material may not be further reproduced, distributed, transmitted, modified, adapted,
performed, displayed, published, or sold in whole or in part, without prior written permission from the publisher."

Permissions for the use of Full Text articles on third party websites are granted on a case by case basis and only in cases where access to the AAAS Material is restricted by some means of password or access control. Alternately, an E-Print may be purchased through our reprints department (brocheleau@rockwaterinc.com).

REGARDING FULL TEXT ARTICLE USE ON THE WORLD WIDE WEB IF YOU ARE AN ‘ORIGINAL AUTHOR’ OF A SCIENCE PAPER

If you chose "Original Author" as the Requestor Type, you are warranting that you are one of authors listed on the License Agreement as a "Licensed content author" or that you are acting on that author's behalf to use the Licensed content in a new work that one of the authors listed on the License Agreement as a "Licensed content author" has written.

Original Authors may post the ‘Accepted Version’ of their full text article on their personal or on their University website and not on any other website. The ‘Accepted Version’ is the version of the paper accepted for publication by AAAS including changes resulting from peer review but prior to AAAS’s copy editing and production (in other words not the AAAS published version).

FOR MOVIES / FILM / TELEVISION:
Permission is granted to use, record, film, photograph, and/or tape the AAAS material in connection with your program/film and in any medium your program/film may be shown or heard, including but not limited to broadcast and cable television, radio, print, world wide web, and videocassette.

The required credit line should run in the program/film's end credits.

FOR MUSEUM EXHIBITIONS:
Permission is granted to use the AAAS material as part of a single exhibition for the duration of that exhibit. Permission for use of the material in promotional materials for the exhibit must be cleared separately with AAAS (please contact us at permissions@aaas.org).

FOR TRANSLATIONS:
Translation rights apply only to the language identified in your request summary above.

The following disclaimer must appear with your translation, on the first page of the article, after the credit line: "This translation is not an official translation by AAAS staff, nor is it endorsed by AAAS as accurate. In crucial matters, please refer to the official English- language version originally published by AAAS."

FOR USE ON A COVER:

Permission is granted to use the AAAS material on the cover of a journal issue, newsletter issue, book, textbook, or annual report in print and electronic formats provided the AAAS material reproduced as permitted herein remains in situ and is not exploited separately

By using the AAAS Material identified in your request, you agree to abide by all the terms and conditions herein.

Questions about these terms can be directed to the AAAS Permissions department permissions@aaas.org.

Other Terms and Conditions:

v 2

If you would like to pay for this license now, please remit this license along with your payment made payable to "COPYRIGHT CLEARANCE CENTER" otherwise you will be invoiced within 48 hours of the license date. Payment should be in the form of a check or money order referencing your account number and this invoice number 501295875. Once you receive your invoice for this order, you may pay your invoice by credit card. Please follow instructions provided at that time.

Make Payment To: Copyright Clearance Center Dept 001
P.O. Box 843006
Boston, MA 02284-3006

For suggestions or comments regarding this order, contact RightsLink Customer Support: customercare@copyright.com or +1-877-622-5543 (toll free in the US) or +1-
978-646-2777.

Gratis licenses (referencing $0 in the Total field) are free. Please retain this printable license for your reference. No payment is required.